

CHALMERS



Evaluation of heat and moisture induced stress and strain of historic building materials and artefacts

Master of Science Thesis in the Master's Programme Structural Engineering and Building Performance Design

NATALIE LEONOR WILLIAMS PORTAL

Department of Civil and Environmental Engineering
Division of Building Technology
Building Physics
CHALMERS UNIVERSITY OF TECHNOLOGY
Göteborg, Sweden 2011
Master's Thesis 2011:82

Master's Thesis 2011:82

Evaluation of heat and moisture induced stress and strain of historic building materials and artefacts

*Master of Science Thesis in the Master's Programme Structural Engineering and
Building Performance Design*

NATALIE LEONOR WILLIAMS PORTAL

Department of Civil and Environmental Engineering
Division of Building Technology
Building Physics
CHALMERS UNIVERSITY OF TECHNOLOGY
Göteborg, Sweden 2011

Evaluation of heat and moisture induced stress and strain of historic building materials and artefacts

Master of Science Thesis in the Master's Programme Structural Engineering and Building Performance Design

NATALIE LEONOR WILLIAMS PORTAL

© NATALIE LEONOR WILLIAMS PORTAL, 2011

Examensarbete / Institutionen för bygg- och miljöteknik,
Chalmers tekniska högskola 2011:82

Department of Civil and Environmental Engineering
Division of Building Technology
Building Physics
Chalmers University of Technology
SE-412 96 Göteborg
Sweden
Telephone: + 46 (0)31-772 1000

Cover:

Historic paintings applied directly to external building assemblies in The Vatican Museums, Italy. Photo credit: N. L. Williams Portal

Chalmers reproservice / Department of Civil and Environmental Engineering
Göteborg, Sweden 2011

Evaluation of heat and moisture induced stress and strain of historic building materials and artefacts

Master of Science Thesis in the Master's Programme Structural Engineering and Building Performance Design

NATALIE LEONOR WILLIAMS PORTAL

Department of Civil and Environmental Engineering

Division of Building Technology

Building Physics

Chalmers University of Technology

ABSTRACT

Climate change can cause not only damage, but can also destroy the basic structure of historic sites, as well as their associated interior artefacts. The evaluation of combined heat and moisture induced stress and strain (HMSS) is a valuable method in which possible damage-related processes can be predicted. The aim was to develop one- and two-dimensional coupled heat and moisture (HM) and HMSS models of building materials and artefacts in the commercial finite element software COMSOL Multiphysics Version 4.1. This multiphysics software package ensures the compatibility of modelling combined physical transports, due to its flexible and adaptable platform. Validation and verification by means of analytical, numerical and experimental solutions are also included in this study, along with numerical simulation results from the developed models. The two-dimensional HM and HMSS models were thereafter implemented into various case studies in order to demonstrate the value and applicability of the models as predictive tools. The one- and two-dimensional HM models were concluded to be valid predictive tools to investigate the impact of a change in climatic conditions on building assemblies and artefacts. The HM model was however found to be limited when faced with moisture transport beyond the storage capacity of the materials defined in the model. Concerning the two-dimensional HMSS model, it was found to be an adequate predictive tool to determine possible damage-related processes in building assemblies and artefacts. The verification of this model was executed based on the material properties and mechanical behaviour of one material, namely lime wood. Accordingly, the functionality of the HMSS model is only valid for this given material.

Key words: Coupled heat and moisture induced stress and strain, finite element method, COMSOL Multiphysics, predictive tools, historical buildings and artefacts, and climate change

Contents

| | | |
|-------|---|----|
| 1 | INTRODUCTION | 1 |
| 1.1 | Background | 1 |
| 1.2 | Objectives | 2 |
| 1.3 | Methodology | 2 |
| 1.4 | Limitations | 2 |
| 2 | COUPLED HEAT AND MOISTURE MODELLING | 3 |
| 2.1 | Heat and moisture transfer | 3 |
| 2.2 | Energy and moisture balance | 4 |
| 2.3 | Boundary conditions | 5 |
| 2.4 | COMSOL modelling | 5 |
| 3 | HM MODEL VERIFICATION | 8 |
| 3.1 | Benchmark test description | 8 |
| 3.2 | HM model setup | 11 |
| 3.3 | Decoupled HM model verification | 14 |
| 3.3.1 | Step response for a slab | 14 |
| 3.3.2 | Heat transfer results | 16 |
| 3.3.3 | Moisture transfer results | 17 |
| 3.4 | Coupled HM model verification | 18 |
| 3.4.1 | Coupled transfer results | 18 |
| 3.4.2 | Model limitations | 20 |
| 4 | HEAT AND MOISTURE INDUCED MECHANICAL STRESS-STRAIN MODELLING | 22 |
| 4.1 | Mechanical stress and strain | 22 |
| 4.2 | COMSOL modelling | 25 |
| 5 | HMSS MODEL VERIFICATION | 28 |
| 5.1 | Verification test description | 28 |
| 5.1.1 | Material properties | 29 |
| 5.2 | HMSS Model setup | 31 |
| 5.2.1 | Numerical simulation results | 33 |
| 5.2.2 | Model limitations | 34 |
| 6 | CASE STUDIES | 35 |
| 6.1 | Model parameters | 35 |
| 6.1.1 | Climate conditions | 35 |
| 6.1.2 | Boundary heat sources | 37 |

| | | |
|--------|-------------------------------------|----|
| 6.1.3 | Boundary moisture sources | 38 |
| 6.1.4 | Selected materials and assemblies | 38 |
| 6.2 | Two-dimensional HM modelling | 39 |
| 6.2.1 | Model setup | 39 |
| 6.2.2 | Numerical simulation results | 43 |
| 6.3 | Two-dimensional HMSS modelling | 45 |
| 6.3.1 | Background | 45 |
| 6.3.2 | Model setup | 46 |
| 6.3.3 | Numerical simulation results | 48 |
| 7 | SENSITIVITY ANALYSIS | 52 |
| 7.1 | One-dimensional HM modelling | 52 |
| 7.1.1 | Thermal impact | 52 |
| 7.2 | Two-dimensional HM modelling | 55 |
| 7.2.1 | Additional boundary moisture source | 55 |
| 7.3 | Two-dimensional HMSS modelling | 57 |
| 7.3.1 | Thermal impact | 57 |
| 7.3.2 | Additional boundary heat source | 58 |
| 7.3.3 | Result comparison | 60 |
| 8 | CONCLUSIONS | 64 |
| 9 | RECOMMENDATIONS | 65 |
| 10 | REFERENCES | 66 |
| 11 | APPENDICES | 68 |
| 11.1 | Network analysis | 68 |
| 11.1.1 | Heat Transfer | 68 |
| 11.1.2 | Moisture Transfer | 71 |
| 11.2 | Material properties | 74 |
| 11.3 | Matlab files | 79 |
| 11.3.1 | Saturation vapour pressure | 79 |
| 11.3.2 | M-file for HM model | 79 |
| 11.3.3 | M-file for HMSS model | 91 |

Preface

This study has been executed as a collaborative effort between Chalmers University of Technology, Sweden and Eindhoven University of Technology (TU/e), the Netherlands. The first portion of this project was carried out from September to December 2010 at the Department of Civil and Environmental Engineering, Building Technology, Chalmers University of Technology under the supervision of Professor Angela Sasic Kalagasidis. From January to April 2011, the project was undertaken at the Department of Architecture, Building and Planning, Building Physics and Systems, TU/e under the supervision of Assistant Professor Jos van Schijndel. The concluding remarks for this project have been accomplished in May 2011 at Chalmers University of Technology.

This project could not have been completed without Angela Sasic Kalagasidis and Jos van Schijndel who not only served as my supervisors but also encouraged and guided me throughout the development of this research. I would also like to thank my research colleague and opponent David van Reenen for his co-operation and valuable brainstorming sessions.

Göteborg June 2011

Natalie Leonor Williams Portal

Notations

THEORETICAL PARAMETERS

Roman upper case letters

| | |
|--------------|---|
| C | Constitutive matrix |
| D_M | Moisture diffusion coefficient (m^2/s) |
| D_w | Liquid transport coefficient (m^2/s) |
| E | Young's modulus (MPa) |
| E_{Radial} | Young's modulus in radial direction (MPa) |
| E_{Tang} | Young's modulus in tangential direction (MPa) |
| F | Body force (N) |
| Fo | Fourier number (-) |
| G | Shear modulus (MPa) |
| I_{sol} | Solar radiation energy flux (W/m^2) |
| K | Liquid conductivity (s) |
| L | Length or thickness (m) |
| M | Moisture source (kg/m^3) or moisture content (%) Eqn (5.1) |
| M_w | Molar mass of water (kg/mol) |
| R_w | Individual gas constant for water (J/mol·K) |
| S | Heat source or sink (W) |
| $S_{h,g}$ | Entire boundary for traction and displacement vectors |
| T | Temperature at a point ($^{\circ}C$, K) |
| T_0 | Initial temperature ($^{\circ}C$, K) |
| T_1 | Step change in temperature at boundary $x=0$ ($^{\circ}C$, K) |
| T_e | Exterior temperature ($^{\circ}C$, K) |
| T_i | Interior temperature ($^{\circ}C$, K) |
| T_{ref} | Initial reference temperature ($^{\circ}C$) |

Roman lower case letters

| | |
|------------|---|
| a_d | Thermal diffusivity (J/kg·K) or moisture diffusivity (m^2/s) |
| a | Conservative flux convection coefficient (-) |
| c | Diffusion coefficient (-) |
| c_p | Specific heat capacity (J/kg·K) |
| c_{pa} | Specific heat capacity of air (J/kg·K) |
| d_a | Damping or a mass coefficient (-) |
| e_a | Mass coefficient (-) |
| f | Source term (-) |
| g | Density of moisture flow rate ($kg/m^2 \cdot s$) or boundary source term (-) Eqn (2.21) |
| g_{ℓ} | Density of moisture liquid flow rate ($kg/m^2 \cdot s$) |
| g_p | Density of convective moisture flow rate for partial vapour pressure ($kg/m^2 \cdot s$) |

| | |
|------------------|---|
| g_v | Density of moisture vapour flow rate ($\text{kg}/\text{m}^2 \cdot \text{s}$) |
| g_{vp} | Density of convective moisture flow rate for humidity by volume ($\text{kg}/\text{m}^2 \cdot \text{s}$) |
| g_φ | Density of convective moisture flow rate for relative humidity ($\text{kg}/\text{m}^2 \cdot \text{s}$) |
| h | Boundary coefficient (-) |
| k | Stiffness term (-) |
| m | Mass term (-) |
| n | Outward unit normal vector on $\partial\Omega$ (-) |
| p | Pressure at a point (Pa) |
| p_0 | Initial pressure (Pa) |
| p_1 | Step change in pressure at boundary $x=0$ (Pa) |
| p_v | Partial vapour pressure (Pa) |
| p_{sat} | Vapour pressure at saturation (Pa) |
| q | Density of heat flow rate (W/m^2) or boundary absorption coefficient Eqn (2.20) |
| q_c | Density of convective heat flow rate (W/m^2) |
| q_{cd} | Density of conductive heat flow rate (W/m^2) |
| q_{sol} | Density of solar radiation flow rate (W/m^2) |
| r | Known vector (-) |
| s | Capillary suction pressure (Pa) |
| t | Time (s) or traction vector Eqn |
| $u(x, t)$ | Dimensionless solution (-) |
| u | Vector of dependent variables (-) or displacement vector (-) Eqn (4.4) |
| u_w | Wind speed (m/s) |
| w | Moisture content at a point or defined for a material (kg/m^3) |

Greek upper case letters

| | |
|------------------|---|
| Δ | Laplace operator (-) |
| ∇ | Vector differential operator (gradient) (-) |
| $\nabla\theta$ | Temperature increment (K) |
| ∇w | Moisture increment (%m) |
| Ω | Computational domain – union of all domains (-) |
| $\partial\Omega$ | Domain boundary (-) |
| C | Fourth-order stiffness tensor (-) |

Greek lower case letters

| | |
|-----------------------|---|
| α | Absorption coefficient (-) |
| α_c | Convective surface heat transfer coefficient ($\text{W}/\text{m}^2 \cdot \text{K}$) |
| α_e | Exterior heat transfer coefficient ($\text{W}/\text{m}^2 \cdot \text{K}$) |
| α_i | Interior heat transfer coefficient ($\text{W}/\text{m}^2 \cdot \text{K}$) |
| α_{sol} | Absorptivity of solar radiation (-) |
| α_t | Dimensional change coefficient due to thermal increment (1/K) |

| | |
|-----------------------|---|
| β | Convection coefficient (-) |
| β_e | Exterior moisture transfer coefficient ($\text{kg}/\text{m}^2\cdot\text{s}$) |
| β_i | Interior moisture transfer coefficient ($\text{kg}/\text{m}^2\cdot\text{s}$) |
| β_v | Moisture transfer coefficient for humidity by volume (m/s) |
| β_φ | Moisture transfer coefficient for relative humidity ($\text{kg}/\text{m}^2\cdot\text{s}$) |
| γ | Conservative flux source term (-) |
| δ_p | Vapour permeability for partial vapour pressure ($\text{kg}/\text{m}\cdot\text{s}\cdot\text{Pa}$) |
| ε_o | Initial strain (m) |
| $\varepsilon_{x,y,z}$ | Strain component (m) |
| ϵ | Strain tensor |
| κ | Dimensional change coefficient due to moisture increment (1/%m) |
| λ | Thermal conductivity ($\text{W}/\text{m}\cdot\text{K}$) |
| μ | Lagrange multiplier (-) |
| ν | Poisson's ratio (-) |
| ξ | Moisture capacity (kg/m^3) or damping parameter Eqn (4.14) |
| ρ | Density (kg/m^3) or mass density (-) Eqn (4.14) |
| ρ_a | Density of air (kg/m^3) |
| $\rho_o c_o$ | Volumetric heat capacity ($\text{J}/\text{m}^3\cdot\text{K}$) |
| ρ_w | Density of water (kg/m^3) |
| σ | Stress tensor |
| σ_o | Initial stress (N/m^2) |
| $\sigma_{x,y,z}$ | Stress components (N/m^2) |
| τ | Shear stress (N/m^2) |
| φ | Relative humidity (%) |
| φ_e | Exterior relative humidity (%) |
| φ_i | Interior relative humidity (%) |
| φ_o | Initial relative humidity (%) |
| φ_1 | Step change in relative humidity at boundary $x=0$ (%) |

COMSOL MODEL PARAMETERS

Equivalent theoretical parameter indicated by '[-]'

Roman upper case letters

| | |
|--------------|--|
| Cpv | Specific heat capacity ($\text{J}/\text{m}^3\cdot\text{K}$), [$\rho_o c_o$] |
| Dl_mat | Liquid transport coefficient (m^2/s), [D_w] |
| Dw_mat | Moisture diffusion coefficient (m^2/s), [D_M] |
| Igrad_year | Global radiation from climate data (W/m^2), [I_{sol}] |
| K_mat | Thermal conductivity ($\text{W}/\text{m}\cdot\text{K}$), [λ] |
| Modrad_mat | Modulus of Elasticity in radial direction (MPa), [E_{Radial}] |
| Modshear_mat | Shear modulus (MPa), [G] |
| Modtan_mat | Modulus of Elasticity in tangential direction (MPa), [E_{Tang}] |
| Psat | Vapour pressure at saturation (Pa), [p_{sat}] |

| | |
|-----------|---|
| Rain_year | Precipitation from climate data (mm/h) |
| Rhi | Interior relative humidity (-, %), [φ_i] |
| Rho | Initial relative humidity (-, %), [φ_0] |
| Rhstep | Step change in relative humidity (-, %), [φ_1] |
| Rhe_year | Exterior relative humidity from climate data (%), [φ_e] |
| Rhe_10 | Exterior relative humidity from climate data for 2010 (%), [φ_e] |
| Te | Exterior temperature ($^{\circ}\text{C}$, K), [T_e] |
| Ti | Interior temperature ($^{\circ}\text{C}$, K), [T_i] |
| To | Initial temperature ($^{\circ}\text{C}$, K), [T_0] |
| Tstep | Step change in temperature ($^{\circ}\text{C}$, K), [T_1] |
| Te_year | Exterior temperature from climate data ($^{\circ}\text{C}$), [T_e] |
| Te_10 | Exterior temperature from climate data for 2010 ($^{\circ}\text{C}$), [T_e] |

Roman lower case letters

| | |
|------------|---|
| alpha | Dimensional change coefficient due to moisture increment (1/%m), [κ] |
| beta_e | Exterior moisture transfer coefficient ($\text{kg}/\text{m}^2\cdot\text{s}$), [β_e] |
| betae_10 | Exterior moisture transfer coefficient calculated from climate data for 2010 ($\text{kg}/\text{m}^2\cdot\text{s}$), [β_e] |
| beta_i | Interior moisture transfer coefficient ($\text{kg}/\text{m}^2\cdot\text{s}$), [β_i] |
| deltap_mat | Vapour permeability ($\text{kg}/\text{m}\cdot\text{s}\cdot\text{Pa}$), [δ_p] |
| g_e | Exterior moisture convection ($\text{kg}/\text{m}^2\cdot\text{s}$), [g_φ] |
| g_i | Interior moisture convection ($\text{kg}/\text{m}^2\cdot\text{s}$), [g_φ] |
| he | Exterior heat transfer coefficient ($\text{W}/\text{m}^2\cdot\text{K}$), [α_e] |
| he_10 | Exterior heat transfer coefficient calculated from climate data for 2010 ($\text{W}/\text{m}^2\cdot\text{K}$), [α_e] |
| hi | Interior heat transfer coefficient ($\text{W}/\text{m}^2\cdot\text{K}$), [α_i] |
| ksi_mat | Moisture capacity defined for a material (kg/m^3), [ξ] |
| nuvector | Poisson's ratio (-), [ν] |
| qc_e | Exterior heat convection (W/m^2), [q_c] |
| qc_i | Interior heat convection (W/m^2), [q_c] |
| w_mat | Moisture content defined for a material (kg/m^3 , %), [w, M] |

1 Introduction

1.1 Background

The driving force of this study is the Climate for Culture project found within the European Union's 7th framework program. This project attempts to face the challenges of climate change, while acknowledging the need for the preservation of cultural heritage. The effects of climate change on selected cultural heritage sites from 16 countries in Europe and North Africa are being examined over a period of five years. It is important to consider that a change in climatic conditions can cause not only damage, but can also destroy the basic structure of these sites, as well as their associated interior artefacts.

The need for establishing attainable environmental guidelines for museums is on the emerging front. As of late, there has been not only a push to reduce energy consumption and carbon emissions, but also a concern regarding the preservation of natural resources and cultural heritage (International Institute of Conservation, 2010). As such, it is of interest to gain knowledge of the past and present conditions of artefacts in order to understand causes of previous damage, predict forthcoming damage, and also aid in developing preservation guidelines for artefacts.

Experimental and simulation work on indoor climate and control in historic and monumental buildings has been to a great extent the focal point in building physics research at the Technical University of Eindhoven in the Netherlands (Schellen & van Schijndel, 2007). It is of particular interest to observe the simulation work that has been executed to evaluate the heat and mass transfer through monumental materials along with their associated dimensional effects. For instance, an investigation of the moisture related shrinkage of wood in a monumental organ located in the Walloon Church in Delft, the Netherlands, was investigated by means of wood deformation tests. Guidelines regarding the indoor climate conditions for this monumental church were thereafter recommended based on experimentally validated numerical simulation results (Schellen, 2002). It is thought that further investigations regarding the prediction of the effects of changing environmental conditions on historical buildings and their associated artefacts can be supported by means of computer simulations (Sulaiman et al., 2010).

The development of finite element based numerical models have been deemed as valuable tools for predicting past and future behaviour of artefacts. For example, the numerical modelling of moisture induced stress fields in a lime wood cylinder subjected to changing climate conditions has been established by Jakiela et al (2007). The purpose of this model was to determine the response of the specimen to step changes in thermal and hygric conditions, as well as the maximum stress levels. A similar coupled model was also developed in COMSOL Multiphysics by Schellen & van Schijndel (2010) as a comparative benchmark to numerically model the moisture related mechanical stress in wooden cylindrical objects. It is however of interest to further develop such coupled multiphysics models by including varying outdoor and indoor thermal and hygric climates in order to generate a more realistic predictive tool for use in historical buildings. The main focus of this study was thus to develop models of this type in the commercial finite element software COMSOL Multiphysics Version 4.1. This software was selected primarily due to its flexible and adaptable platform ensuring the compatibility of modelling combined heat and moisture induced stresses and strains in building materials and artefacts found in historic buildings.

1.2 Objectives

The main objective of this study is to develop a predictive tool to determine possible damage-related processes caused by change in climatic conditions on building assemblies and artefacts particularly sited in historical buildings. More specifically, the predictive tool is based on one- and two-dimensional coupled heat and HMSS modelling in COMSOL Multiphysics. A secondary objective is to verify and validate the developed models by means of analytical solutions, as well as by experimental and numerical results. Also, the sensitivity of the predictive tool to varying model parameters and boundary conditions is investigated. The prediction of damage-related processes in building assemblies and artefacts is simply demonstrated and the evaluation of the numerical simulation results is beyond the scope of this study.

1.3 Methodology

The methodology used in the development of a predictive tool in COMSOL Multiphysics comprised of the following steps:

- Development of one- and two-dimensional coupled heat and moisture (HM) models in COMSOL Multiphysics.
- Verification of the one-dimensional decoupled HM model in stationary and transient time studies using network calculations and analytical solutions.
- Verification of the one-dimensional transient coupled HM model using the normative benchmark test namely the European Provisional Standard prEN 15026.
- Development of a two-dimensional transient HMSS model in COMSOL Multiphysics. Includes the integration of the two-dimensional transient coupled HM model in a two-dimensional transient linear elastic solid mechanics model.
- Verification of the two-dimensional transient HMSS model by means of a numerical and experimental study evaluating the response of lime wood supports in historical panel paintings subjected to changing climate conditions.
- Implementation of the two-dimensional HM and HMSS models into various case studies in order to demonstrate the value and applicability of the models as predictive tools.
- Investigation of critical model parameter changes in the one-dimensional HM model and also in both two-dimensional HM and HMSS models.

1.4 Limitations

The HM and HMSS models were developed in one- and two-dimensions. The development of the HM model excluded air transport occurring interstitially and through materials. Additional heat and moisture generation, such as latent heat, was also neglected. Concerning the HMSS model, it was developed exclusively to numerically simulate linear elastic mechanical behaviour of materials. As such, plastic deformation and failure criterion were excluded from this study.

The temperature used in the numerical simulations ranged between -30°C to 80°C . Moisture freezing in materials was not considered in the models. Overall, simulation time studies were limited to a period of one year.

2 Coupled Heat and Moisture Modelling

The evaluation of coupled heat and moisture transport is a valuable method in which possible damage-related processes can be predicted. Heat and moisture transport mechanisms can be described individually by Partial Differential Equations (PDEs). These PDEs can be fluently combined thereby allowing coupled transport to be modelled.

In this study, the commercial finite element software COMSOL Multiphysics Version 4.1 was utilized to develop a coupled heat and moisture model, which is denoted as HM model in this paper. This multiphysics software package ensures the compatibility of modelling combined heat and moisture transport in building assemblies due to its flexible and adaptable platform. The combined transport described by PDEs was integrated into a multiphysics modelling tool entitled Coefficient Form PDE Interface (c), and thereafter, parameterized by advanced material and boundary functions.

2.1 Heat and moisture transfer

The model includes two-dimensional conductive heat transfer according to Fourier's Law:

$$q = q_{cd} \quad (2.1)$$

$$q_{cd} = -\lambda \nabla T = - \left(\lambda \frac{\partial T}{\partial x}, \lambda \frac{\partial T}{\partial y} \right) \quad (2.2)$$

The total moisture transfer considered includes both vapour and liquid flow. Moisture transfer can be characterized by various potentials. The partial vapour pressure and the relative humidity were both considered in the HM model. The following expressions describe the total moisture transfer corresponding to both cases:

$$g = g_v + g_\ell \quad (2.3)$$

$$g_v = -\delta_p \nabla p = - \left(\delta_p \frac{\partial p}{\partial x}, \delta_p \frac{\partial p}{\partial y} \right) \quad (2.4)$$

$$g_\ell = -D_w \cdot \frac{\xi}{p_{sat}} \nabla p = -D_w \cdot \frac{\xi}{p_{sat}} \left(\frac{\partial p}{\partial x}, \frac{\partial p}{\partial y} \right) \quad (2.5)$$

$$g_v = -\delta_p \cdot p_{sat} \nabla \varphi = -\delta_p \cdot p_{sat} \left(\frac{\partial \varphi}{\partial x}, \frac{\partial \varphi}{\partial y} \right) \quad (2.6)$$

$$g_\ell = -D_w \cdot \xi \nabla \varphi = -D_w \cdot \xi \left(\frac{\partial \varphi}{\partial x}, \frac{\partial \varphi}{\partial y} \right) \quad (2.7)$$

Partial vapour pressure as a potential was shown to pose certain limitations during verification, particularly when combined with non-isothermal conditions. These limitations are further discussed in Section 3.4.2.

2.2 Energy and moisture balance

The PDEs for energy and moisture balance are necessary to model the combined dynamic heat and moisture transport. The methodology presented to combine the balance equations is based on Sasic Kalagasidis (2010). As such, the final forms of the balance equations are provided in Equations (2.8), (2.13) and (2.14).

$$c_p \rho \frac{\partial T}{\partial t} = -\nabla(-\lambda \nabla T) \pm S \quad (2.8)$$

$$\frac{\partial w}{\partial t} = -\nabla \left(\underbrace{(-\delta_p - D_w \cdot \frac{\xi}{p_{\text{sat}}}) \nabla p}_{g_v + g_\ell} \right) \pm M \quad (2.9)$$

The moisture balance can be further simplified in order to reduce the number of associated dependent variables. The expansion of the partial derivative of moisture content using the chain rule leads to an expression associated to moisture content, relative humidity, and partial vapour pressure, shown below:

$$\frac{\partial w}{\partial t} = \frac{\partial w}{\partial p} \cdot \frac{\partial p}{\partial t} = \frac{\partial w}{\partial \varphi} \cdot \frac{\partial \varphi}{\partial p} \cdot \frac{\partial p}{\partial t} \quad (2.10)$$

The following two relationships, expressed in Equations (2.11) and (2.12), help further transform the above equation:

$$\frac{\partial w}{\partial \varphi} = \xi \quad (2.11)$$

$$\varphi = \frac{p}{p_{\text{sat}}} \rightarrow \frac{\partial \varphi}{\partial p} = \frac{1}{p_{\text{sat}}} \quad (2.12)$$

The moisture capacity of a material is defined in Equation (2.11) as the slope of the sorption isotherm which represents the relationship between moisture content and relative humidity. As per Equation (2.12), the relative humidity is defined as the ratio between the partial vapour pressure and the saturated vapour pressure. Subsequently introducing these relationships into the moisture balance equation yields the following final forms for both the partial vapour pressure and relative humidity potentials:

$$\frac{\partial w}{\partial t} = \frac{\xi}{p_{\text{sat}}} \frac{\partial p}{\partial t} = -\nabla \left((-\delta_p - D_w \cdot \frac{\xi}{p_{\text{sat}}}) \nabla p \right) \pm M \quad (2.13)$$

$$\frac{\partial w}{\partial t} = \xi \frac{\partial \varphi}{\partial t} = -\nabla \left((-\delta_p \cdot p_{\text{sat}} - D_w \cdot \xi) \nabla \varphi \right) \pm M \quad (2.14)$$

As observed in Equations (2.13) and (2.14), the moisture balance is now a function of one dependent variable, namely partial vapour pressure or relative humidity.

2.3 Boundary conditions

The boundary value problem is formulated with the inclusion of two Neumann boundary conditions: convective thermal and hygric fluxes. The heat flux, denoted as q_c , is prescribed at both the external and internal boundaries by means of Equation (2.15). Temperature as a function of time is defined as the dependent variable.

$$q_c = \alpha_c \cdot (T_s - T_a) \quad (2.15)$$

The moisture flux is typically expressed as a moisture transfer coefficient multiplied by the difference between vapour content across a given surface, as observed in the following:

$$g_{vp} = \beta_v \cdot (v_s - v_a) \quad (2.16)$$

It is however of interest to define the driving force for moisture transport as partial vapour pressure, and furthermore as relative humidity. Firstly, the following Equation (2.17), which describes the relationship between the partial pressure and vapour content based on the General Gas Law (Hagentoft, 2001), was utilized to modify Equation (2.16), thus yielding Equation (2.18):

$$p_v = 461.4 \cdot (T + 273.15) \cdot v \quad (2.17)$$

$$g_p = \frac{\beta_v}{461.4 \cdot (T + 273.15)} \cdot (p_{vs} - p_{va}) \quad (2.18)$$

Further, Equation (2.18) can be expressed with relative humidity as the driving force by introducing the relationship stated in Equation (2.12) to yield the following:

$$g_\varphi = \beta_\varphi \cdot (\varphi_s - \varphi_a) \quad (2.19)$$

All moisture potentials expressed in Equations (2.16) to (2.19) are functions of temperature and time.

2.4 COMSOL modelling

One of the main goals of this study is to develop models describing coupled heat and moisture transport using COMSOL. In order to achieve this goal, the PDEs

describing the energy and moisture balances, Equations (2.8), (2.13) and/or (2.14), need to be modelled in COMSOL.

As aforementioned, COMSOL contains a multiphysics modelling tool entitled Coefficient Form PDE Interface (c) that can be tailored to suit the study in question. This tool contains the feature of a scalar coefficient form equation that is described by a balance equation. The balance equation contains a single dependent variable u that is an unknown function on the computational domain Ω . The PDE problem is described by the following:

$$e_a \frac{\partial^2 u}{\partial t^2} + d_a \frac{\partial u}{\partial t} + \nabla(-c\nabla u - \alpha u + \gamma) + \beta \nabla u + au = f \quad \text{in } \Omega \quad (2.20)$$

$$\mathbf{n} \cdot (c\nabla u + \alpha u - \gamma) + qu = g - h^T \boldsymbol{\mu} \quad \text{on } \partial\Omega \quad (2.21)$$

$$u = r \quad \text{on } \partial\Omega \quad (2.22)$$

Equation (2.20) is the PDE that must be satisfied in the computational domain Ω . Whereas, Equations (2.21) and (2.22) are the Neumann and Dirichlet boundary conditions, respectively, that must hold on the domain boundary Ω .

Since the convective heat transfer inside the material is neglected in this study, the coefficients e_a , α , γ , β , and a are equal to zero. Thus, Equations (2.20) and (2.21) simplify to:

$$d_a \frac{\partial u}{\partial t} = -\nabla(-c\nabla u) \pm S \quad (2.23)$$

$$\mathbf{n} \cdot (c\nabla u) = g - h^T \boldsymbol{\mu} \quad (2.24)$$

The energy and moisture balance equations can be coupled in COMSOL by means of the simplified equation presented above. In order to adequately model the combined heat and moisture transport, the PDE must be modified to contain two dependent variables. In this study, it is of particular interest to observe the correlation between temperature and partial vapour pressure or relative humidity, denoted as T , p , and φ respectively. As such, the single dependent variable u must become a vector of dependent variables T and p or φ , as shown in Equation (2.25).

$$\mathbf{u} = \begin{bmatrix} T \\ p \end{bmatrix} \quad \text{or} \quad \mathbf{u} = \begin{bmatrix} T \\ \varphi \end{bmatrix} \quad (2.25)$$

Since u is a vector, the storage and transport coefficients also need to be defined in matrix form. The damping/mass and diffusion coefficients, d_a and c , can be defined as the corresponding variables found in the energy and moisture balance Equations (2.8), (2.13) and (2.14). Accordingly, for a one-dimensional case assuming isotropic behaviour, the following matrices can describe the coefficients considering both moisture potentials:

$$d_a = \begin{bmatrix} d_{a,T} & 0 \\ 0 & d_{a,p} \end{bmatrix} = \begin{bmatrix} \rho c_p & 0 \\ 0 & \frac{\xi}{p_{sat}} \end{bmatrix} \quad (2.26)$$

$$d_a = \begin{bmatrix} d_{a,T} & 0 \\ 0 & d_{a,\varphi} \end{bmatrix} = \begin{bmatrix} \rho c_p & 0 \\ 0 & \xi \end{bmatrix} \quad (2.27)$$

$$-c = - \begin{bmatrix} c_T & 0 \\ 0 & c_p \end{bmatrix} = - \begin{bmatrix} \lambda & 0 \\ 0 & \delta_p + D_w \cdot \frac{\xi}{p_{sat}} \end{bmatrix} \quad (2.28)$$

$$-c = - \begin{bmatrix} c_T & 0 \\ 0 & c_\varphi \end{bmatrix} = - \begin{bmatrix} \lambda & 0 \\ 0 & \delta_p p_{sat} + D_w \cdot \xi \end{bmatrix} \quad (2.29)$$

Introducing the above coefficients into the simplified PDE yields the following matrix forms shown in Equations (2.30) to (2.32). The formulation for relative humidity is simply shown here; however, the same procedure applies to the potential of partial vapour pressure.

$$d_a \cdot \frac{\partial u}{\partial t} = \begin{bmatrix} d_{a,T} & 0 \\ 0 & d_{a,\varphi} \end{bmatrix} \cdot \begin{bmatrix} \frac{\partial T}{\partial t} \\ \frac{\partial \varphi}{\partial t} \end{bmatrix} = \begin{bmatrix} \rho c_p & 0 \\ 0 & \xi \end{bmatrix} \cdot \begin{bmatrix} \frac{\partial T}{\partial t} \\ \frac{\partial \varphi}{\partial t} \end{bmatrix} \quad (2.30)$$

$$-\nabla(-c \cdot \nabla u) = \nabla \begin{bmatrix} c_T & 0 \\ 0 & c_\varphi \end{bmatrix} \cdot \begin{bmatrix} \nabla T \\ \nabla \varphi \end{bmatrix} = \begin{bmatrix} \lambda & 0 \\ 0 & \delta_p \cdot p_{sat} + D_w \cdot \xi \end{bmatrix} \cdot \nabla \begin{bmatrix} \frac{\partial T}{\partial x} \\ \frac{\partial \varphi}{\partial x} \end{bmatrix} \quad (2.31)$$

$$\begin{bmatrix} \rho c_p & 0 \\ 0 & \xi \end{bmatrix} \begin{bmatrix} \frac{\partial T}{\partial t} \\ \frac{\partial \varphi}{\partial t} \end{bmatrix} + \begin{bmatrix} \lambda & 0 \\ 0 & \delta_p \cdot p_{sat} + D_w \cdot \xi \end{bmatrix} \begin{bmatrix} \nabla^2 T \\ \nabla^2 \varphi \end{bmatrix} \pm \begin{bmatrix} S \\ M \end{bmatrix} \quad (2.32)$$

The methodology presented above also holds for two-dimensional cases. For non-isotropic materials, the coefficients can be described according to directional properties.

Furthermore, the development of the coupled HM model can be visualized by means of an example of the Matlab code generated in COMSOL along with screenshots, which is provided in Section 11.3.2.

3 HM Model Verification

The validity of the HM model developed in COMSOL was verified in stages using several approaches, namely network analysis and two analytical benchmark tests.

The first step in verification involved a simplified version of the model, such that the transfer methods were verified individually. The numerical results for decoupled one-dimensional stationary heat and moisture transports were verified by network analysis. The model results agreed with the network analysis and are provided as an appendix in Section 11.1.

Furthermore, the normative benchmark test of the European Provisional Standard prEN 15026, described in Section 3.1, was used as the basis of the verification of the one-dimensional HM model in a transient study.

The one-dimensional HM model was firstly decoupled such that heat and moisture transports were verified separately. The prEN 15026 benchmark test parameters were used to set up the model, while the verification was accomplished by means of an analytical solution of a step response for a slab as discussed in Section 3.3.1. The numerical results for both transport mechanisms were found to satisfy the analytical solutions.

Lastly, the coupled one-dimensional transient HM model was verified using the normative benchmark test of the European Provisional Standard prEN 15026 as presented in Section 3.4. The numerical results were observed to fall within the error limits required by the standard.

3.1 Benchmark test description

The verification of the HM model was executed by means of the normative benchmark test of European Provisional Standard prEN 15026. The benchmark test is based on a one-dimensional analytical solution for coupled thermal and hygric transport in a homogeneous semi-infinite domain of 20 m that is initially in equilibrium with constant surrounding conditions of $T_0=20^\circ\text{C}$ and $R_h=50\%$. The domain is thereafter exposed to a step change to $T=30^\circ\text{C}$ and $R_h=95\%$. Boundary resistances and moisture sources (rain) are neglected in this benchmark. Temperature and moisture profiles after 7, 30 and 365 days are to be calculated by the model. These profile results are required to fall within $\pm 2.5\%$ of the analytical solution in accordance with the benchmark test.

At the beginning of the numerical simulation, the boundary conditions undergo a step change according to the temperature and relative humidity step changes prescribed by the test and thereafter remain constant over the course of the calculation. These boundary conditions are introduced by means of Neumann boundary conditions, such that thermal and hygric convective fluxes are calculated according to the previously defined Equations (2.15) and (2.19). The benchmark test specifies that no surface transfer resistances are to be applied to the boundaries; however the magnitude of the heat and moisture transfer coefficients were selected to ensure constant boundary conditions in the calculations. For example, high influence surface transfer coefficients were applied at the interior boundary in order to eliminate any influence that the internal boundary conditions may have on the domain. As a result, the

temperature and moisture distributions occurring from the exterior to the interior can be depicted in the numerical simulation results.

The hygrothermal material properties and the general data used in the verification are specified by the prEN15026 benchmark test and are summarized in Table 3.1. The moisture-dependent material properties, with the exception of the volumetric heat capacity, are calculated according to the analytical functions presented in Equations (3.1) to (3.9). It is of interest to note that the units presented in Table 3.1 to Table 3.3 are declared in square brackets and converted according to SI derived units in COMSOL.

Table 3.1 Summary of data used in HM model for prEN15026 verification

| Variable Name | | Expression | Description |
|-------------------------------|------------|------------------------------|-------------------------------|
| General | COMSOL | | |
| T_{ref} | To | 20 [degC] | Initial reference temperature |
| ρ_w | – | 1000 [kg/m ³] | Density of water |
| R_w | – | 8,314 [J/(mol*K)] | Universal gas constant |
| M_w | – | 0,018 [kg/mol] | Molar mass of water |
| w | w_mat | Equation (3.1) or (3.3) | Moisture content |
| p_{suc} | – | Equation (3.2) | Suction pressure |
| ξ | ksi_mat | Equation (3.4) | Moisture capacity |
| D_w | DI_mat | Equation (3.5) | Liquid transport coefficient |
| K | – | Equation (3.6) | Liquid conductivity |
| $\partial p_{suc}/\partial w$ | – | Equation (3.7) | Change in suction pressure |
| δ_p | deltap_mat | Equation (3.8) | Vapour permeability |
| λ | K_mat | Equation (3.9) | Thermal conductivity |
| $\rho_0 c_0$ | Cpv | 1,824e6 [J/m ³ K] | Volumetric heat capacity, dry |

The moisture storage function is expressed as either a function of the capillary suction pressure or as a function of the relative humidity as per the benchmark test:

$$w = \frac{146}{(1 + (8 \times 10^{-8} s)^{1.6})^{0.375}} \quad (3.1)$$

$$s = p_{\text{suc}} = 0.125 \times 10^8 \left(\left(\frac{146}{w} \right)^{\frac{1}{0.375}} - 1 \right)^{0.625} \quad (3.2)$$

$$w(\varphi) = \frac{146}{(1 + (-8 \times 10^{-8} R_w \cdot T_{\text{ref}} \cdot \rho_w \cdot \ln(\varphi))^{1.6})^{0.375}} \quad (3.3)$$

As previously discussed in Section 2.2, the HM model is based on the moisture balance PDE which necessitates the moisture capacity of the material. The moisture capacity can be approximated by the slope of the moisture storage function stated in Equation (3.3):

$$\frac{dw(\varphi)}{d\varphi} = \xi = \frac{948.90 \cdot (10.83 \cdot \ln(\varphi))^{0.6}}{(\varphi \cdot (-10.83 \cdot \ln(\varphi))^{1.6} + 1)^{1.375}} \quad (3.4)$$

Concerning the liquid transport component of the moisture balance PDE, the HM model particularly requires the liquid transport coefficient:

$$D_w = -K \cdot \frac{\partial p_{\text{suc}}}{\partial w} \quad (3.5)$$

The benchmark test defines the moisture-dependent liquid conductivity according to:

$$K = \exp(-39.2619 + 0.0704 \cdot (w - 73) - 1.7420 \cdot 10^{-4} \cdot (w - 73)^2 - 2.7953 \cdot 10^{-6} \cdot (w - 73)^3 - 1.1566 \cdot 10^{-7} \cdot (w - 73)^4 + 2.5969 \cdot 10^{-9} \cdot (w - 73)^5) \quad (3.6)$$

Subsequently, the derivative of Equation (3.2) with respect to the moisture content yields the change in suction pressure:

$$\frac{\partial p_{\text{suc}}}{\partial w} = -p_{\text{suc}} \cdot \frac{0.625}{1 - \left(\frac{146}{w} \right)^{\frac{1}{0.375}}} \cdot \frac{1}{0.375 \cdot w} \quad (3.7)$$

The moisture-dependent vapour permeability for the benchmark material is defined according to:

$$\delta_p = \frac{M_w}{R_w T_{\text{ref}}} \cdot \frac{26.1 \times 10^{-6}}{200} \cdot \frac{1 - \frac{w}{146}}{0.503 \left(1 - \frac{w}{146} \right)^2 + 0.497} \quad (3.8)$$

The thermal conductivity is defined as moisture-dependent according to the following linear function:

$$\lambda = 1.5 + \frac{15.8}{1000} \cdot w \quad (3.9)$$

3.2 HM model setup

The model includes a one-dimensional semi-infinite homogeneous domain measuring 20 m in accordance to the benchmark test. The domain is shown below in Figure 3.1.

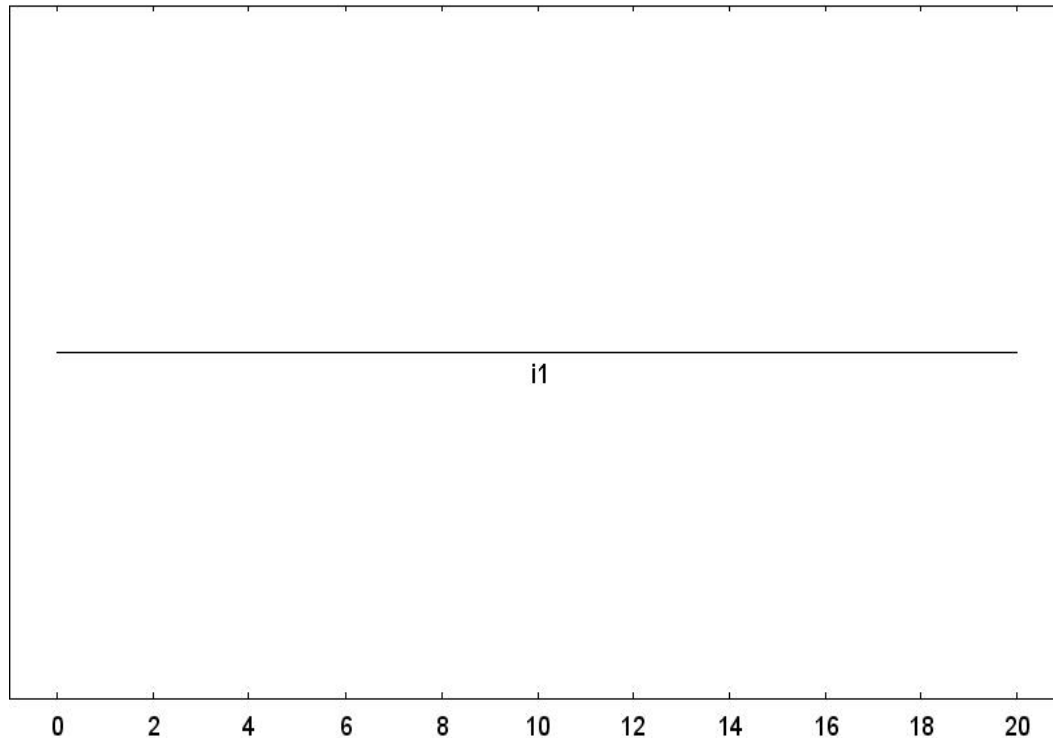


Figure 3.1 Overview of the geometry of the homogeneous domain used in the one-dimensional HM model verification.

The initial and boundary conditions specified by the benchmark are introduced into the HM model by means of global definitions. In COMSOL Multiphysics, global definitions are variables or functions that are accessible throughout the entirety of the *Model Builder* which is the root node of the model tree structure. Global definitions are particularly useful in an organizational sense when coupling models. The global parameters used in the HM model are summarized below in Table 3.2.

Table 3.2 Global parameters used in HM model for prEN15026 verification

| Name | | Expression | Description |
|----------------|--------|------------|---------------------|
| General | COMSOL | | |
| T ₀ | To | 20 [degC] | Initial temperature |
| T ₁ | Tstep | 30 [degC] | Step in temperature |

| | | | |
|-------------|--------|-----------------------------------|---|
| φ_0 | Rho | 0.50 [-] | Initial relative humidity |
| φ_1 | Rhstep | 0.95 [-] | Step in relative humidity |
| p_0 | Pvo | 1171 [Pa] | Initial partial vapour pressure |
| p_1 | Pvstep | 2225 [Pa] | Step in partial vapour pressure |
| α_e | he | 1.00E4 [W/(m ² *K)] | Exterior heat transfer coefficient |
| α_i | hi | 1.11E-10 [W/(m ² *K)] | Interior heat transfer coefficient (adiabatic) |
| β_e | beta_e | 1.00E2 [kg/(m ² *s)] | Exterior moisture transfer coefficient (for relative humidity) |
| β_i | beta_i | 7.78E-05 [kg/(m ² *s)] | Interior moisture transfer coefficient (adiabatic, for relative humidity) |

As observed in Table 3.2, initial and step values are expressed for both relative humidity and partial vapour pressure. Both moisture potentials are considered in the decoupled HM model verification discussed subsequently in Section 3.3.

Furthermore, it is of interest to illustrate that the initial conditions defined in Table 3.2 are specified for the entire homogeneous domain in COMSOL as per Figure 3.2.

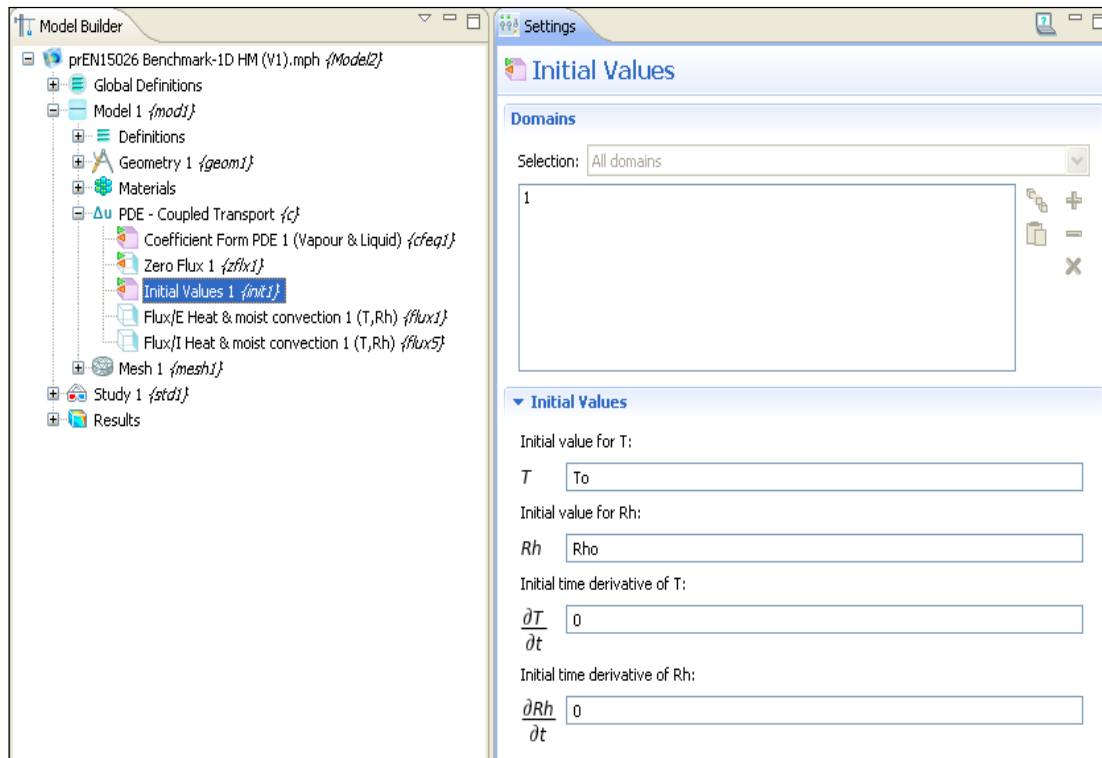


Figure 3.2 Overview of the Model Builder and initial values defined in the HM model in COMSOL.

In general, the material properties presented in Section 3.1 are tabulated and inputted into the HM model in COMSOL by means of interpolation functions. An example of an interpolation function defined in COMSOL is presented in Figure 3.3.

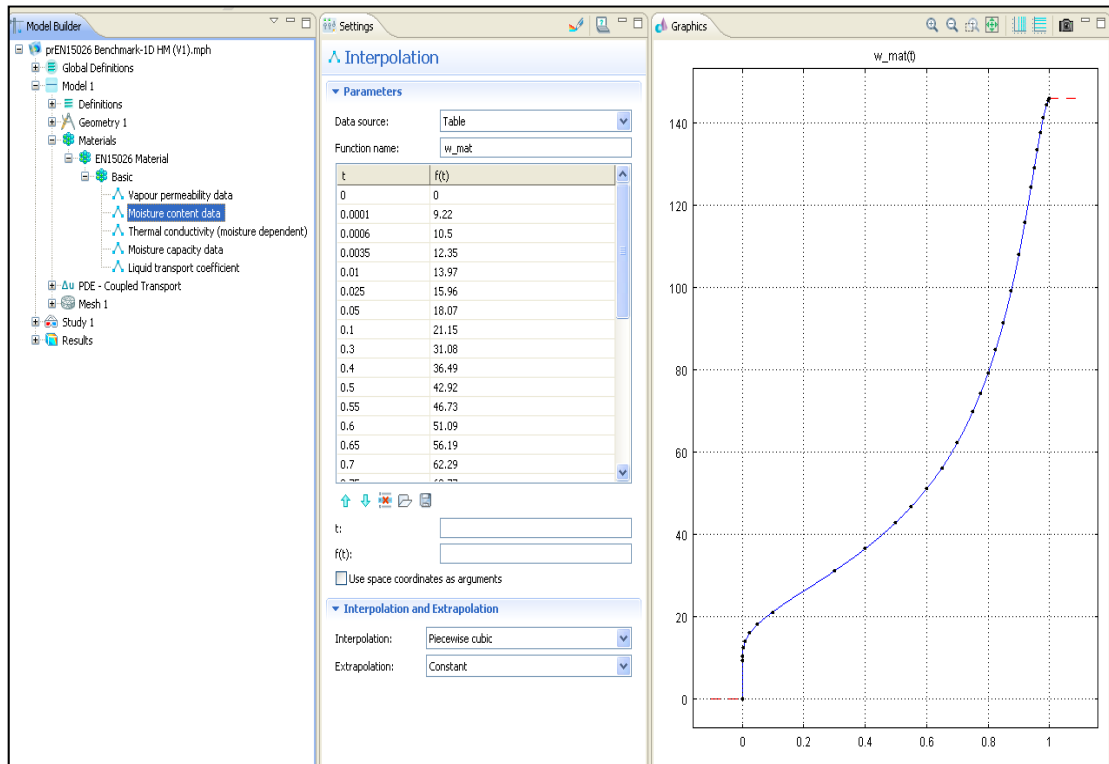


Figure 3.3 Overview of a material interpolation function in COMSOL.

The COMSOL calculation period covered 365 days and incorporated time steps of 3600 seconds. The mesh that was implemented contains 1000 elements distributed with a geometric sequence and an element ratio of 10. The geometric sequence implies that the element size exponentially increases as the distance increases away from the leftmost exterior boundary. This mesh thus allows the numerical simulation to simultaneously capture the rapidly decreasing moisture profile, as well as the slower declining temperature profile.

3.3 Decoupled HM model verification

The one-dimensional HM model was decoupled in order to verify the heat and moisture transfer problems separately. An analytical case consisting of a step response for a slab was used to verify the decoupled HM model. Due to the decoupled state of the transfer mechanisms, using constant thermal and moisture material properties corresponding to the initial surrounding conditions was found to be more practical. These constant material properties are summarized in Table 3.3.

Table 3.3 *Material properties for decoupled HM model verification*

| Name | Expression | Description |
|------------|---------------------------------|-----------------------------|
| λ | 1.5 [W/(m*K)] | Thermal conductivity, dry |
| C_{pv} | 1.824e6 [J/(m ³ *K)] | Volumetric heat capacity |
| δp | 9.078e-13 [kg/(m*s*Pa)] | Vapour permeability, Rh=50% |
| ξ | 78.314 [kg/m ³] | Moisture capacity, Rh=50% |

3.3.1 Step response for a slab

The analytical case considered provides individual solutions for one-dimensional transient heat and moisture transfer problems. The case incorporates the response of a homogeneous slab to a step change at one boundary having no surface resistance. The prescribed conditions for the analytical model are shown below in Figure 3.4 for the heat transfer problem.

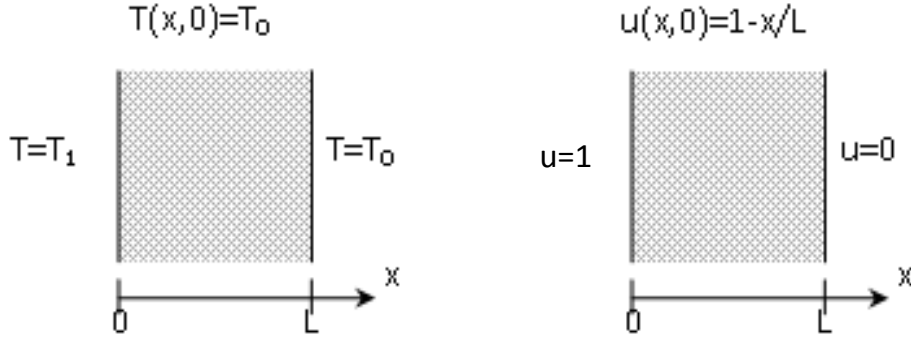


Figure 3.4 A step change at one boundary with no surface resistance (on the left), and the dimensionless deviation from steady-state (on the right) (Hagentoft, 2001).

The steady-state heat and moisture solution derived from Figure 3.4 are described in the following equations:

$$T(x, t) = T_0 + (T_1 - T_0) \cdot \left(1 - \frac{x}{L}\right) - (T_1 - T_0) \cdot u(x, t) \quad (3.10)$$

$$p(x, t) = p_0 + (p_1 - p_0) \cdot \left(1 - \frac{x}{L}\right) - (p_1 - p_0) \cdot u(x, t) \quad (3.11)$$

$$\varphi(x, t) = \varphi_0 + (\varphi_1 - \varphi_0) \cdot \left(1 - \frac{x}{L}\right) - (\varphi_1 - \varphi_0) \cdot u(x, t) \quad (3.12)$$

The dimensionless part found in Equations (3.10) to (3.12), denoted as $u(x, t)$, can be expressed by the Fourier number solution:

$$u(x, t) = \frac{2}{\pi} \sum_{n=1}^N \frac{1}{n} \cdot \sin\left(\frac{n\pi x}{L}\right) e^{-n^2 \pi^2 Fo(t)} \quad (3.13)$$

$$Fo(t) = a_d \cdot \frac{t}{L^2} \quad (3.14)$$

The Fourier number included in the above solution describes the relation between the rate of conduction and the rate of storage for the homogeneous domain. The variable a_d , defines either the thermal or moisture diffusivity for the domain.

In order to determine the size of the domain for the verification, an analytical solution for a step response of a semi-infinite slab with no surface resistance was considered. The steady-state heat solution is expressed by:

$$T(x, t) = T_0 + (T_1 - T_0) \cdot \operatorname{erfc}\left(\frac{x}{\sqrt{4a_d t}}\right) \quad 0 \leq x < \infty \quad (3.15)$$

The temperature response to a step change at the boundary of a semi-infinite slab was calculated for a time period of one year using Equation (3.15) and is depicted below in Figure 3.5. It should be noted that only the temperature response was considered due to the fact that the heat front propagates more rapidly than the moisture front.

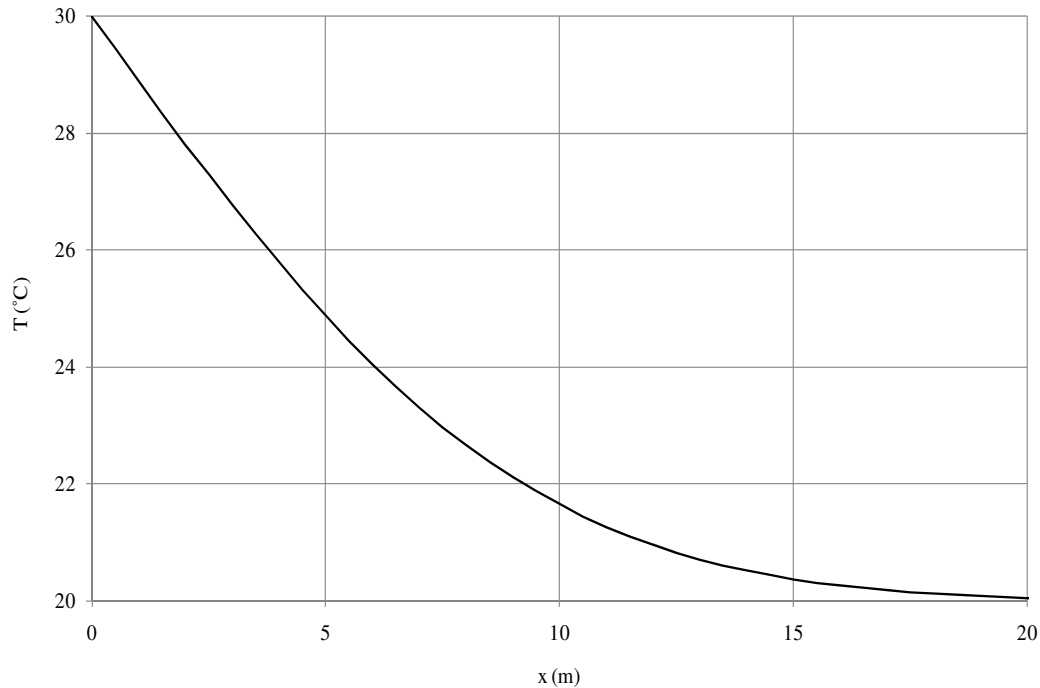


Figure 3.5 Temperature response to a step change at the boundary of a semi-infinite slab for one year.

As the size of the domain increases, the heat flow at the semi-infinite boundary is shown to approach zero in Figure 3.5. It is to say that the difference between the initial constant temperature of the domain and the temperature response at the semi-infinite boundary can be considered as negligible. Thus, it is of interest to use the domain size of 20 m in order to obtain accurate model verification and also to be consistent with that specified in the prEN15026 benchmark test.

3.3.2 Heat transfer results

Temperature profiles after 7, 30 and 365 days were calculated by the COMSOL model and compared to the analytical solution, as shown below in Figure 3.6.

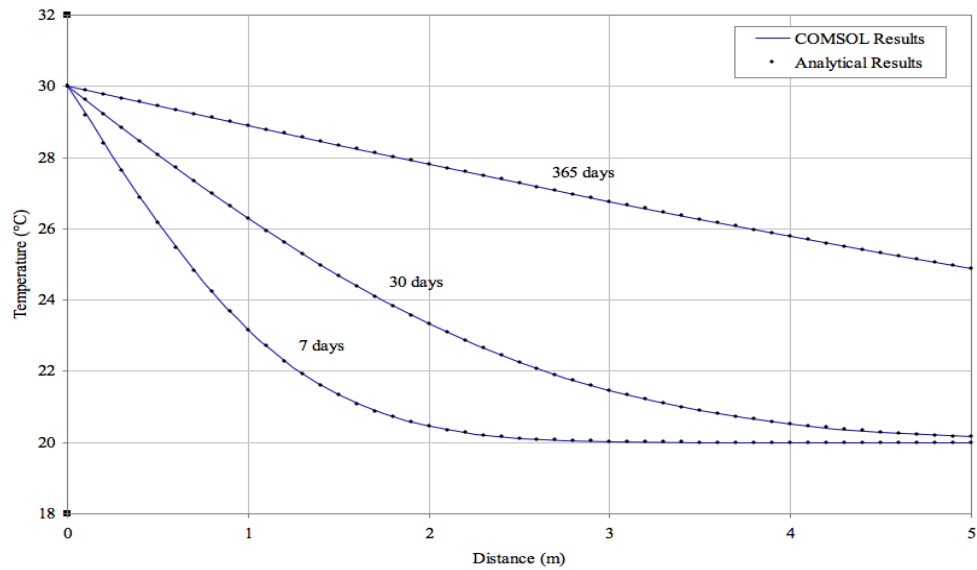


Figure 3.6 Graphical comparison of the numerical simulation results from the one-dimensional transient heat transfer model with the analytical results.

From Figure 3.6, the temperature profiles numerically simulated by the decoupled HM COMSOL are consistent with those obtained from the analytical solution.

3.3.3 Moisture transfer results

The one-dimensional transient moisture transfer problem was considered using both potentials of partial vapour pressure and relative humidity. Moisture profiles after 7, 30 and 365 days were calculated by the COMSOL model and compared to the analytical solution for both potentials as depicted below in Figure 3.7 and Figure 3.8.

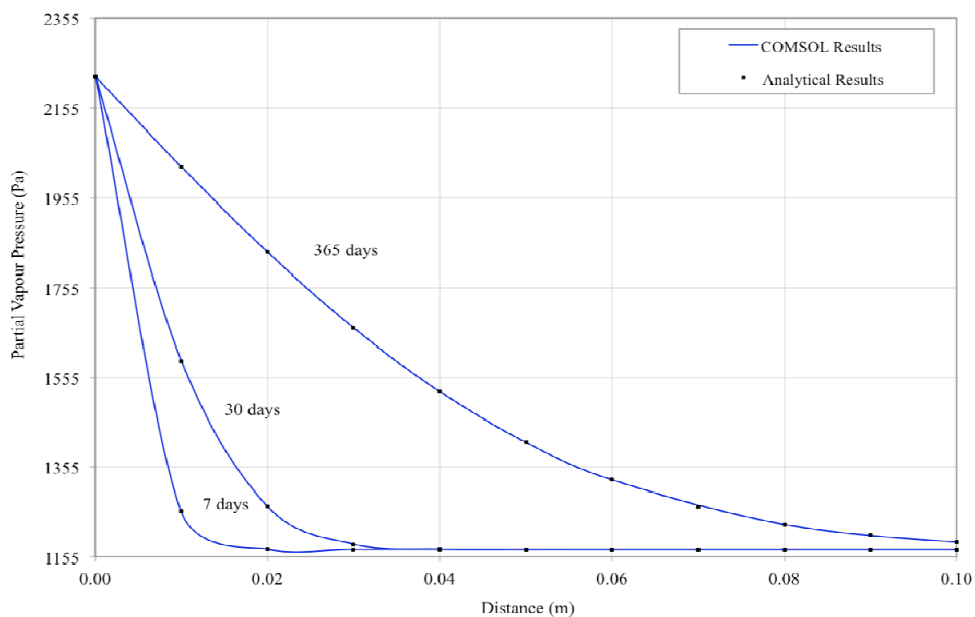


Figure 3.7 Graphical comparison of the numerical simulation results from the one-dimensional transient moisture transfer model (partial vapour pressure as potential) with the analytical results.

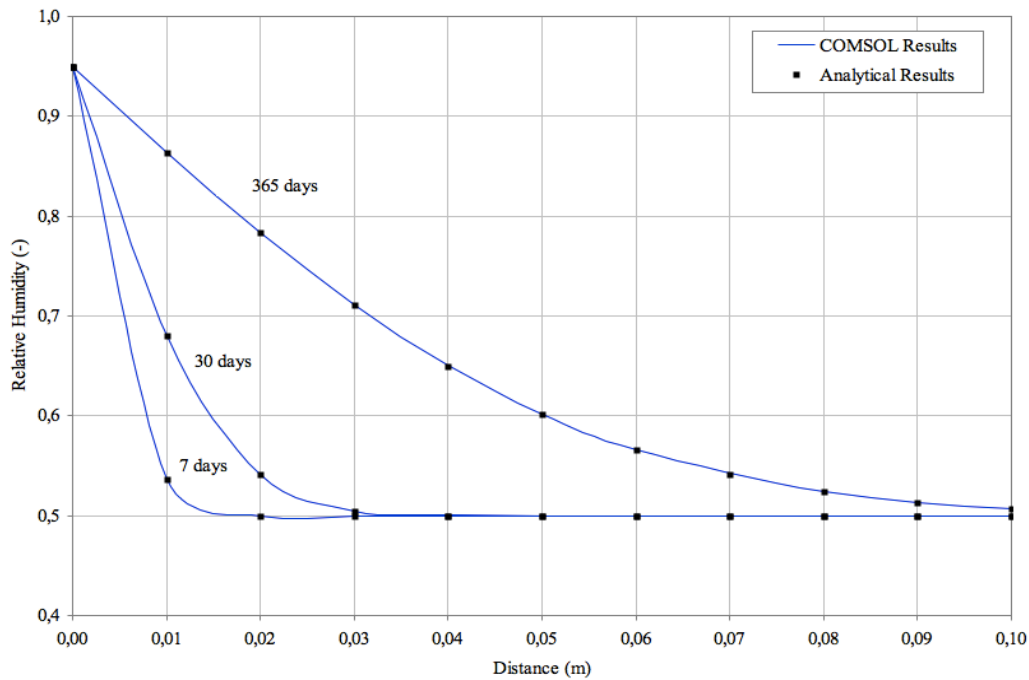


Figure 3.8 Graphical comparison of the numerical simulation results from the one-dimensional transient moisture transfer model (relative humidity as potential) with the analytical results.

The moisture profiles numerically simulated by the decoupled COMSOL model for both partial vapour pressure and relative humidity are consistent with those obtained from the analytical solution, as shown in Figure 3.7 and Figure 3.8.

3.4 Coupled HM model verification

The verification of the one-dimensional coupled HM model was executed by means of the normative benchmark test of European Provisional Standard prEN 15026. The HM model includes the general and material data specified by the benchmark test described in Section 3.1.

3.4.1 Coupled transfer results

In order for the coupled HM model to meet the prEN 15026 benchmark test, as previously mentioned in Section 3.1, both the numerically simulated heat and moisture profiles must fall within $\pm 2.5\%$ of the analytical solution. The heat and moisture profiles obtained from the COMSOL model were plotted for 7, 30, and 365 days against the required permissible error ranges, as depicted in Figure 3.9 and Figure 3.10.

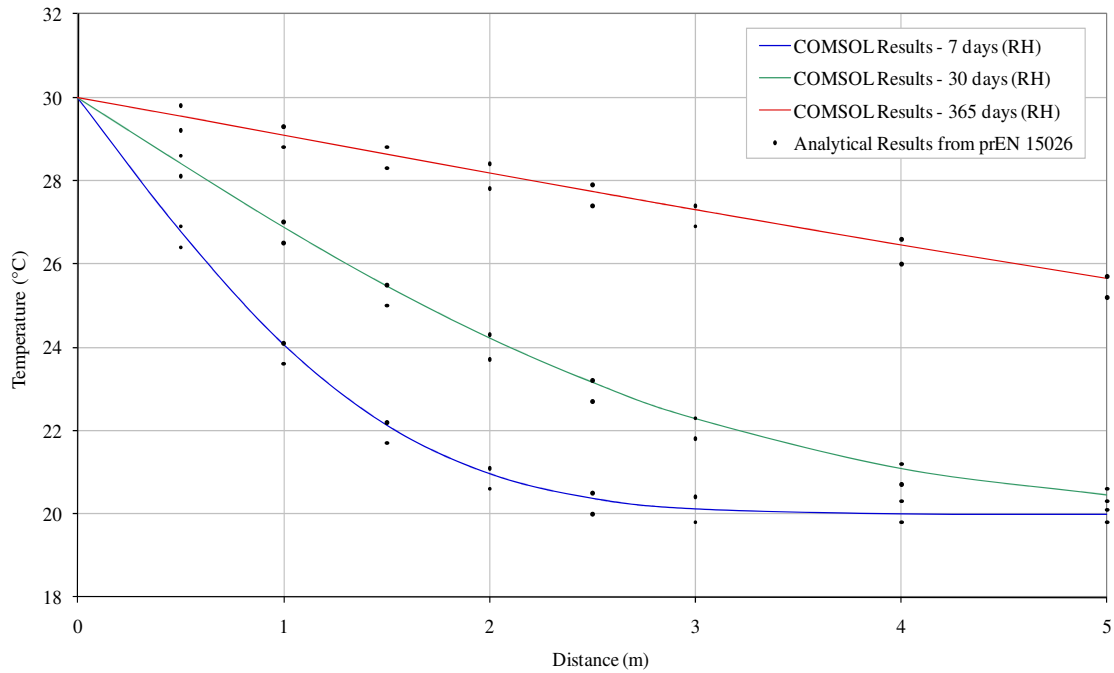


Figure 3.9 The numerically simulated water content distribution profile meeting the limits of validity stated by prEN15026 at 7 days, 30 days and 365 days.

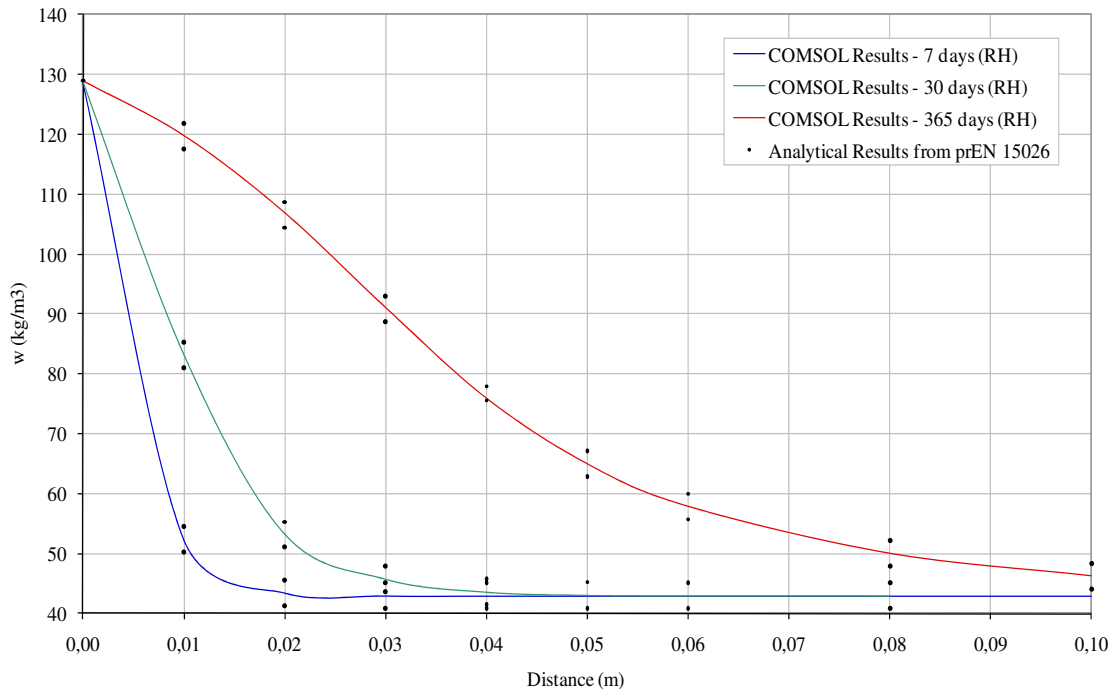


Figure 3.10 The numerically simulated water content distribution profile meeting the limits of validity stated by prEN15026 at 7 days, 30 days and 365 days.

As can be noted from the above figures, Figure 3.9 and Figure 3.10, the coupled heat and moisture COMSOL model complies with the general requirements of the prEN 15026 benchmark test.

3.4.2 Model limitations

The HM model was originally developed using partial vapour pressure as the moisture potential. Through model verification however it was observed that this model setup posed limitations specifically under non-isothermal conditions with a simultaneous step change in hygric conditions.

The prescribed step change in relative humidity at the exterior boundary was observed to have a delayed response in the homogeneous domain, as shown in Figure 3.11.

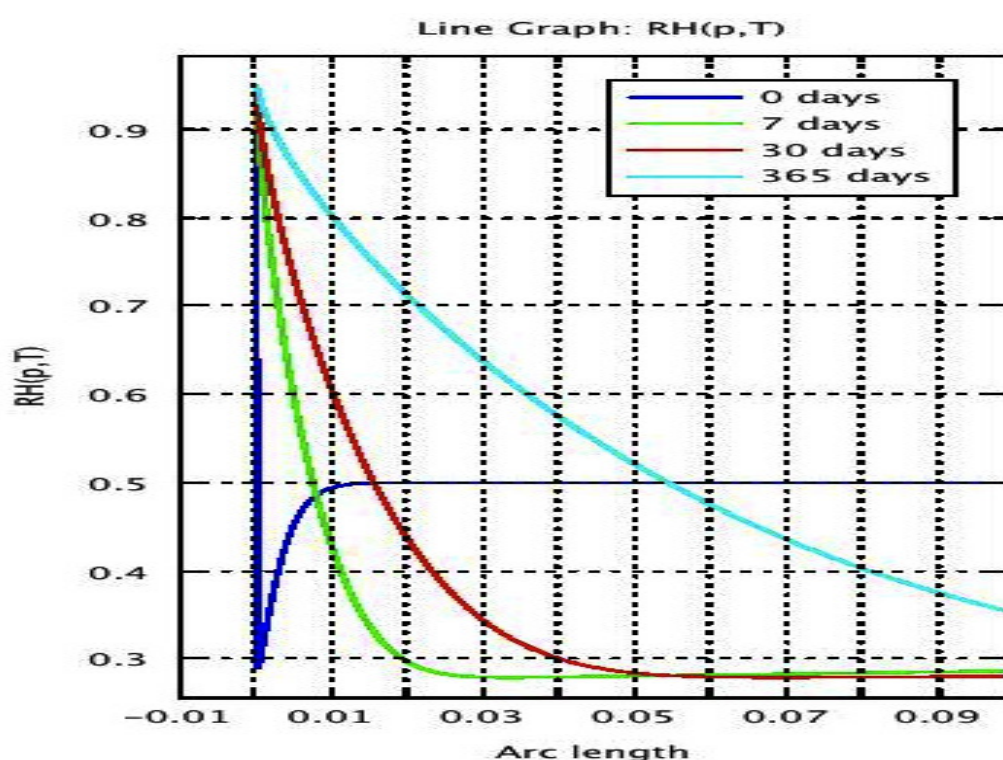


Figure 3.11 The delayed response in the numerical simulation results from the HM model using vapour partial pressure as moisture potential.

The model's behaviour to the boundary step change, shown in Figure 3.11, caused the calculated moisture profiles to deviate outside $\pm 2.5\%$ of the analytical solution. It is thought that the delayed response can be explained by the fact that the heat front propagates approximately 50 000 times faster than the moisture front in the homogeneous material specified by the prEN 15026 benchmark test.

Various measures were undertaken in order to attempt to improve the delayed response of the material to the boundary step change. For example, fine discretization of the mesh at the boundary was implemented, but this change did not appear to have a significant impact on the rate of reaction. The change that yielded the most significant improvement was the implementation of the relative humidity as an alternative to partial vapour pressure. A simplified psychrometric chart shown in

Figure 3.12 can be used to concisely illustrate how the model is thought to react to a step change for both moisture potentials.

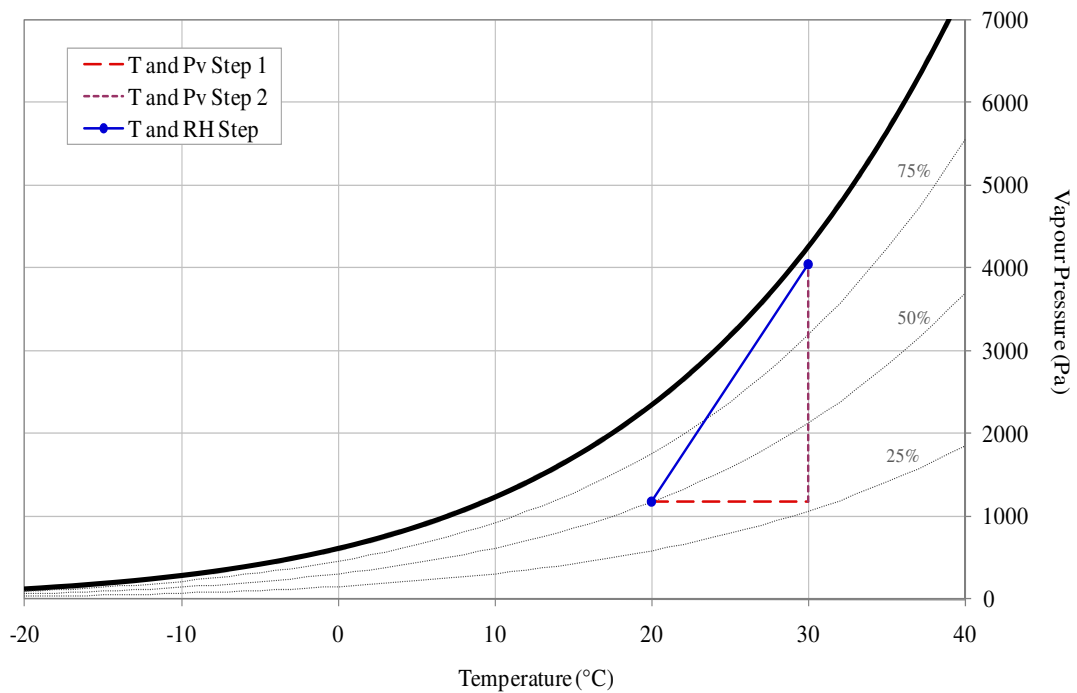


Figure 3.12 Simplified psychrometric chart with response to a step change in both partial vapour pressure and relative humidity.

As a result of this modification, a simultaneous convergence of the thermal and moisture step changes was observed. This potential is effective in this particular case because a prescribed step change in relative humidity is in fact a function of temperature, therefore being directly correlated to the non-isothermal conditions.

4 Heat and Moisture Induced Mechanical Stress-strain Modelling

It is of further interest to develop a model that can predict the possible damage-related processes in hygroscopic materials particularly those found in historical building environments due to climatic changes. It is known that variable boundary conditions influence the moisture content in hygroscopic materials, which in turn induces elastic or plastic thermal and moisture deformations (Schellen & van Schijndel, 2010). As such, this study primarily focuses on the development of a general model that can be adapted to simulate heat and moisture induced mechanical stresses and strains of various hygroscopic materials found in historical buildings subjected to variable indoor and outdoor climates. The results obtained from this model can be used to understand causes of previous damage, predict forthcoming damage, and also help develop preservation guidelines for artefact objects in historical buildings.

The Solid Mechanics physics interface provided in the Structural Mechanics Module was utilized to couple mechanical stress and strain to the verified COMSOL model developed in the Coefficient Form PDE Interface (c). This coupling allows the numerical simulation of the temperature and moisture profiles, as well as the resulting mechanical stresses and strains in a defined hygroscopic material.

4.1 Mechanical stress and strain

The HMSS model was developed as a linear elastic boundary value problem. This type of problem is based on equilibrium, compatibility and constitutive relationships of a three-dimensional volume element in a continuous body. The formulation presented in this section is generally based on Eschenauer et al (1997), else it is otherwise stated.

The mechanical equilibrium is based on three tensor partial differential equations that can be summarized by the equation of motion such that conditions of static equilibrium are considered:

$$\nabla\sigma + F = 0 \quad (4.1)$$

Equilibrium conditions are derived from the undeformed configuration of an elemental volume as per Figure 4.1.

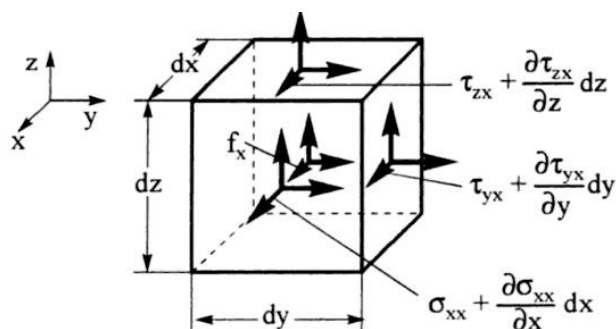


Figure 4.1 Equilibrium for an infinitesimal volume element in Cartesian coordinates (Eschenauer et al., 1997).

The three tensor partial differential equations can thus be described by:

$$\begin{aligned} \frac{\partial \sigma_{xx}}{\partial x} + \frac{\partial \tau_{xy}}{\partial y} + \frac{\partial \tau_{xz}}{\partial z} + f_x &= 0 \\ \frac{\partial \tau_{xy}}{\partial x} + \frac{\partial \sigma_{yy}}{\partial y} + \frac{\partial \tau_{yz}}{\partial z} + f_y &= 0 \\ \frac{\partial \tau_{xz}}{\partial x} + \frac{\partial \tau_{yz}}{\partial y} + \frac{\partial \sigma_{zz}}{\partial z} + f_z &= 0 \end{aligned} \quad (4.2)$$

For a two-dimensional case, the partial differential equations simplify to:

$$\begin{aligned} \frac{\partial \sigma_{xx}}{\partial x} + \frac{\partial \tau_{xy}}{\partial y} + f_x &= 0 \\ \frac{\partial \tau_{xy}}{\partial x} + \frac{\partial \sigma_{yy}}{\partial y} + f_y &= 0 \end{aligned} \quad (4.3)$$

Compatibility is expressed by six equations describing the small strain-displacement of a continuous body. The total strain tensor is written in the compact form as:

$$\epsilon = \frac{1}{2} [\nabla u + \nabla u^T] \quad (4.4)$$

The six equations of displacements can be derived from the following figure, Figure 4.2 , which depicts the deformed elemental surface:

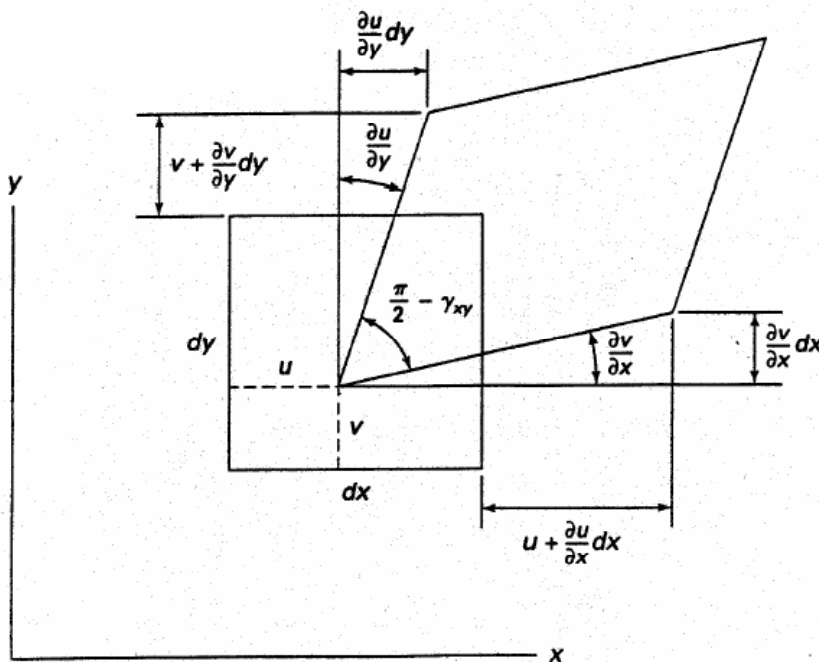


Figure 4.2 Deformed elemental surface (Chandrupatla & Belegundu, 1997)

As such, the displacements are defined as per the following relationships:

$$\begin{aligned}\varepsilon &= \nabla \mathbf{u}^T = [\varepsilon_{xx} \ \varepsilon_{yy} \ \varepsilon_{zz} \ \gamma_{xy} \ \gamma_{xz} \ \gamma_{yz}]^T \\ \varepsilon &= \left[\frac{\partial u}{\partial x}, \frac{\partial v}{\partial y}, \frac{\partial w}{\partial z}, \frac{\partial u}{\partial y} + \frac{\partial v}{\partial x}, \frac{\partial u}{\partial z} + \frac{\partial w}{\partial x}, \frac{\partial v}{\partial z} + \frac{\partial w}{\partial y} \right]^T\end{aligned}\quad (4.5)$$

The constitutive relationships are based on the linear proportionality between stress and strain tensors as described by Hooke's law:

$$\sigma = \mathbf{C} : \varepsilon \quad (4.6)$$

The Voigt notation can be used to express the above relationship in matrix form, shown for a two-dimensional isotropic problem:

$$\begin{bmatrix} \sigma_{xx} \\ \sigma_{yy} \\ \tau_{xy} \end{bmatrix} = \begin{bmatrix} C_{11} & C_{12} & C_{13} \\ C_{21} & C_{22} & C_{23} \\ C_{31} & C_{32} & C_{33} \end{bmatrix} \begin{bmatrix} \varepsilon_{xx} \\ \varepsilon_{yy} \\ \gamma_{xy} \end{bmatrix} \quad (4.7)$$

Two general conditions can be considered for a two-dimensional isotropic case, namely plane stress and plane strain. These stress and strain states are defined by the following conditions, respectively:

$$\sigma_{zz} = \tau_{xz} = \tau_{yz} = 0 \quad (4.8)$$

$$\varepsilon_{zz} = \tau_{xz} = \tau_{yz} = 0 \quad (4.9)$$

The *C-matrix* included in Equation (4.7) can be further expressed by means of two independent material coefficients, namely Young's modulus, E , and Poisson's ratio, ν (Ottosen, & Petersson, 1992). The *C-matrix* can be expressed by the following matrices for plane stress and strain states, in that order:

$$\mathbf{C} = \frac{E}{1-\nu^2} \begin{bmatrix} 1 & \nu & 0 \\ \nu & 1 & 0 \\ 0 & 0 & \frac{1-\nu}{2} \end{bmatrix} \quad (4.10)$$

$$\mathbf{C} = \frac{E}{(1+\nu)(1-2\nu)} \begin{bmatrix} 1-\nu & \nu & 0 \\ \nu & 1-\nu & 0 \\ 0 & 0 & \frac{1-2\nu}{2} \end{bmatrix} \quad (4.11)$$

The Hooke-Duhamel's law for thermo-elastic materials can be used to relate the stress and strain tensors, along with temperature and moisture. In this study, the displacement formulation is used, as it is of interest to solve for unknown displacements as per the following:

$$\sigma = \sigma_o + C : (\epsilon - \epsilon_o - \alpha_t \Delta\theta - \kappa \Delta w)$$

$$\text{where, } \alpha_t \Delta\theta \begin{bmatrix} 1 \\ 1 \\ 0 \end{bmatrix} \text{ and } \kappa \Delta w \begin{bmatrix} 1 \\ 1 \\ 0 \end{bmatrix} \quad (4.12)$$

Moreover, the boundary value problem using the displacement formulation requires prescribed displacements as boundary conditions. The boundary conditions can be defined as traction vectors (natural) or displacements (essential), shown respectively (Ottosen, & Petersson, 1992):

$$\begin{aligned} t = S_n = h & \quad \text{on } S_h \\ u = g & \quad \text{on } S_g \end{aligned} \quad (4.13)$$

Since the displacement formulation is used as the basis of this model, it is simply necessary to prescribe displacements as boundary conditions. Accordingly, a prescribed displacement, u , is defined as a vector, g , acting on a part of the boundary S_g . It should be noted that the prescribed displacements in the HMSS model vary depending on the geometry and orientation of the domain taken in consideration.

4.2 COMSOL modelling

The heat and moisture induced stress model is developed by coupling the Solid Mechanics physics interface provided in the Structural Mechanics Module to the Coefficient Form PDE Interface (c) that was tailored and verified to solve the coupled heat and moisture transfer. The coupling of the two models can be visualized by means of a flow chart in Figure 4.3.

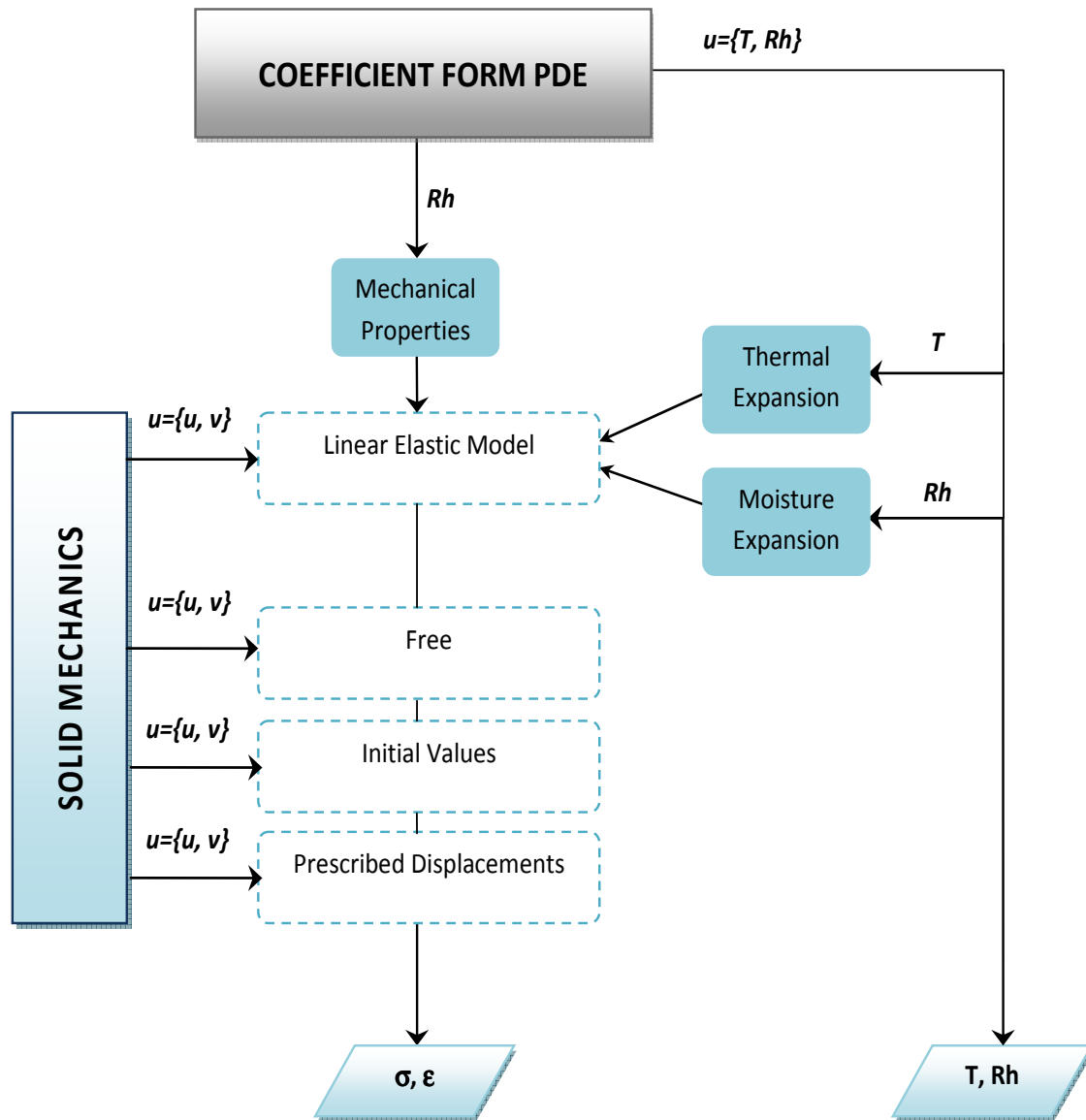


Figure 4.3 Flow chart showing the coupling of the HM and HMSS models.

The Solid Mechanics physics tool is developed in accordance with the mathematical formulation for mechanical stress and strain stated in Section 4.1. An additional concept that is introduced in the numerical modelling is the concept of time-dependency. For time-dependent studies, COMSOL Multiphysics uses the equation of motion that includes Rayleigh damping:

$$m \frac{\partial^2 \mathbf{u}}{\partial t^2} + \xi \frac{\partial \mathbf{u}}{\partial t} + k \mathbf{u} = \mathbf{f}(t) \quad (4.14)$$

Since damping is neglected in this study, the damping parameter, ξ , is set to zero. The equation of motion is altered such that the mass term, m , becomes the mass density, ρ , and the stiffness term, k , is replaced by the displacement formulation expressed in Equation (4.12):

$$\rho \frac{\partial^2 \mathbf{u}}{\partial t^2} - \nabla \sigma = \mathbf{F} \quad (4.15)$$

The above solid mechanics PDE is defined in COMSOL with a displacement field, u ,

containing three field components, namely u , v , w . In this study, it is of interest to numerically simulate heat and moisture induced mechanical stresses and strains in two-dimensions, therefore, prescribed parameters are only necessary for the u and v field components.

The Solid Mechanics physics tool is specified as a linear elastic material model, which provides the option to input isotropic, orthotropic, or anisotropic material properties. This feature allows the HMSS model to be altered to incorporate various types of hygroscopic materials. The model inputs include the parameters defining the *C-matrix* according to the assigned material for a given domain. For example, an orthotropic solid model prompts for a C-matrix that is a function of Young's modulus, Poisson's ratio and Shear modulus. The interaction between the HM and HMSS models can be accomplished in this portion of the model by incorporating moisture dependent mechanical properties, as referred to in the above flow chart.

Furthermore, the linear elastic material model in COMSOL provides the option to incorporate thermal expansion, initial stress and strain, as well as damping to the displacement formulation. Including the thermal and moisture strain deformations in the strain tensor are of particular interest in this study as this allows for the coupling of the HM and HMSS models. The two types of deformations are defined in the same form and should be implemented into the model in a similar manner.

In the Solid Mechanics physics tool, the thermal expansion feature is limited to one use and is overridden otherwise. By revisiting Equation (4.12) it is observed that the initial strain is introduced into the strain tensor similarly to the thermal and moisture expansion. As such, it is valid to introduce the thermal or moisture expansion into the strain tensor by means of the initial stress and strain feature in COMSOL.

As observed in Figure 4.3, the Solid Mechanics tool also includes features denoted as Free, Initial Values, and Prescribed Displacements. These conditions are prescribed in order to formulate the boundary value problem. Concerning the prescribed displacements in the HMSS model, they are defined in the x - and y -directions and are generally assigned as zero to simulate a fixed connection.

For a more visual explanation of the development of the HMSS model, an example of the Matlab code generated in COMSOL along with screenshots are presented in Section 11.3.3.

5 HMSS Model Verification

The HMSS model developed in COMSOL was verified by experimental and numerical simulated results presented in a study by Rachwal et al. (2010). This study evaluates the response of lime wood supports in historical panel paintings subjected to changing climate conditions in regards to moisture. A two-dimensional HMSS model was configured in COMSOL to incorporate the test parameters stated in the study. The numerical simulation results from the HMSS model were observed to generally meet the experimental and numerical results. This model is thus validated as an adequate predictive tool based on the fact that it simulates the expected response behaviour of lime wood.

5.1 Verification test description

A study by Rachwal et al. (2010) which evaluates the response of lime wood supports in historical panel paintings subjected to changing climate conditions related to moisture is used to support the validity of the two-dimensional transient HMSS model. Examples of the use of historical panel paintings are depicted in Figure 5.1 shown below.



Figure 5.1 Use of wood panels in historical paintings (The Getty Conservation Institute, 1995)

One of the various tests executed in this study is the tangential dimensional response of a lime wood specimen to two cycles of 100 hours with relative humidity step variations between 47 and 35% under a constant temperature of 24°C. Both experimental and numerical results of the dimensional response of a lime wood specimen under the test scenario are provided in the study. The numerical results were simulated by a model developed using a finite element method software package.

5.1.1 Material properties

The material properties of lime wood (*Tilia sp.*) were determined experimentally and utilized in the numerical simulations. Further details regarding the methodology used for the measurements of wood properties can be found in Rachwal et al. (2010). A thin layer of gesso is included in this study to model a realistic picture panel having a preparatory gesso layer. In this verification however, the interaction and mismatch between the mechanical behaviour of the two layers is beyond the scope of this project.

Lime wood being treated as an orthotropic material (Rachwal et al., 2010) requires directional material properties in order to adequately model the mechanical behaviour of the material. As such, this study includes the radial and tangential directional mechanical properties for this material. Gesso is defined as an isotropic material and possesses mechanical properties valid for all directions. A summary of the material properties used in the HMSS model are summarized below in Table 5.1.

Table 5.1 Summary of material data used in HMSS model verification

| Variable Name | | Expression | Units | Description |
|---------------------|--------------|-----------------|-------------------|--|
| General | COMSOL | | | |
| <i>Lime wood</i> | | | | |
| M | w_mat | Figure 5.1 | % | Moisture content |
| D_M | Dw_mat | Equation (5.1) | m ² /s | Moisture diffusion coefficient |
| E_{Radial} | Modrad_mat | Figure 5.3 | MPa | Modulus of Elasticity radial direction |
| E_{Tang} | Modtan_mat | Figure 5.3 | MPa | Modulus of Elasticity tangential direction |
| G | Modshear_mat | Equation (5.4) | MPa | Shear modulus |
| ν | nuvector | {0.346,0.630,0} | - | Poisson's ratio |
| κ | alpha | {0.13,0.28,0} | 1/%-m | Dimensional change coefficient - moisture |
| <i>Gesso</i> | | | | |
| E | Mod_mat | Equation (5.5) | MPa | Modulus of Elasticity |
| ν | nuvector | {0.25} | - | Poisson's ratio |
| κ | alpha | {6.8e-5} | 1/%-m | Dimensional change coefficient - moisture |

The water vapour sorption isotherms for lime wood are plotted in Figure 5.2. The re-adsorption curve was utilized as the moisture content in the HMSS model verification.

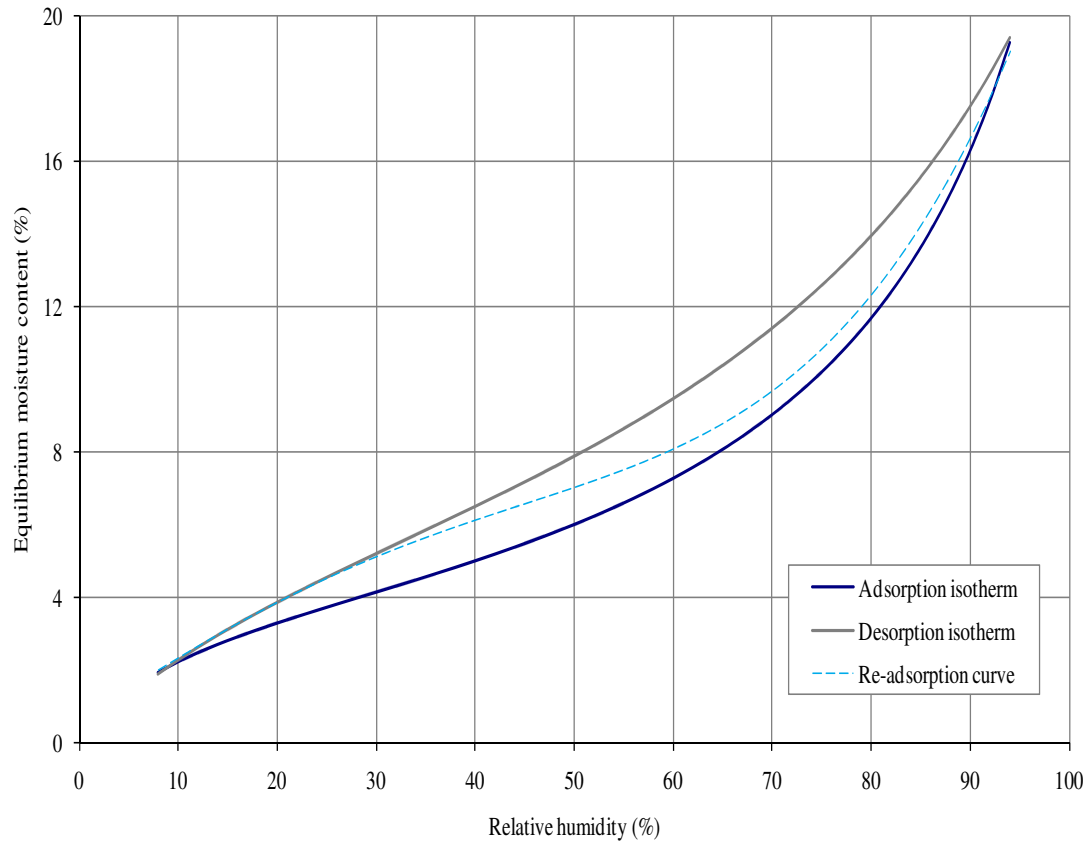


Figure 5.2 Adsorption and desorption isotherms of lime wood, along with the re-adsorption curve at 24 °C (Rachwal et al., 2010).

The moisture diffusion coefficient for lime wood is expressed as a function of the moisture content:

$$D_M = 1.1 \times 10^{-10} - 9.5 \times 10^{-11} \times M + 2.63 \times 10^{-11} \times M^2 - 1.31 \times 10^{-12} \times M^3 \quad (5.1)$$

It is important to note that the moisture diffusion coefficient is expressed by the following relationship:

$$D_M = \frac{\delta_p \cdot p_{sat}}{\xi} \quad (5.2)$$

The inclusion of this coefficient simplifies the moisture balance PDE stated in Equation (2.14). While neglecting the liquid transport, the equation becomes:

$$\frac{\partial w}{\partial t} = \frac{\partial \varphi}{\partial t} = -\nabla(-D_M \nabla \varphi) \pm M \quad (5.3)$$

Moreover, the tensile properties of lime wood are functions of moisture content. The moduli of elasticity along the radial and tangential directions are expressed by the following functions:

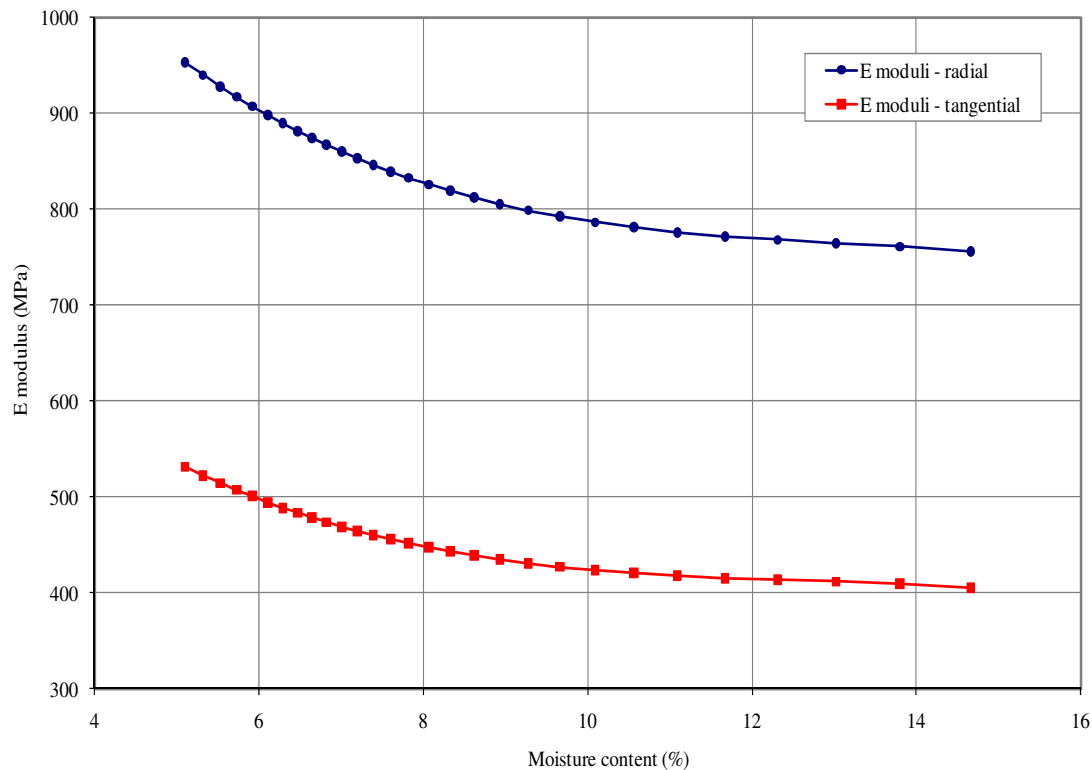


Figure 5.3 Moduli of elasticity of lime wood in the radial and tangential directions as a function of moisture content (Rachwal et al., 2010).

The shear modulus, G , is used to express the relationship between shear stresses and shear strains. The shear modulus of lime wood is expressed as a function of moisture content according to the following:

$$G = 2.39 \times 10^2 - 2.67 \times 10^1 \times M + 2.01 \times M^2 - 5.18 \times 10^{-2} \times M^3 \quad (5.4)$$

The modulus of elasticity for gesso is a function of relative humidity and is described by:

$$E = 4.09 \times 10^3 + 5.86 \times 10^1 \times \varphi - 1.31 \times \varphi^2 \quad (5.5)$$

5.2 HMSS Model setup

The two-dimensional transient HMSS model was setup in COMSOL in order to meet the numerical and experimental test conditions and results established by Rachwal et al., 2010. The global parameters used in the HM model are summarized below in Table 5.2. The units are declared in square brackets and converted according to SI derived units in COMSOL.

Table 5.2 Global parameters used in HMSS model for verification

| Name | | Expression | Description |
|-------------|--------|-------------------------------|--|
| General | COMSOL | | |
| T_0 | To | 24 [degC] | Initial temperature |
| T_e | Te | 24 [degC] | Exterior temperature |
| φ_0 | Rho | 42 [%] | Initial relative humidity |
| α_e | he | 7.7 [W/(m ² *K)] | Exterior heat transfer coefficient |
| β_e | beta_e | 8E-6 [kg/(m ² *s)] | Exterior moisture transfer coefficient |

The panel painting consists of a 10 mm thick lime wood panel with a 1 mm gesso finish in accordance with typical dimensions and material properties stated in the study. Figure 5.4 depicts the geometry for the two-dimensional HMSS model.

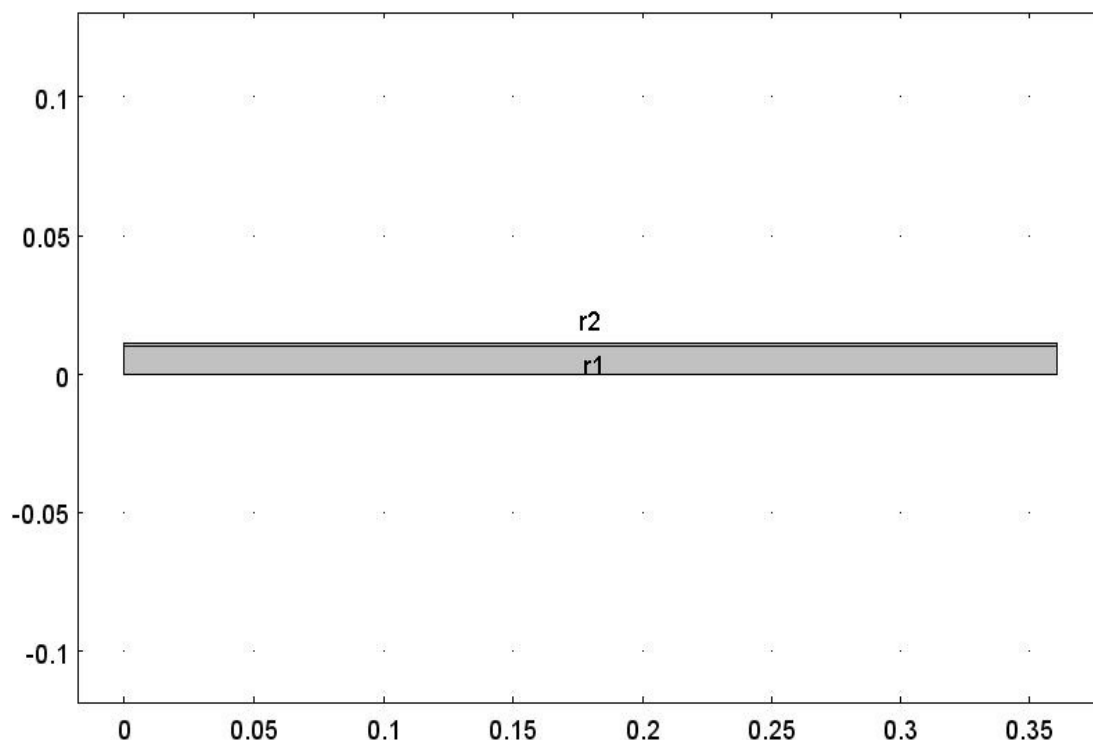


Figure 5.4 Overview of the geometry of the panel painting used in the two-dimensional HMSS model verification.

The hygrothermal and mechanical material properties presented in Section 5.1.1 are generally incorporated into the HMSS model by means of analytical functions or

constants. Accordingly, the material properties are calculated using the relative humidity solved by the coupled heat and moisture physics of the model.

In the HMSS model, both domains, including the lime wood and gesso, are initially under a constant temperature of 24°C and relative humidity of 42%. The domains undergo two cycles, each spanning 100 hours, of relative humidity step variations between 47 and 35%.

The numerical simulation period covered 11 days and incorporated time steps of 3600 seconds. The time study is set for a longer duration than that specified by the two cycles of 100 hours due to the fact that the picture panels were found to respond more significantly to increased fluctuation periods (Rachwal et al., 2010). In addition, a mesh with an extra fine element size was implemented in the model.

5.2.1 Numerical simulation results

The numerical simulation results from the HMSS model were compared to both experimental and numerical results from the study, as shown in Figure 5.5. It should be noted that the critical strain of lime wood was determined to be 0.002 (Rachwal et al., 2010).

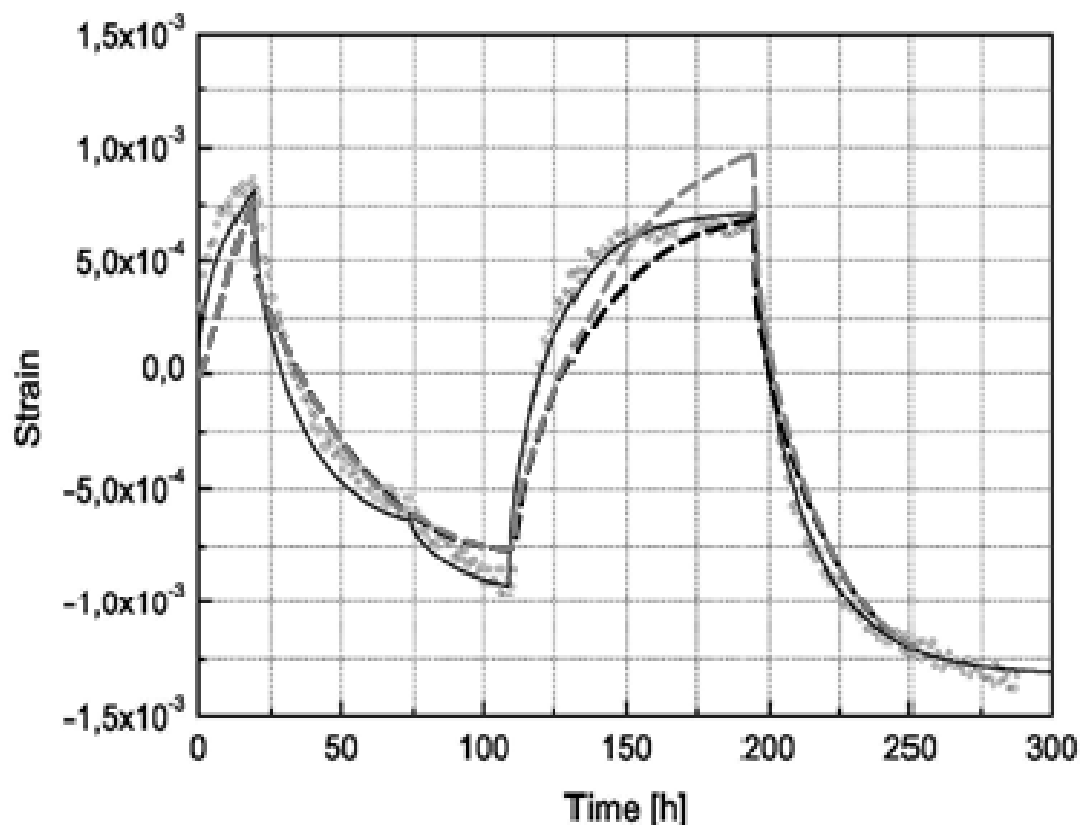


Figure 5.5 Dimensional response in the tangential direction of a lime wood specimen to two variations of relative humidity between 47 and 35%: experimental data – circles, study numerical results – solid line, HMSS numerical results – dashed lines (Rachwal et al, 2010)

The numerical simulation results from the HMSS model follow a similar trend to that presented by the experimental and numerical results. The deviation observed in the results is due to a lack of information regarding the relative humidity step variations. The sensitivity of the dimensional response to minimal dissimilarities in the prescribed relative humidity step variation is made evident by the two numerical simulation results from the HMSS model particularly between 125 and 200 hours. As such, additional refinement of the boundary conditions would be necessary to increase the precision of the HMSS numerical simulation results. Nevertheless, the HMSS model simulates the expected response behaviour of lime wood and is thus considered an adequate predictive tool.

The numerical simulation results for stress are not presented in this study particularly because these results are not discussed in the numerical and experimental verification case study. However, given that the stress and strain are linearly proportional according to that described in Section 4.1, there is simply a need to verify one of the solutions.

5.2.2 Model limitations

The HMSS model is an adequate predictive tool to determine possible damage-related processes in building assemblies and artefacts. The verification of the HMSS model is however based on the mechanical behaviour of lime wood, which in turn signifies that additional verification using other desired materials may need to be executed.

6 Case Studies

Various case studies were considered in this study to demonstrate the value and applicability of both the verified two-dimensional HM and HMSS models to historical buildings. The case studies include exterior climatic conditions predicted for the Netherlands, as well as recorded interior climate data from a heritage site located in Belgium. The studies also reflect typical heritage building assemblies and the interaction of artefacts within the building environment.

6.1 Model parameters

6.1.1 Climate conditions

The outdoor climate data used in the case studies were obtained from the REMO climate model provided by the Max Planck Institute in Hamburg, Germany. This climate data spans over a period from 1950 to 2099, which is stated to be necessary to adequately predict the effects of climate change on heritage sites and their associated artefacts. The climate data utilized represent average data for several areas near De Bilt, Netherlands (Kramer, 2011). The selected climate data that were utilized in the case studies are summarized in Table 6.1. These data were sorted per year, tabulated and inputted in COMSOL as interpolation functions.

Table 6.1 The variables utilized in COMSOL derived from the REMO model.

| Description | Unit | COMSOL variable |
|-------------------|------------------|-----------------|
| Temperature | °C | Te_year |
| Relative humidity | % | Rhe_year |
| Wind speed | m/s | – |
| Precipitation | mm/h | Rain_year |
| Global radiation | W/m ² | Igrad_year |

Several limitations were observed in this study particularly in regards to the model development in COMSOL Multiphysics. Firstly, the inclusion of climate data was incorporated into COMSOL by means of a global interpolation functions. An interpolation function however has a table cell capacity. The insertion of larger data sets would need to be implemented by means of a Matlab function node which links an actual Matlab function to a defined Matlab function in COMSOL. The integration of Matlab into COMSOL via LiveLink was beyond the scope of this study, thereby limiting the numerical simulation time period to one year corresponding to datasets defined by interpolation functions. In addition, a shorter time period was found to be feasible due to the fact that the coupled multiphysics modelling consumes a great deal of simulation time.

More specifically, climate data spanning over a timeseries of one year corresponding to January 2010 to January 2011 is utilized in the presented case studies. The

prescribed outdoor temperature, relative humidity, as well as wind speed are plotted in Figure 6.1 to Figure 6.3.

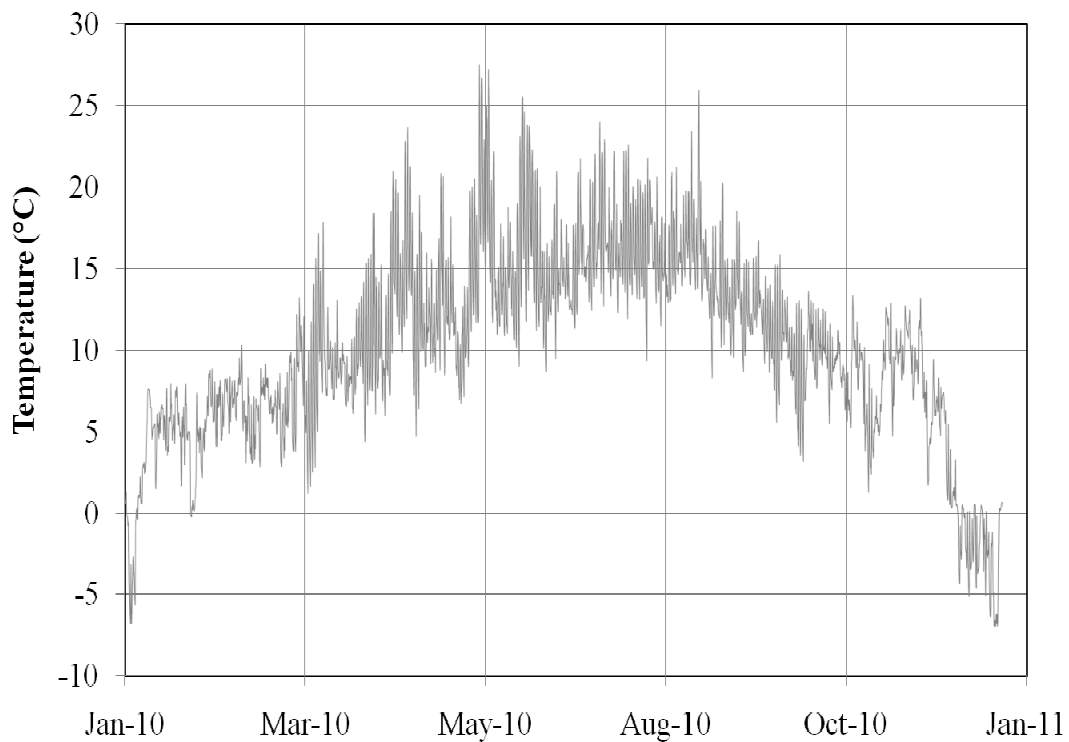


Figure 6.1 External temperature from the REMO climate model for January 2010 to January 2011.

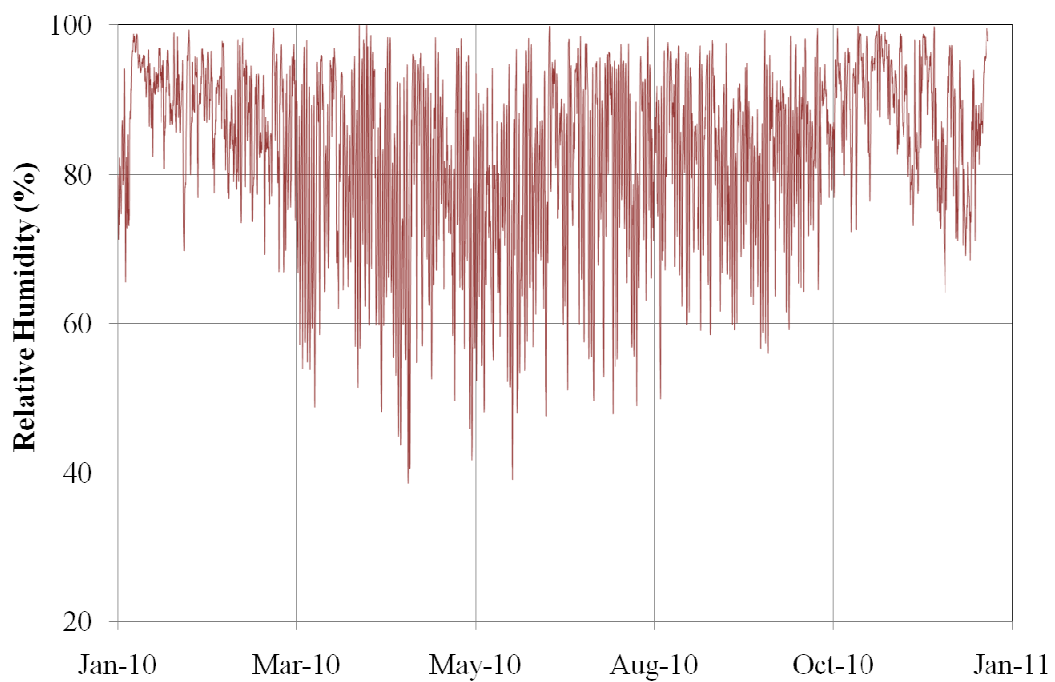


Figure 6.2 Outdoor relative humidity from the REMO climate model for January 2010 to January 2011.

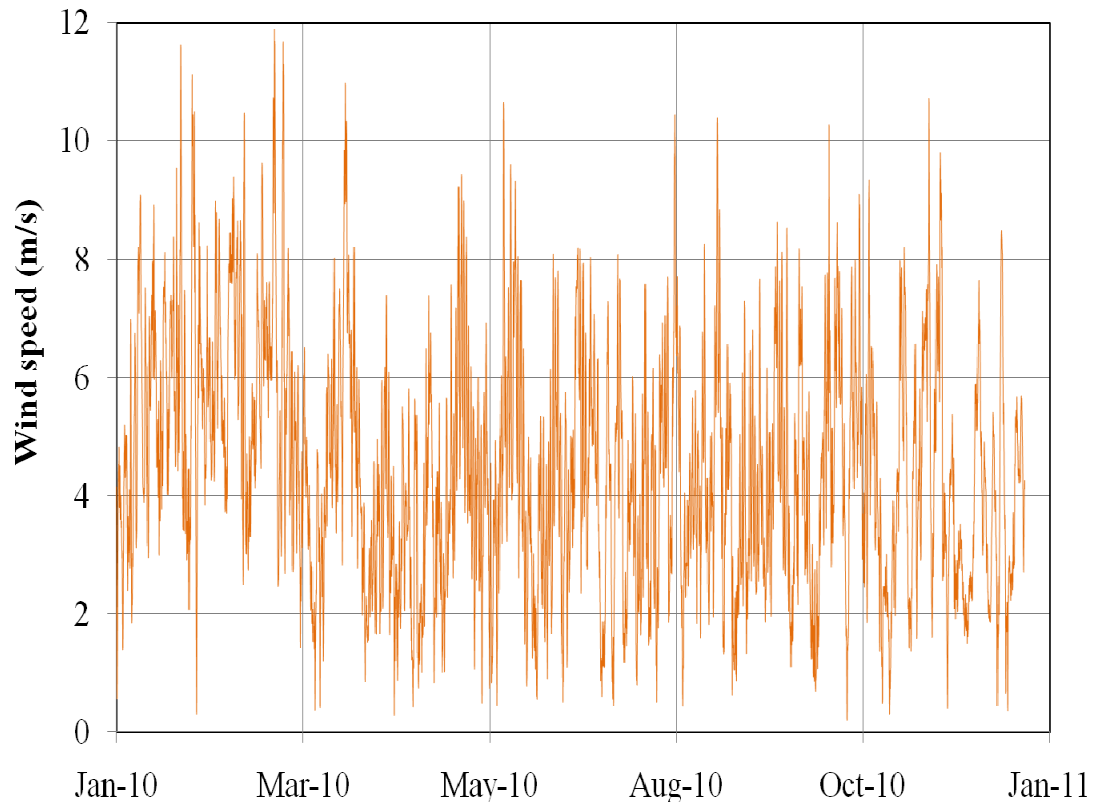


Figure 6.3 Outdoor wind speed from the REMO climate model for January 2010 to January 2011.

Furthermore, the precipitation and global radiation data are considered in the sensitivity analyses that are described in Section 7. These data were included in order to observe the effects and limitations of additional heat and moisture sources in both the HM and HMSS models.

Concerning the indoor climate data, a combination of constant average values and annual climate data measured from a heritage site in Belgium. The measured data was retrieved from the Technical University of Eindhoven's online database entitled Physics of Monuments (Smulders & Martens, 2008). The indoor data that is primarily included in the numerical simulations are temperature and relative humidity. The prescribed indoor climate conditions are further discussed in each case study.

6.1.2 Boundary heat sources

The boundary heat sources considered in the case studies include convective heat flow as per the aforementioned Equation (2.15), as well as global radiation. The internal heat source, namely convective heat flow, was assumed to be constant in the case studies.

The convective heat flow between a surface and its surrounding air is affected by the temperature and pressure differences, and also by air movements. In this study, forced convection parallel to the surface, expressed by Equations (6.1) and (6.2), was assumed as the type of air flow to determine the most suitable external heat transfer coefficients (Hagentoft, 2001).

$$\alpha_c = 6 + 4 \cdot u_w \quad u_w \leq 5m/s \quad (6.1)$$

$$\alpha_c = 7.41 \cdot u_w^{0.78} \quad u_w \geq 5m/s \quad (6.2)$$

Solar radiation emitted in the form of short wave radiation is assumed to cause measurable heat gain at an exposed surface due to partial absorption. The amount of heat flow that takes place at a given surface is dependent on the absorptivity of the surface material, as well as its respective orientation and incident angle to the thermal radiation source. The net absorbed heat flow at a given surface was calculated using Equation (6.3):

$$q_{sol} = \alpha_{sol} \cdot I_{sol} \quad (6.3)$$

The solar radiation energy flux, I_{sol} , is the sum of direct and diffuse radiation components.

6.1.3 Boundary moisture sources

The boundary moisture sources considered in the case studies include convective moisture flow according to the previously stated Equation (2.19), as well as precipitation. It is to be noted that the convective moisture flow at the interior was assumed to be constant in this study.

The moisture transfer coefficient for the exterior was calculated by applying the Lewis formula described in the following (Hagentoft, 2001):

$$\beta_v = \frac{\alpha_c}{\rho_a c_{pa}} \quad (6.4)$$

Equation (6.4) is computed based on the convective heat transfer coefficient calculated by Equations (6.1) or (6.2).

Secondly, precipitation was included as a moisture source at the exterior boundary. This data was simply implemented in the sensitivity analysis in order to observe the limitations of the HM model to additional moisture sources. As such, the correction of the precipitation data according to the intensity and distribution at the external boundary surface is beyond the scope of this study.

6.1.4 Selected materials and assemblies

A case study of an exterior wall assembly commonly found in historical buildings is considered in order to observe the functionality of the models. Materials were selected based on typical historical building assemblies, motivated by those used in the Netherlands (Schellen et al., 2008) and Sweden (Björk et al, 2002). A non-insulated two-layer exterior wall assembly was considered: double-wythe historical brick with mortar joints (380 mm) and cement plaster (20 mm). The type of brick used has the dimensions of 250 mm x 120 mm x 65 mm (10''x 5''x 2 1/2'') with 10 mm thick mortar joints. The material properties used in the model were acquired

from the Fraunhofer-Institut Bauphysik (IBP) Holzkirchen material database and are summarized in Section 11.2.

To observe the usefulness of the HMSS model, the lime wood panel painting with gesso layer is used in the case studies. These materials are introduced into the model with the same dimensions, as well as material and mechanical properties stated in Section 5.1.1.

6.2 Two-dimensional HM modelling

This case study has the purpose of demonstrating the application of the two-dimensional HM model to historical building assemblies. The model incorporates a variable outdoor climate along with two different cases of indoor climate conditions.

6.2.1 Model setup

The two-dimensional exterior wall considered in the HM model case study is consistent with that described in Section 6.1.4 and is depicted below in Figure 6.4.

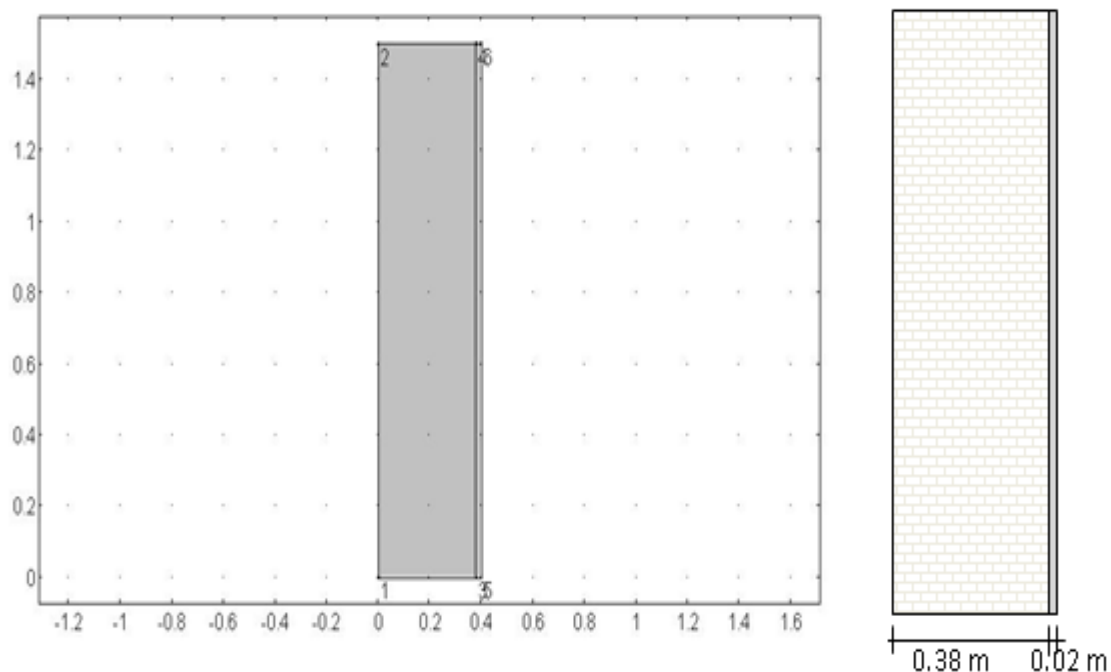


Figure 6.4 Two-dimensional external wall used in HM model case study.

This case study includes variable exterior boundary conditions from the REMO climate model. The interior boundary conditions, consisting of temperature and relative humidity, are defined as constant values or assumed annual mean variations. A comparison of the prescribed temperature and relative humidity for both exterior and interior boundary conditions are presented in Figure 6.5 and Figure 6.6.

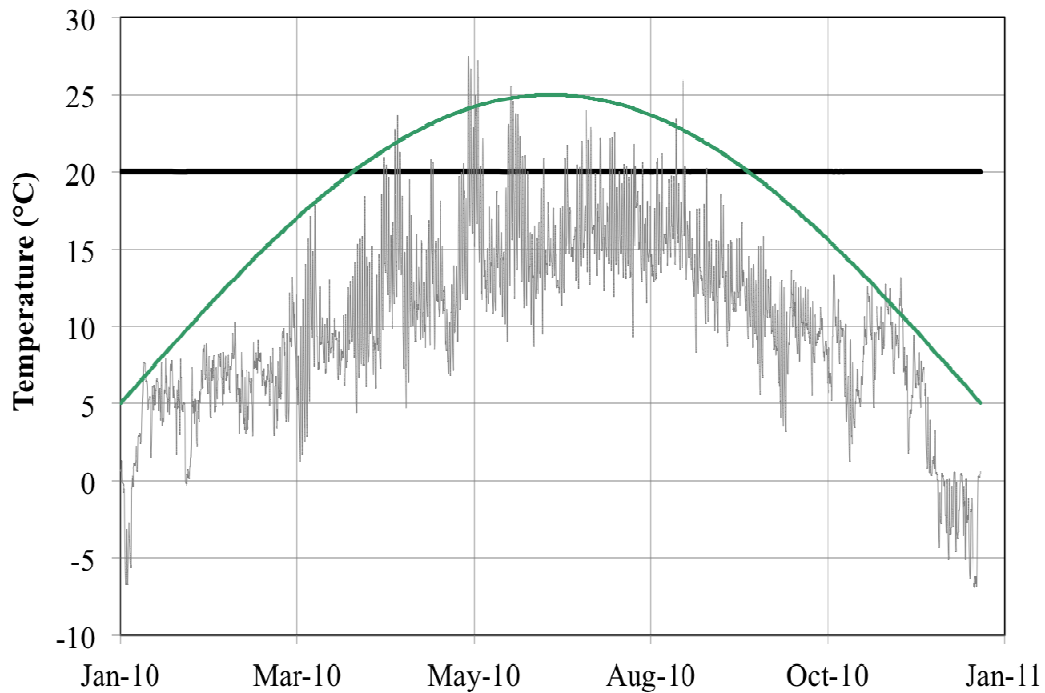


Figure 6.5 Prescribed temperature boundary conditions: outdoor-grey, indoor constant-black (Case A) and indoor variable-green (Case B)

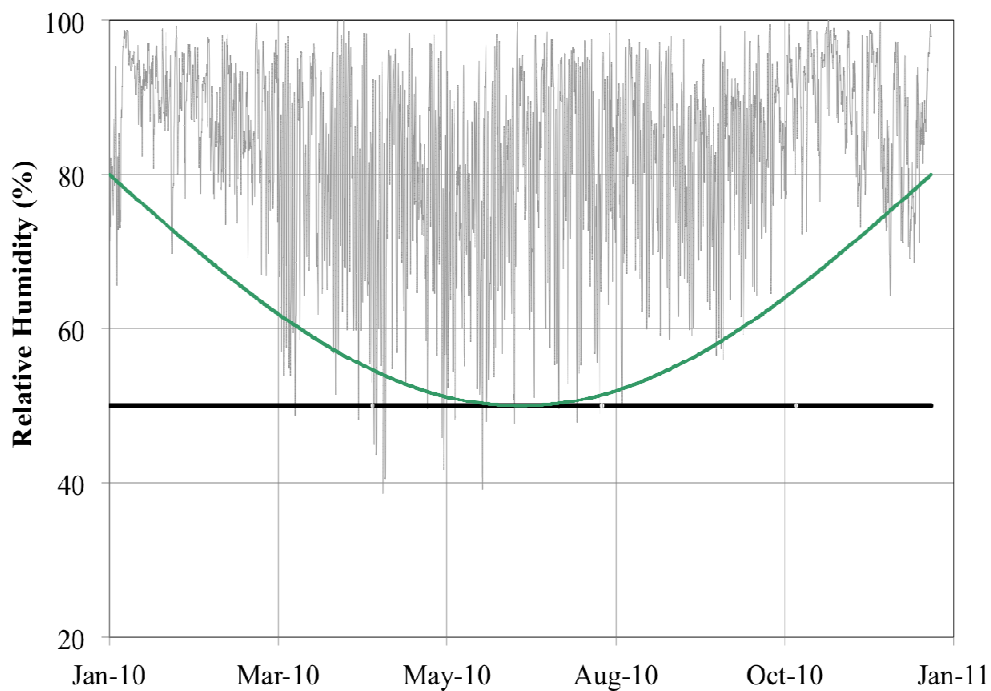


Figure 6.6 Prescribed relative humidity boundary conditions: outdoor-grey, indoor constant-black (Case A) and indoor variable-green (Case B)

As described in Figure 6.5 and Figure 6.6, two cases were considered for the interior boundary conditions, namely Case A and Case B. Case A considers constant interior temperature and relative humidity which are based on commonly used interior

conditions for numerical modelling of heat and moisture in building envelopes (van Schijndel & Schellen, 2009). Whereas Case B includes assumed annual mean variations for the interior temperature and relative humidity.

The global parameters defined in COMSOL for the two-dimensional HM model are summarized in Table 6.2. As observed in the following tables, Table 6.2 Table 6.1 to Table 6.4, the units are declared in square brackets and converted according to SI derived units in COMSOL.

Table 6.2 Global parameters defined in COMSOL for the two-dimensional HM model case study.

| Name | Expression | Description |
|--------|----------------------------------|--|
| To | 10 [degC] | Initial temperature |
| Ti | 20 [degC] | Interior temperature |
| Rho | 0.5 | Initial relative humidity |
| hi | 7.7[W/(m ² *K)] | Interior heat transfer coefficient |
| beta_i | 3.0E-08 [kg/(m ² *s)] | Interior moisture transfer coefficient |

The data for the exterior boundary conditions, as well as vapour saturation pressure are tabulated in the form of global interpolation functions in COMSOL. These functions are provided in Table 6.3.

Table 6.3 Global interpolation functions defined in COMSOL for the two-dimensional HM model case study

| Function name | Units | Description | Source |
|---------------|--|--|--|
| Psat(T) | Psat [Pa], T [degC] | Vapour saturation pressure | Calculation in Section 11.3.1 |
| Te_10(t) | Te_10 [K], t [s] | Exterior temperature | REMO |
| Rhe_10(t) | Rhe_10 [%], t [s] | Exterior relative humidity | REMO |
| he_10(t) | he_10 [W/(m ² *K)], t [s] | Exterior heat transfer coefficient | Calculated by Equations (6.1) or (6.2) |
| betae_10(t) | betae_10 [kg/(m ² *s)], t [s] | Exterior moisture transfer coefficient | Calculated by Equation (6.4) |

Various global analytic functions were defined to compute conditions occurring at the boundaries. The analytic functions listed in Table 6.4 include the convective heat and moisture fluxes, as well as the annual mean variations for interior temperature and relative humidity related to Case B.

Table 6.4 Global analytical functions defined in COMSOL for the two-dimensional HM model case study.

| Function name | Units | Expression | Description |
|------------------------|--------------------------|-----------------|------------------------------|
| <i>Cases A & B</i> | | | |
| qc_e(T,t) | [W/(m ²)] | Equation (6.5) | Exterior heat convection |
| g_e(Rh,t) | [kg/(m ² *s)] | Equation (6.8) | Exterior moisture convection |
| <i>Case A</i> | | | |
| qc_i(T) | [W/(m ²)] | Equation (6.6) | Interior heat convection |
| g_i(Rh) | [kg/(m ² *s)] | Equation (6.9) | Interior moisture convection |
| <i>Case B</i> | | | |
| qc_i(T,t) | [W/(m ²)] | Equation (6.7) | Interior heat convection |
| g_i(Rh,t) | [kg/(m ² *s)] | Equation (6.10) | Interior moisture convection |
| Ti(t) | [degC] | Equation (6.11) | Interior temperature |
| Rhi(t) | [%] | Equation (6.12) | Interior relative humidity |

The heat convection is formulated for the exterior and interior according to:

$$q_{c,e}(T, t) = h_{e,10}(t) \cdot (T_{e,10}(t) - T) \quad (6.5)$$

$$q_{c,i}(T) = h_i \cdot (T_i - T) \quad (6.6)$$

$$q_{c,i}(T, t) = h_i \cdot (T_i(t) - T) \quad (6.7)$$

The following expressions define the moisture convection for the exterior and interior:

$$g_e(Rh, t) = \beta_{e,10}(t) \cdot (Rh_{e,10}(t) - Rh) \quad (6.8)$$

$$g_i(\text{Rh}) = \text{beta}_i \cdot (\text{Rh}_o - \text{Rh}) \quad (6.9)$$

$$g_i(\text{Rh}, t) = \text{beta}_i \cdot (\text{Rh}_i(t) - \text{Rh}) \quad (6.10)$$

The annual mean variations for interior temperature and relative humidity related to Case B are described according to:

$$T_i(t) = 5 + 20 \cdot \sin(\pi \cdot t / 365 \cdot 24 \cdot 3600) \quad (6.11)$$

$$\text{Rh}_i(t) = 80 - 30 \cdot \sin(\pi \cdot t / 365 \cdot 24 \cdot 3600) \quad (6.12)$$

It is important to note that in COMSOL the units for interpolation functions need to be declared when implemented in the analytical functions.

6.2.2 Numerical simulation results

Two numerical simulations were computed for a time period of one year with time steps of 3600 seconds for the purpose of demonstrating the possible numerical results that can be yielded from the HM model. A mesh with an extra fine element size was implemented in the model.

The temperature and moisture distribution results obtained for both model scenarios, Cases A and B, are provided in Figure 6.7 and Figure 6.8. More specifically, the numerical simulation results occurring at the interior surface of the wall assembly (0.40m) are presented and compared for the two cases.

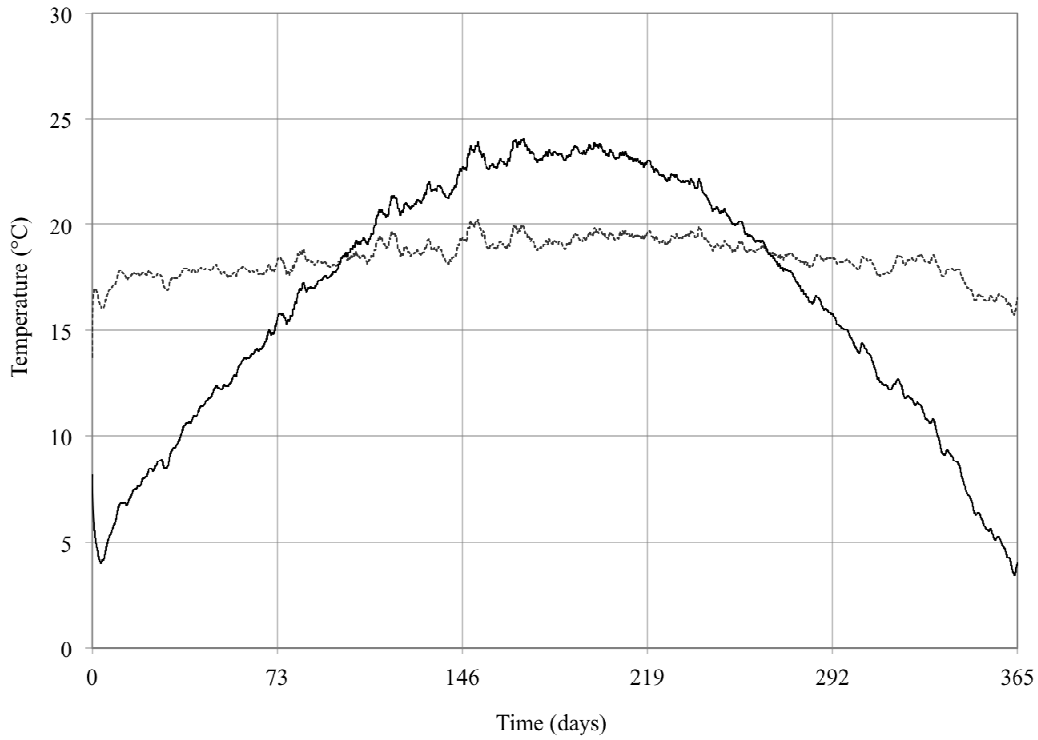


Figure 6.7 Numerical simulation results for the temperature distribution at the interior surface of the wall assembly ($x=0.4m$): Case A – grey dashed line, Case B– black solid line

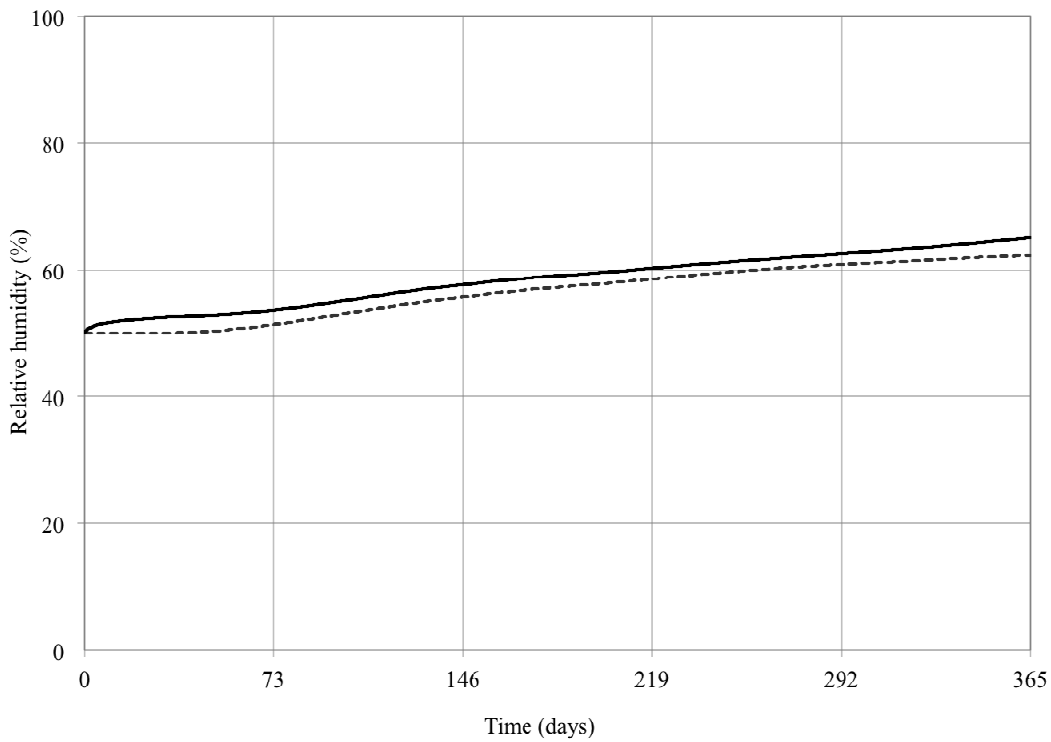


Figure 6.8 Numerical simulation results for the relative humidity distribution at the interior surface of the wall ($x=0.4m$): Case A – grey dashed line, Case B–black solid line

From Figure 6.7 and Figure 6.8, it is observed that the temperature and relative humidity at the interior surface of the wall are consistent with the prescribed boundary conditions.

6.3 Two-dimensional HMSS modelling

A case study is used in order to demonstrate the use of variable outdoor and indoor climate conditions in the two-dimensional HMSS model, as well as the applicability of the model to historical buildings and artefacts.

6.3.1 Background

The chosen case study involves the heritage site of the Castle of Gaasbeek located in Gaasbeek, Belgium as shown in Figure 6.9. This building was originally constructed in 1240 AD and has been reconstructed and modified various times since then (Kasteel van Gaasbeek, 2011).



Figure 6.9 Overview of the north east elevation of the Castle of Gaasbeek (Kasteel van Gaasbeek, 2011), (Kunsten en Erfgoed, 2006).

This Castle functions principally as a museum, but also contains offices and storage rooms. The interior of the Castle contains a multitude of art treasures, such as historic oil paintings and wooden furniture and statues, which can alone be considered as a cultural heritage site (Kramer, 2011).

In historical buildings of this type, microclimates existing near the interior surfaces of exterior walls were found to be one of the many sources causing damage to paintings (Mecklenburg, 2007). For example, as shown in Figure 6.10, the occurrence of condensation is probable behind a picture frame particularly during the winter when the internal relative humidity is excessively increased (Mecklenburg, 2007). Consequently, additional moisture can induce related mechanical stresses and strains which could lead to damage in the given exposed artefacts.



Figure 6.10 Condensed moisture running down the wall from behind one of several painting at the Renwick Gallery of the Smithsonian Institution in Washington, D.C. (Photograph courtesy of Ehrenkrantz, Eckstut & Kuhn, Architects)(Mecklenburg, 2007).

Accordingly, a two-dimensional HMSS model of a lime wood panel painting fixed to an exterior brick wall is considered in order to observe the interaction of artefacts with their surrounding building assemblies in historic buildings. In this case study the exterior wall assembly as defined in Section 6.1.4 is coupled with the panel painting described in Section 5.1.1.

6.3.2 Model setup

A general overview of the geometry for the two-dimensional HMSS model is shown in Figure 6.11. It should be noted that air movement between the panel painting and the wall was neglected in this numerical simulation.

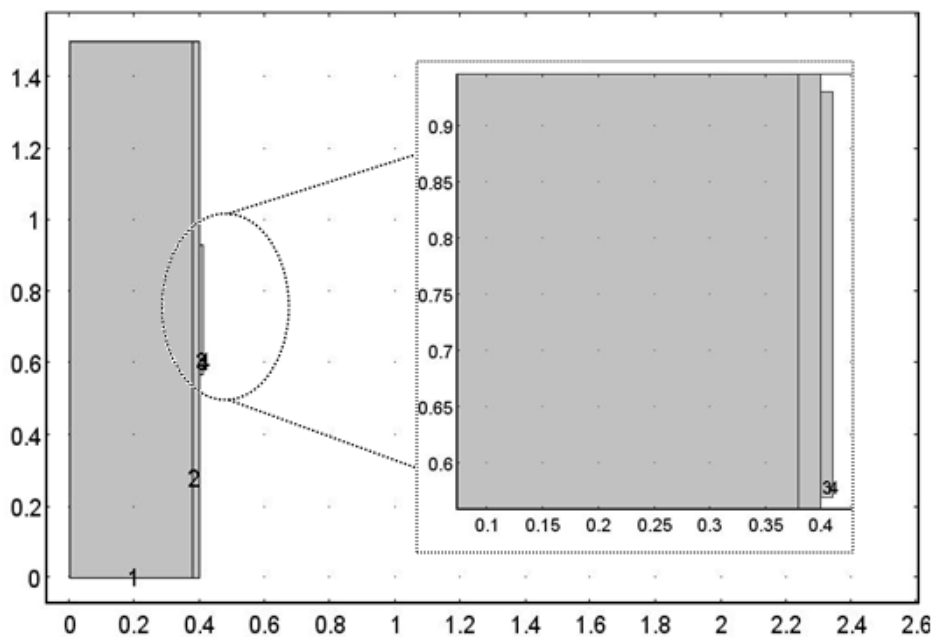


Figure 6.11 Overview of the geometry for the two-dimensional HMSS model in COMSOL.

The numerical simulation was carried out by computing the HM transports occurring in both the exterior wall and panel painting according to the prescribed boundary conditions, as well as the corresponding thermal and hygric material properties. Thereafter, the HMSS was calculated simply for the lime wood panel painting.

The indoor climate data includes recorded temperature and relative humidity measurements from the Castle of Gaasbeek. The data used in this numerical simulation was obtained from a data collector situated at the interior of the first floor adjacent to the south east perimeter wall as per Figure 6.12. This location was chosen particularly because it is relatively sheltered and thus the effects of external wind driven rain can be neglected in this simulation.

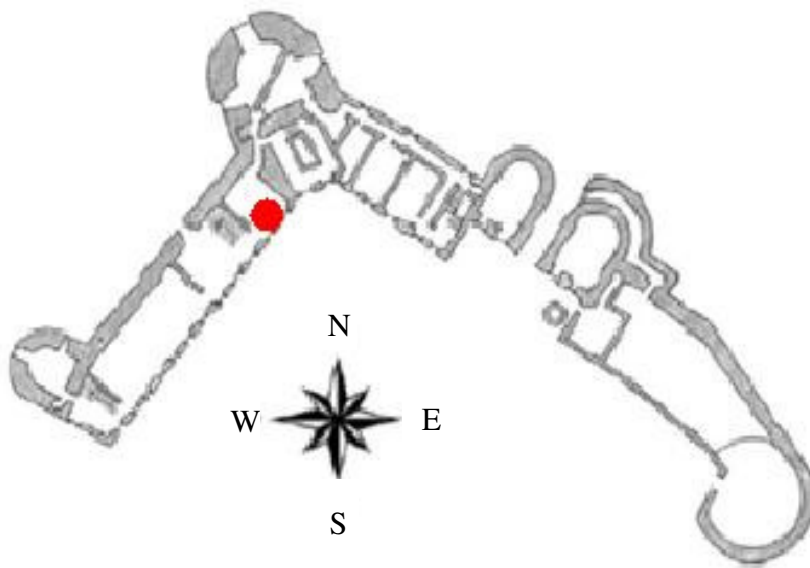


Figure 6.12 Floor plan of the Castle of Gaasbeek and location of the data collector (Kramer, 2011).

The prescribed indoor temperature and relative humidity boundary conditions are plotted against the outdoor REMO climate data in Figure 6.13 and Figure 6.14.

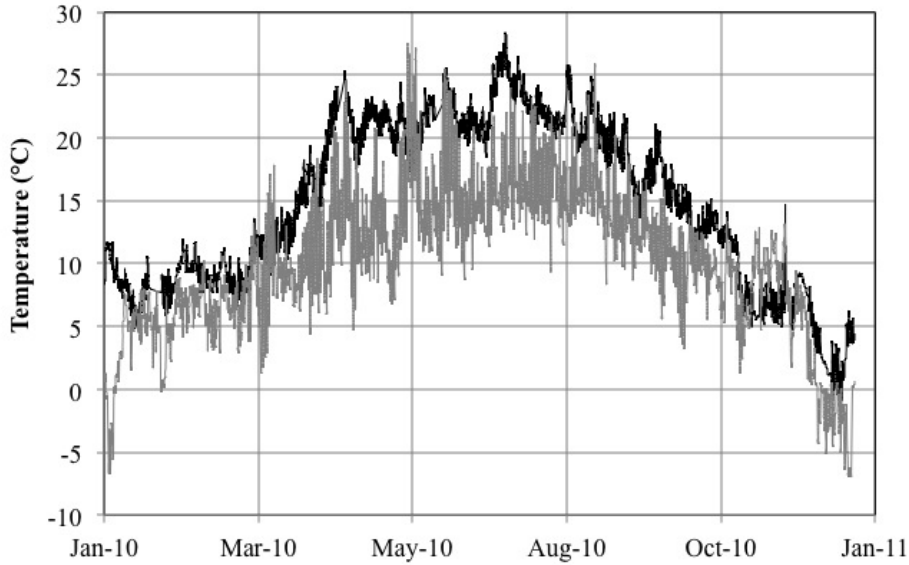


Figure 6.13 Prescribed temperature boundary conditions: outdoor-grey and indoor-black.

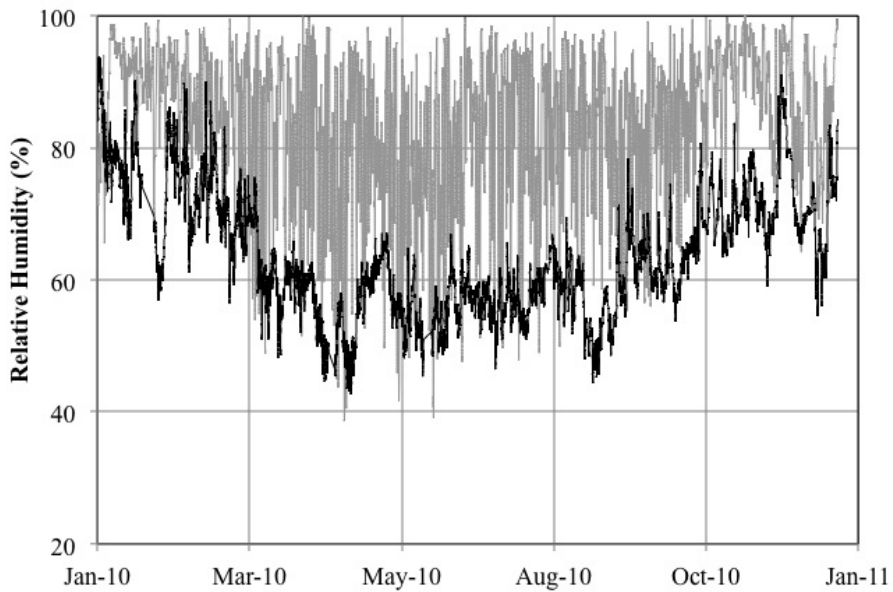


Figure 6.14 Prescribed relative humidity boundary conditions: outdoor-grey and indoor-black.

6.3.3 Numerical simulation results

A numerical simulation was computed for a time period of one year for the purpose of demonstrating the possible numerical results that can be yielded from the HMSS model. Figure 6.15 and Figure 6.16 depict the numerical simulation results for the temperature and moisture distributions along with a depiction of the magnified deformation of the panel painting with a scale factor of 62.5.

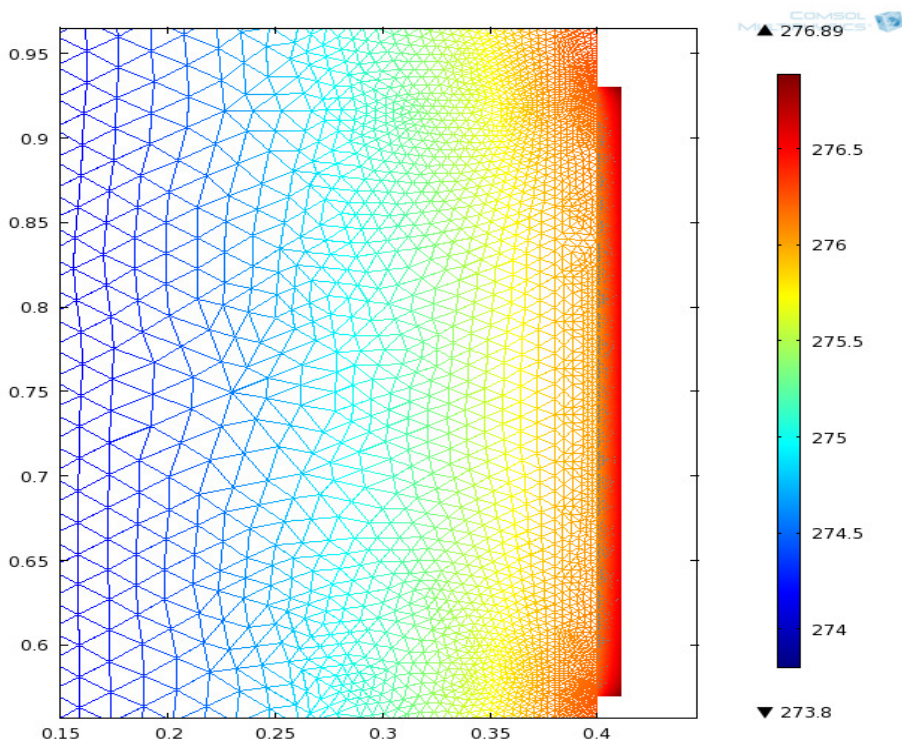
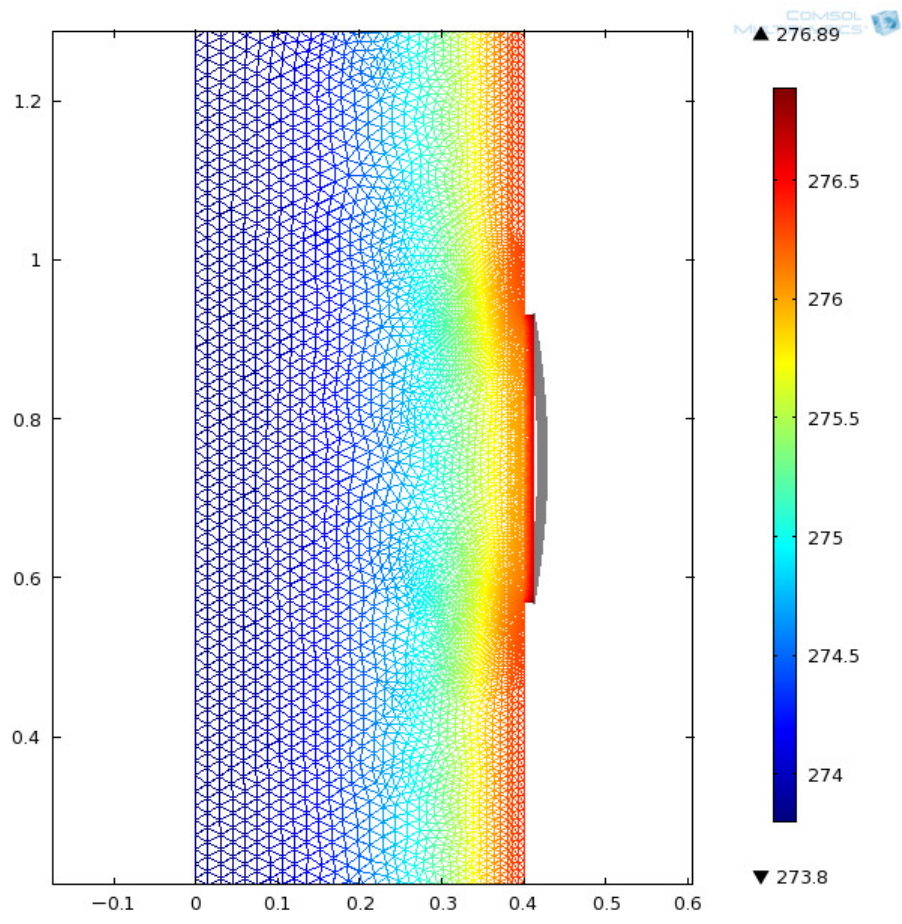


Figure 6.15 Numerical simulation results for the temperature distribution (K) in the exterior wall and panel painting after one year.

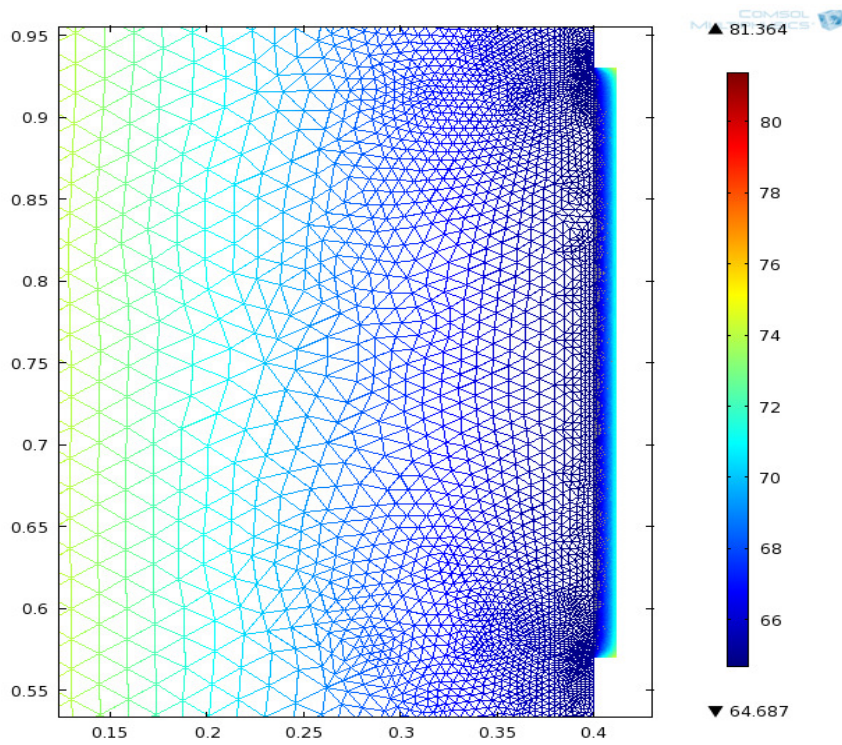
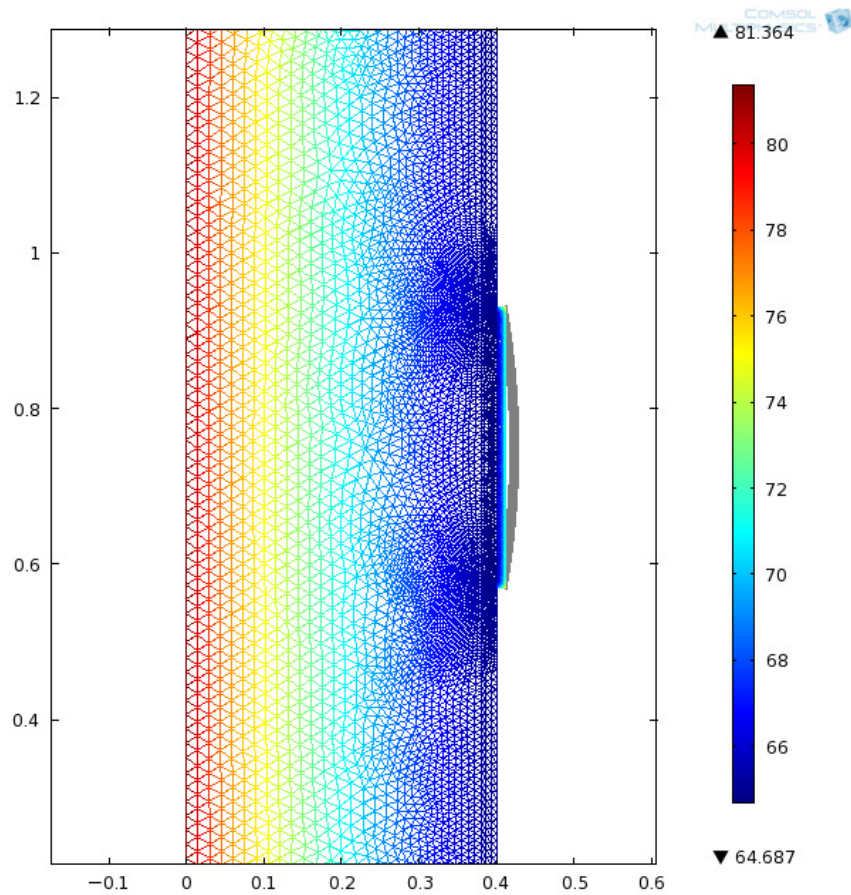


Figure 6.16 Numerical simulation results for the relative humidity distribution (%) in the exterior wall and panel painting after one year.

The numerical simulated displacement results occurring at the centre of the panel painting in the tangential direction are summarized in Figure 6.17.

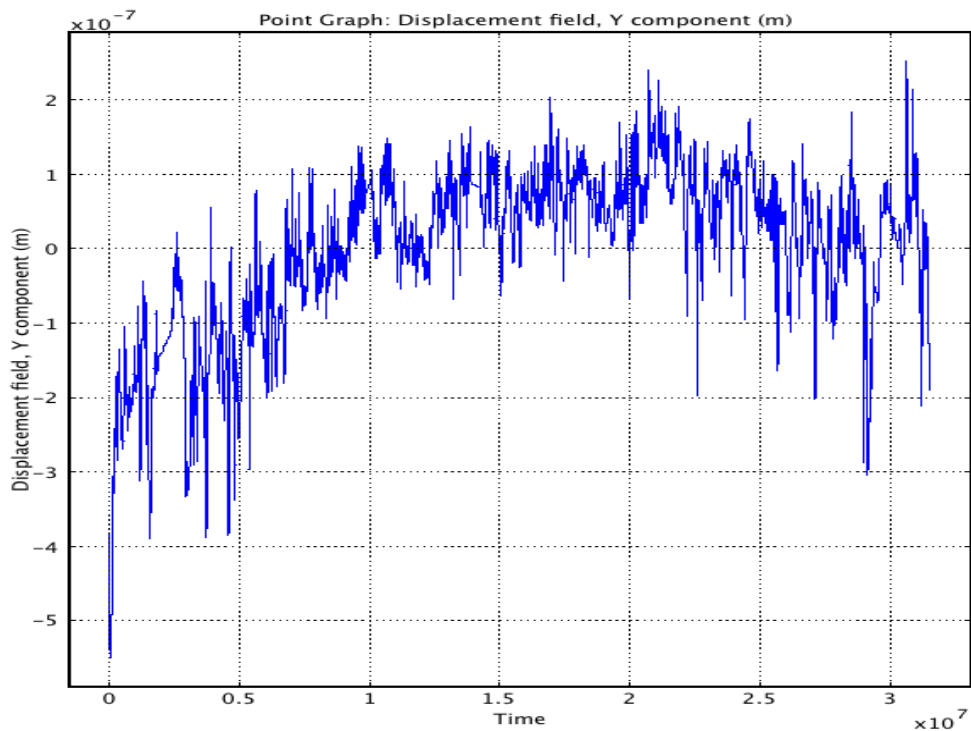


Figure 6.17 Numerical simulation results of the dimensional response in the tangential direction at the centre of the panel painting after one year.

The dimensional response of the panel painting appears to reach a periodic stability over the course of a one year simulation. The displacement curve is however observed in Figure 6.17 to peak or dip from the established periodic stability. This response takes place concurrently with the variations in the boundary conditions, particularly concerning the relative humidity.

7 Sensitivity Analysis

A sensitivity analysis was performed to investigate the outcome of changing critical model parameters in the one-dimensional HM model, and also in both two-dimensional HM and HMSS models. The aim is to analyse the effect of additional heat and moisture sources prescribed at the exterior boundary. Furthermore, the extent of the thermal impact on the computation of the moisture distribution in the HM model, as well as on the mechanical stresses and strains in the HMSS model is also of relevance in this analysis.

7.1 One-dimensional HM modelling

This sensitivity analysis is based on the one-dimensional coupled HM verification scenario presented in Section 3.4.

7.1.1 Thermal impact

The two-dimensional HM model was altered such that two cases were considered in this sensitivity analysis: Case A - decoupled thermal and hygric transport, and Case B - hygric transport with constant temperature. The goal of this analysis is to observe the influence that temperature has on the hygric transport. The prEN 15026 benchmark test was utilized as the basis for this sensitivity analysis in both Cases A and B.

The numerical simulation Case A incorporates decoupled thermal and hygric transport. The temperature and relative humidity undergo step changes as prescribed by the test. The hygric material properties that are influenced by temperature are assigned a constant temperature corresponding to the initial value of 20°C. Also, the thermal conductivity is defined as a constant value corresponding to dry conditions.

The temperature and moisture profiles obtained from the COMSOL model were plotted for 7, 30, and 365 days against the required permissible error ranges, as shown below in Figure 7.1 and Figure 7.2.

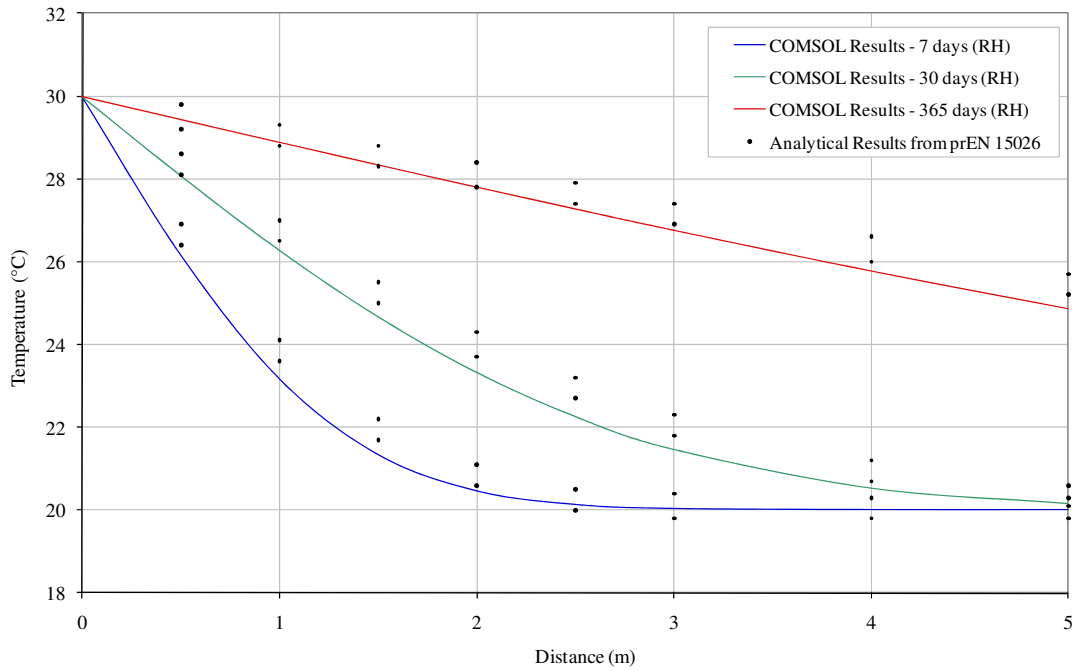


Figure 7.1 The numerically simulated temperature distribution profile for Case A at 7 days, 30 days and 365 days.

As observed in Figure 7.1, the temperature distribution is shown to fall out of the defined permissible error range. The numerical simulation results are on average 1.1% lower than the minimum values specified by the error range. It is observed that the %-error diminishes as time elapses from 7 days to 365 days. The rate of reaction is slower than that observed from the coupled HM model solution likely due to the exclusion of moisture dependent thermal properties.

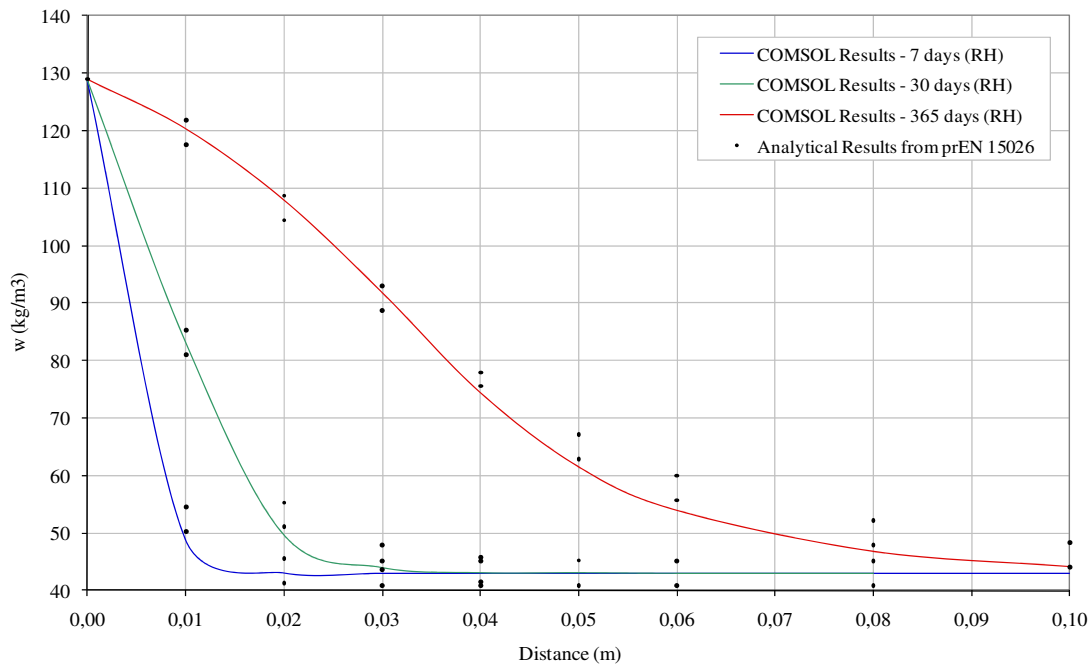


Figure 7.2 The numerically simulated water content distribution profile for Case A at 7 days, 30 days and 365 days.

The water content distribution depicted above in Figure 7.2 is on average 2.5% lower than the minimum values specified by the error range. This discrepancy thus causes the numerically simulated water content distribution profile to fall out of the required permissible error range mandated by the benchmark. It is thought that the exclusion of variable temperature in the hygric transport causes the moisture distribution to occur at a decreased rate.

Moreover, the hygric transport is simply considered in Case B. As such, the relative humidity undergoes a step change as prescribed by the test, while the temperature remains constant over the course of the calculation. The initial temperature of 20°C was defined for the entirety of the simulation. The moisture profile obtained from the COMSOL model was plotted for 7, 30, and 365 days against the required permissible error range, as shown below in Figure 7.3.

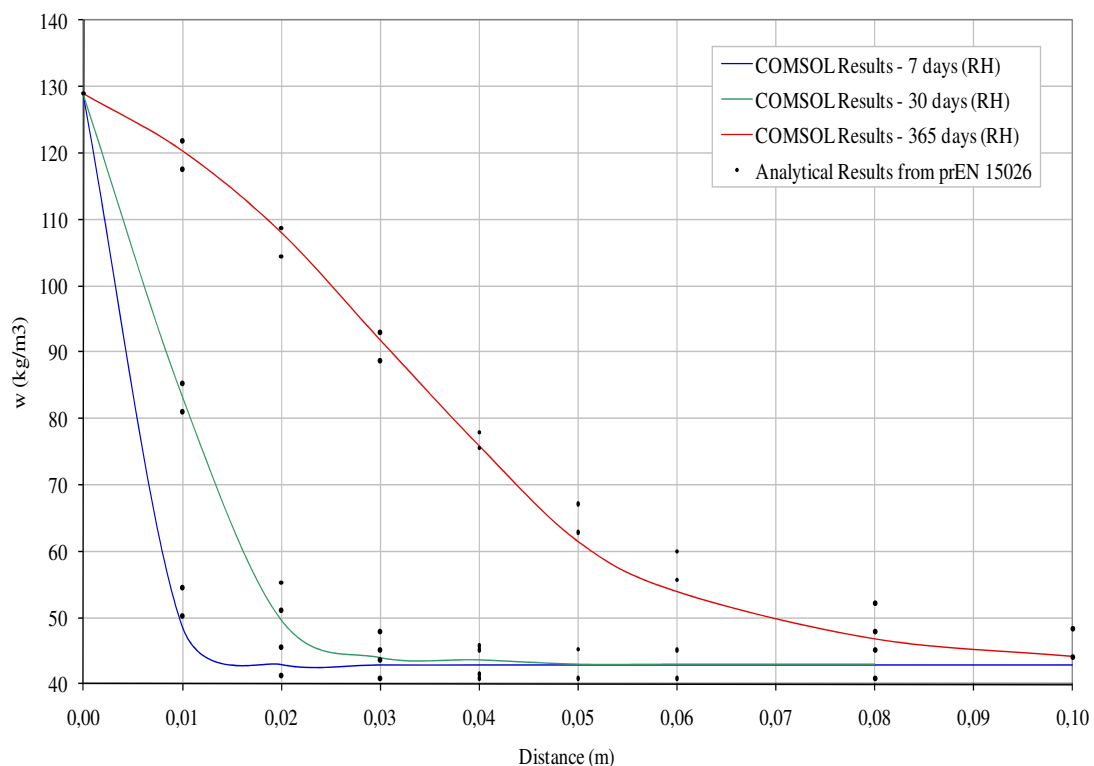


Figure 7.3 The numerically simulated water content distribution profile for Case B at 7 days, 30 days and 365 days.

The water content distribution depicted in Figure 7.3 is on average 2.6% lower than the minimum values specified by the error range. As a result, the numerically simulated water content distribution does not meet the benchmark's permissible error range. The elimination of thermal transfer thus causes the moisture distribution to take place at a slower rate. Through this analysis, it becomes evident that the inclusion of thermal transfer does in fact have a nominal impact on hygric transport.

7.2 Two-dimensional HM modelling

The two-dimensional HM case study discussed in Section 6.2 is used as the basis for this sensitivity analysis. The indoor conditions selected for this analysis are according to Case A which assumes constant interior temperature and relative humidity.

7.2.1 Additional boundary moisture source

Precipitation is incorporated as an additional moisture source at the exterior boundary in order to observe the limitations of the model. The prescribed precipitation data is consistent with that of the climate data prescribed for both the indoor and outdoor that spans over a timeseries of one year corresponding to January 2010 to January 2011. The precipitation data used to prescribe an additional moisture source at the exterior boundary is presented below in Figure 7.4.

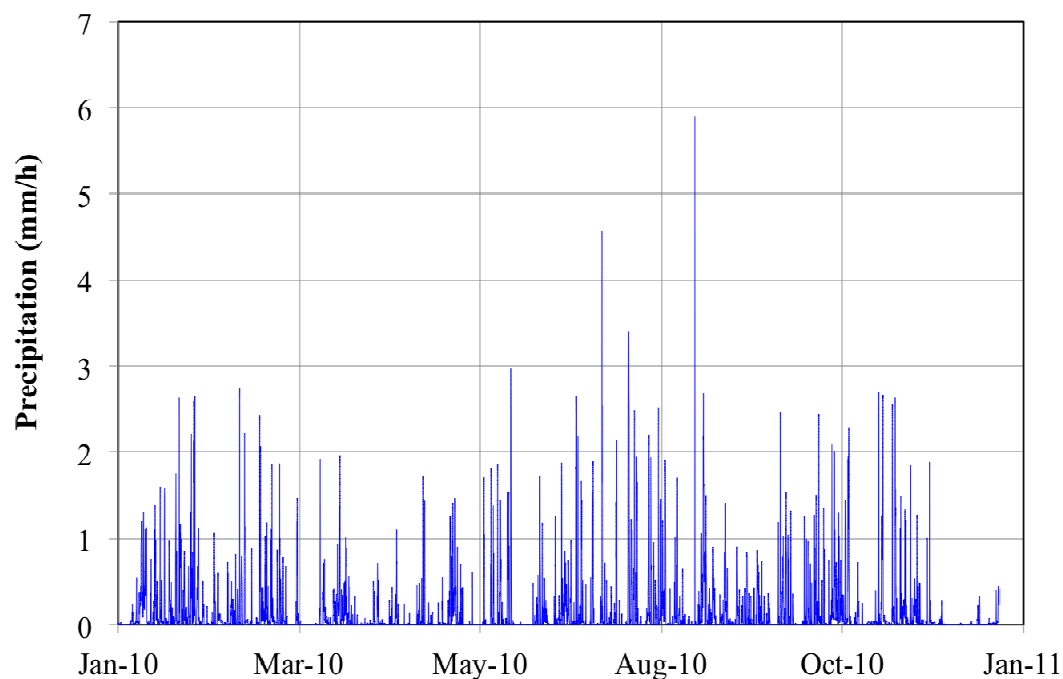


Figure 7.4 *Precipitation data used for the prescribed additional moisture source at the exterior boundary.*

Firstly, it is of interest to observe the moisture storage function shown in Figure 7.5 for the historical solid brick that is defined as the material exposed to the additional moisture source in the two-dimensional HM case study.

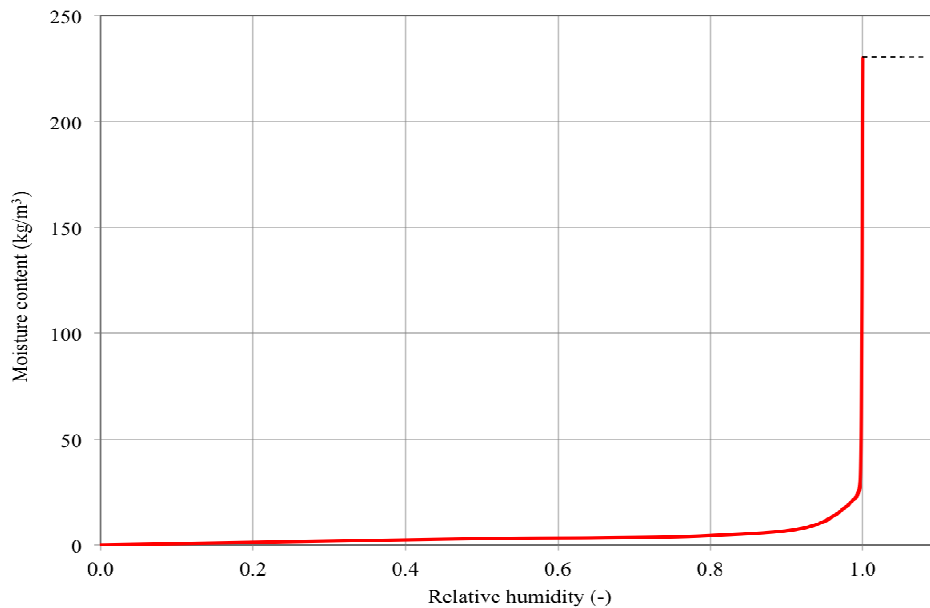


Figure 7.5 *Moisture storage function for historical solid brick used as the material for the exterior wall (IBP, 2010)*

It is of significance to determine if the HM model can generate valid numerical simulations when the relative humidity becomes greater than 100%. In the model, a constant extrapolation of the moisture storage function is prescribed thereby permitting the calculation to continue if the relative humidity becomes greater than 100%.

A numerical simulation was computed for a time period of one year for the purpose of observing the limitations of the HM model to moisture sources. The simulation was however terminated prematurely because the relative humidity in isolated regions of the exterior boundary reached 100%. The results for the moisture content in the brick at the centre of the exterior boundary are depicted below in Figure 7.6.

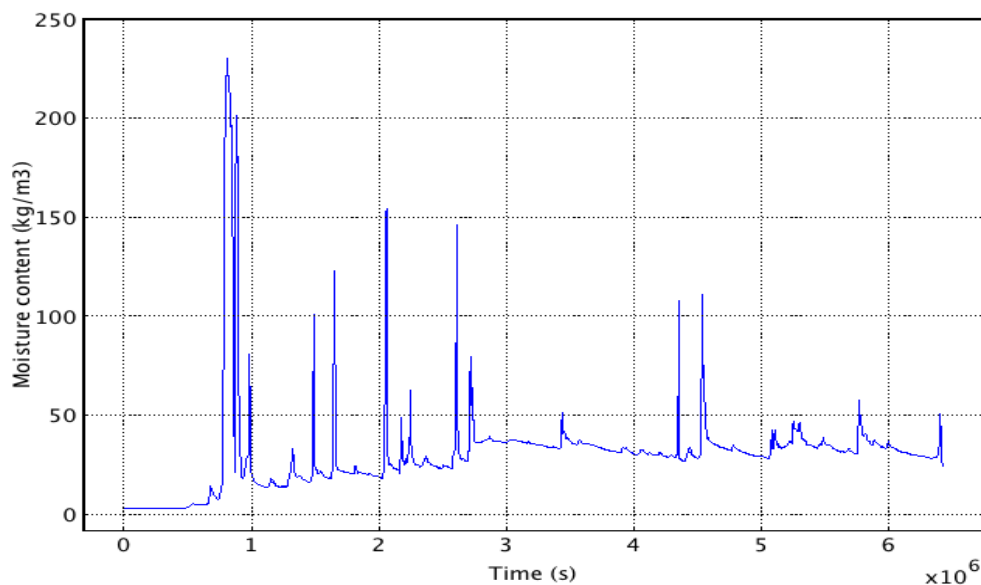


Figure 7.6 *Numerical simulated results of the moisture content in the brick at the centre of the exterior boundary.*

The distribution of the temperature and relative humidity in the brick wall directly before the premature termination of the numerical simulation are presented in Figure 7.7.

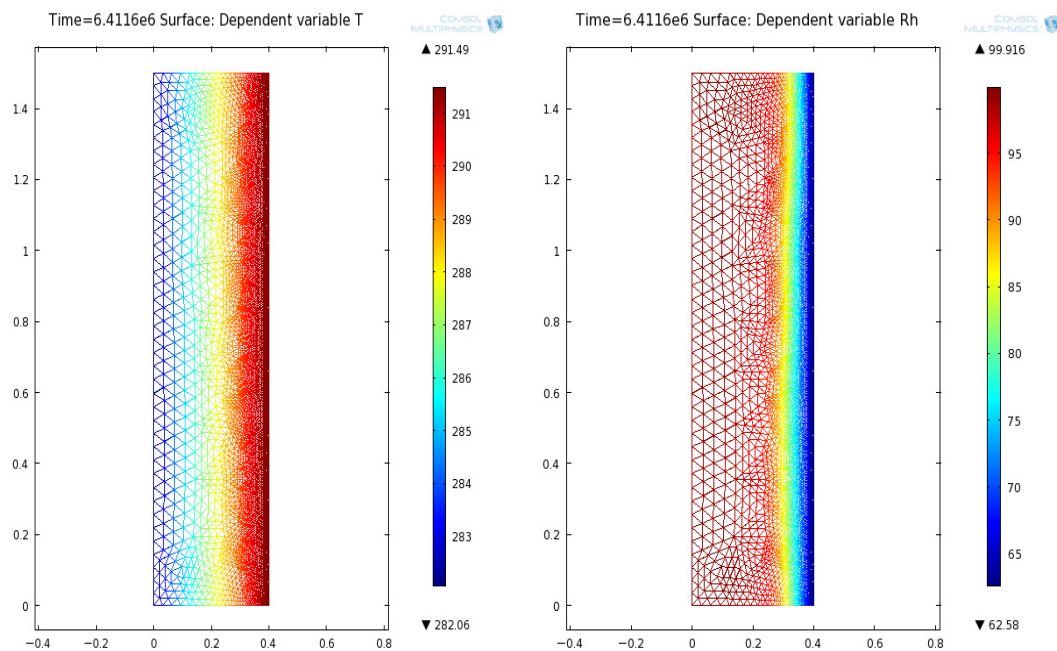


Figure 7.7 Numerical simulation results for the temperature distribution (K) and relative humidity distribution (%) in the exterior wall prior to reaching 100% relative humidity.

The two-dimensional HM model is observed to be bounded by the moisture storage function of the material defined for the domain in question. Consequently, the HM model was not able to extrapolate the moisture storage function accordingly. Further development of the model could consider the refinement of the sorption isotherm outside of the hygroscopic range, the implementation of an alternative moisture potential for hygric transport in place of relative humidity, and also the limitations of modelling liquid transport in materials.

7.3 Two-dimensional HMSS modelling

The two-dimensional HMSS case study described in Section 6.3 is used as a basis to execute sensitivity analyses on the model.

7.3.1 Thermal impact

It is of interest to observe the extent of the temperature effect on the computation of the mechanical stresses and strains in the HMSS model. The coupling of the temperature to the mechanical stress and strain computations was thus disabled to execute this sensitivity analysis. The numerical simulation results obtained from a one-year simulation period are presented and analysed in Section 7.3.3.

7.3.2 Additional boundary heat source

This sensitivity analysis incorporates global radiation as an additional heat source at the exterior boundary. The prescribed global radiation data is consistent with that of the climate data prescribed for both the indoor and outdoor that spans over a timeseries of one year corresponding to January 2010 to January 2011. The prescribed global radiation as an additional exterior heat source is plotted in Figure 7.8.

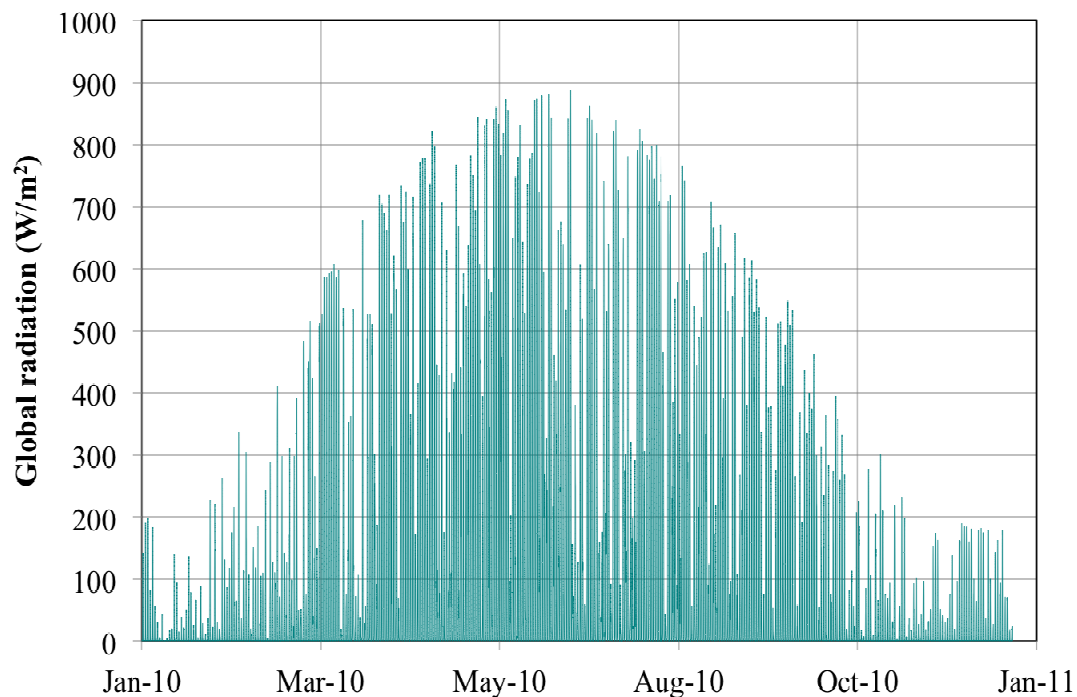


Figure 7.8 Prescribed global radiation as an exterior boundary condition.

A numerical simulation was computed for a time period of one year for the purpose of demonstrating the impact that global radiation acting at the exterior surface has on the results generated by the HMSS model. Comparisons of the numerically simulated equivalent surface temperature and relative humidity occurring at the exterior wall with and without global radiation are depicted below in Figure 7.9 and Figure 7.10.

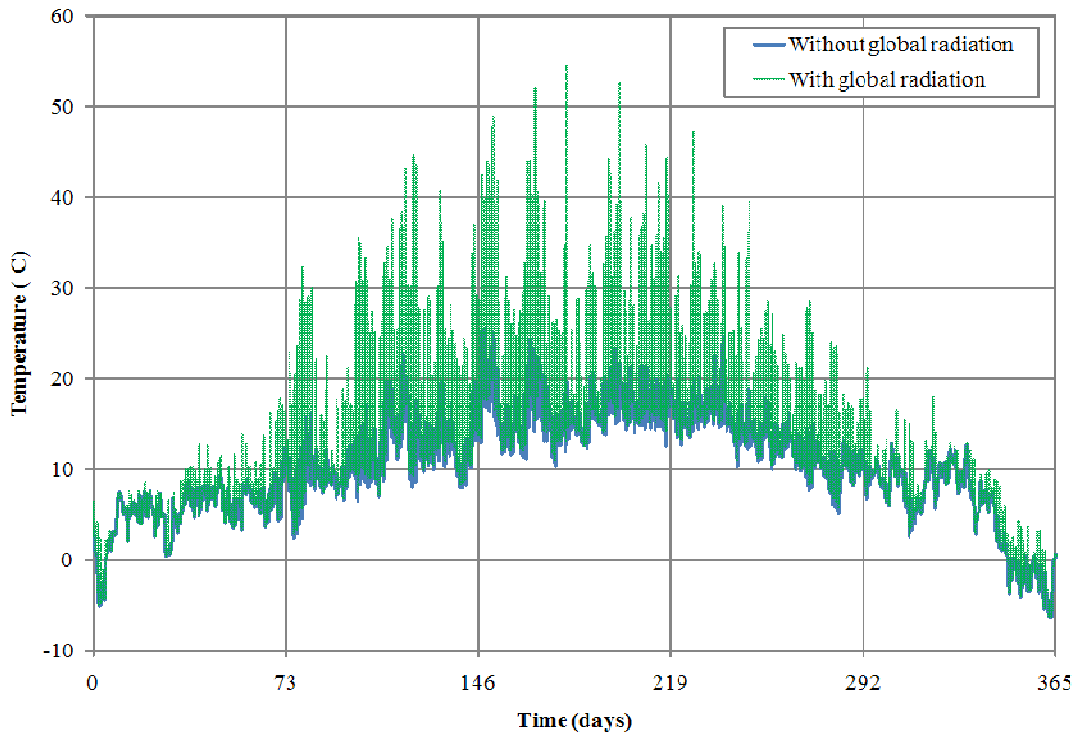


Figure 7.9 Comparison of numerical simulated equivalent surface temperature with and without global radiation at the centre of the exterior wall boundary.

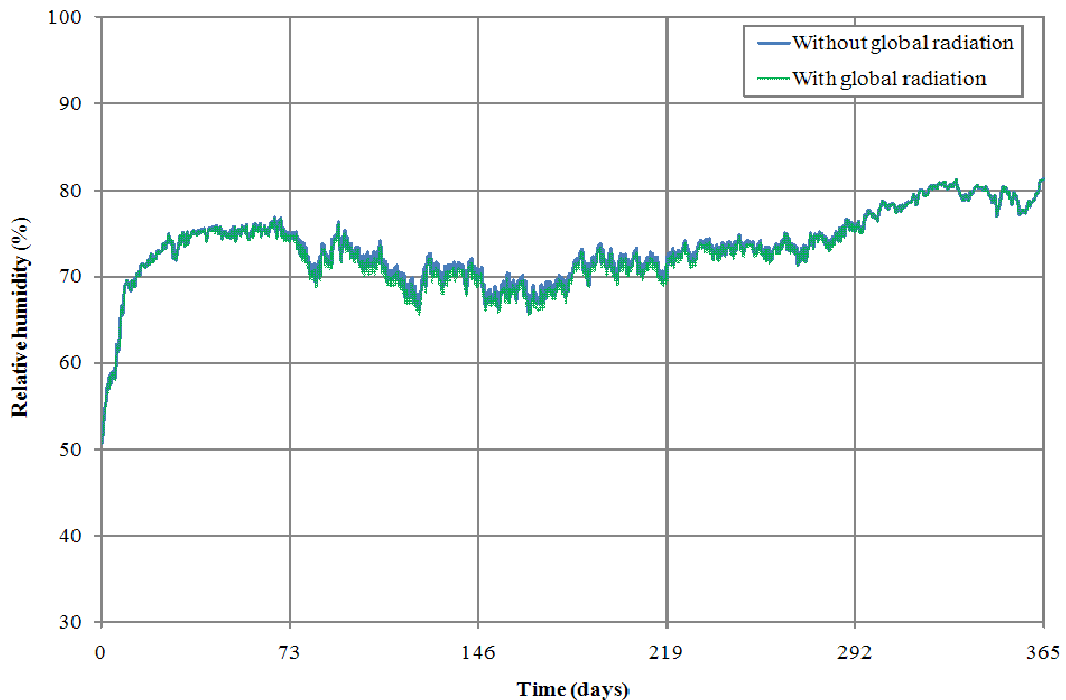


Figure 7.10 Comparison of numerical simulated equivalent surface relative humidity with and without global radiation at the centre of the exterior wall boundary.

The numerically simulated equivalent surface temperature and relative humidity occurring at the exterior wall with and without global radiation are observed to

correlate with the prescribed boundary conditions. The addition of global radiation as an external heat source increases the equivalent surface temperature which in turn decreases the equivalent surface relative humidity.

The numerical simulation results for the temperature and moisture distributions along with the displacement results occurring at the centre of the panel painting in the tangential direction are provided and discussed in Section 7.3.3.

7.3.3 Result comparison

The numerical simulation results for the temperature and moisture distributions along with a depiction of the deformation of the panel painting are provided in Figure 7.11 and Figure 7.12 for both sensitivity analyses.

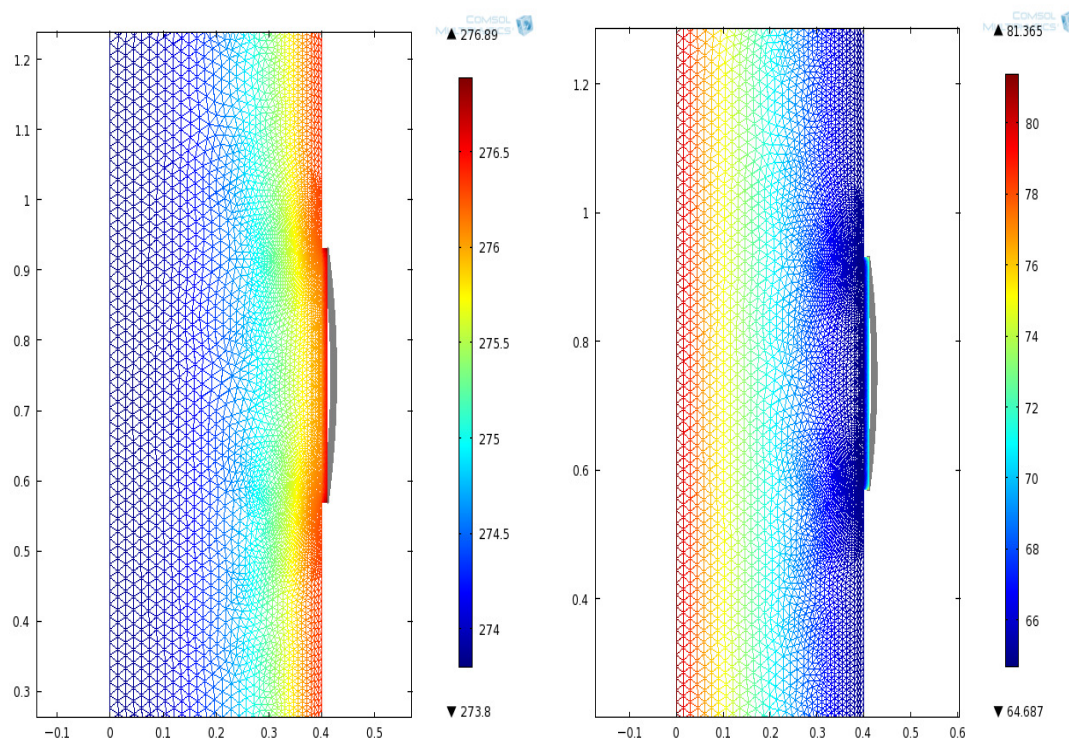


Figure 7.11 Numerical simulation results from the thermal impact analysis showing the temperature distribution (K) and relative humidity distribution (%) in the exterior wall and panel painting after one year.

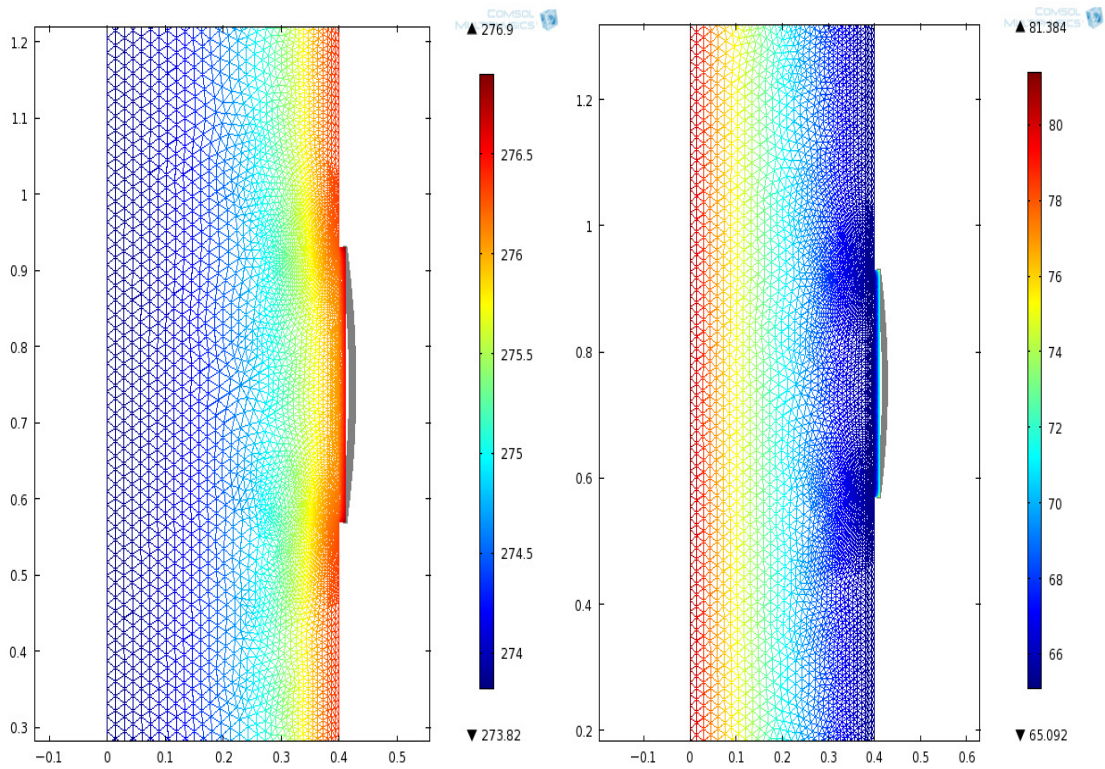


Figure 7.12 Numerical simulation results from the additional heat source analysis showing the temperature distribution (K) and relative humidity distribution (%) in the exterior wall and panel painting after one year.

The numerically simulated temperature and relative humidity distributions for the HMSS case study and sensitivity analyses are compared and presented below in Table 7.1.

Table 7.1 Comparison of temperature and relative humidity distributions after one year between the case study and sensitivity analyses.

| Simulation Results | Case study | Thermal impact | Additional heat source |
|------------------------------------|-------------|----------------|------------------------|
| Temperature distribution (K) | Max: 276.89 | 276.89 | 276.90 |
| | Min: 273.80 | 273.80 | 273.82 |
| Relative humidity distribution (%) | Max: 81.36 | 81.36 | 81.38 |
| | Min: 64.69 | 64.69 | 65.09 |

The analysis considering the thermal impact yields identical results to that obtained for the case study which is an expected outcome. Concerning the sensitivity analysis which includes global radiation as an additional external heat source, a slight variation is noted when comparing the temperature and relative humidity ranges with the results from the case study. The difference could be attributed to an increase in the rate of reaction of the coupled thermal and hygric transfer caused by the additional heat source.

It is however of interest to investigate if this minimal difference has an impact on the induced mechanical stress and strain in the panel painting. Accordingly, the numerical simulated displacement results occurring at the centre of the panel painting in the tangential direction are summarized for both sensitivity analyses in Figure 7.13 and Figure 7.14.

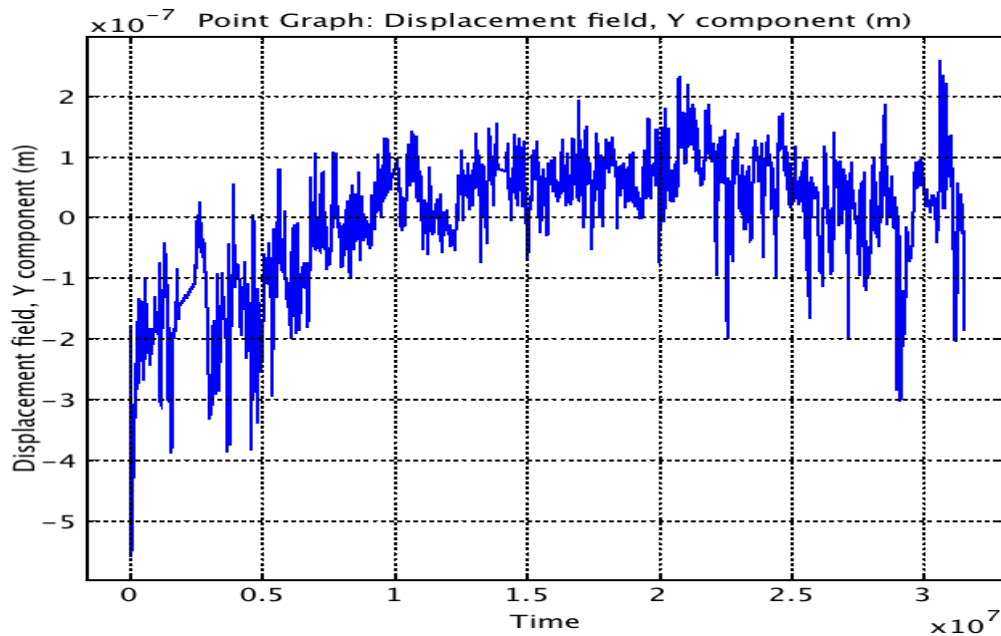


Figure 7.13 Numerical simulation results for the thermal impact analysis showing the dimensional response in the tangential direction at the centre of the panel painting after one year.

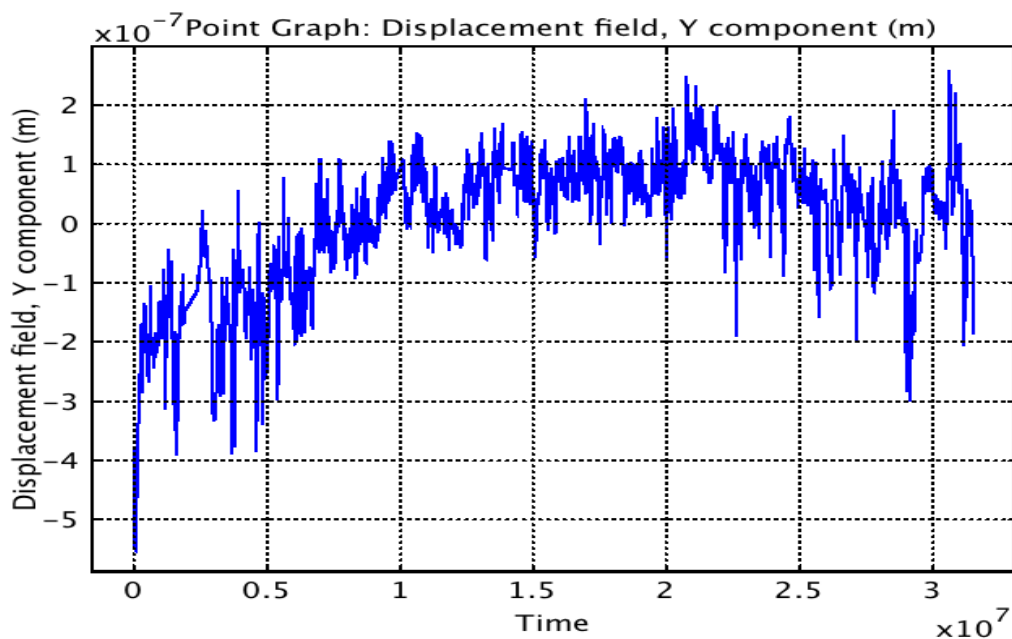


Figure 7.14 Numerical simulation results for the additional heat source analysis showing the dimensional response in the tangential direction at the centre of the panel painting after one year.

A comparison of the annual tangential dimensional response in the panel painting for the HMSS case study and sensitivity analyses is provided in Table 7.2.

Table 7.2 Comparison of the dimensional response in the panel painting after one year between the case study and sensitivity analyses.

| Simulation Results | Case study | Thermal impact | Additional heat source |
|-------------------------------------|---|------------------------|------------------------|
| Tangential dimensional response (m) | <i>Max: 2.59×10^{-7}</i> | 2.59×10^{-7} | 2.59×10^{-7} |
| | <i>Min: -5.50×10^{-7}</i> | -5.50×10^{-7} | -5.50×10^{-7} |

According to the presented dimensional response limits in Table 7.2 , as well as the full dimensional responses shown in Figure 6.17, Figure 7.13, Figure 7.14, no significant differences are observed between the case study and sensitivity analyses.

In the end, the thermal impact on stress and strain is found to be insignificant particularly for the material prescribed in the HMSS model, namely lime wood. This conclusion is concurrent with the reasoning stated by Jakiela et al. (2007):

- The thermal expansion of lime wood is nearly isotropic.
- The rate of heat diffusion through lime wood is rapid in comparison to the rate of temperature changes in the surrounding environment.

It is presumed that if a more temperature sensitive material was defined in the HMSS model that temperature would have a more significant effect on the computation of mechanical stress and strain.

8 Conclusions

One- and two-dimensional transient coupled heat and moisture induced mechanical stress and strain (HMSS) models were developed in COMSOL Multiphysics. To commence, one-dimensional transient decoupled and coupled heat and moisture (HM) models were implemented and verified by means of analytical solutions and benchmarks. Subsequently, the heat and moisture induced stress and strain mechanisms were included into the verified HM model to formulate a two-dimensional HMSS transient model. The latter model was validated through experimental and numerical results derived from a study evaluating the response of lime wood supports in historical panel paintings subjected to changing climate conditions. The verified HM and HMSS models were thereafter tailored to various case studies in order to demonstrate the applicability of the model to the interaction of artefacts and building assemblies of historical buildings. Sensitivity analyses were finally performed in order to investigate the impact of various model parameters and boundary conditions in the one- and two-dimensional HM model and also in the two-dimensional HMSS model.

The following conclusions can be summarized for this study:

- The one- and two-dimensional HM models are valid predictive tools to investigate the impact of a change in climatic conditions on building assemblies and artefacts.
- The one- and two-dimensional HM models are limited to liquid moisture transport within the storage capacity of the defined material, thereby restricting the incorporation of additional boundary moisture sources into the model.
- The two-dimensional HMSS model is an adequate predictive tool to determine possible damage-related processes in building assemblies and artefacts.
- The verification of the HMSS model is based on the material properties and mechanical behaviour of lime wood, which in turn signifies that additional verification using other desired materials may need to be executed.

9 Recommendations

This study can be further developed by incorporating the following components:

- Investigate the limitations of modelling liquid transport in materials. For example, an alternative moisture potential can be integrated in the mass balance PDE. This sensitivity of this moisture potential to simulations using non-isothermal conditions with a simultaneous step change in hygric conditions should be examined.
- Include air transport in the HM model in order to evaluate coupled heat, air and moisture transport.
- Verification of the HMSS model based on the mechanical behaviour of other common materials found in heritage items and buildings.
- Development of a three-dimensional HMSS model for a more realistic visual approach. The two-dimensional HMSS model can easily be expanded to a three-dimensional space. It consists of sketching the desired three-dimensional geometry in COMSOL and assigning the suitable material properties according to the material behaviour (i.e. isotropic, anisotropic, etc.).
- Incorporate larger climate data sets in the model by means of Matlab functions as to observe the effects of past and present climate change.
- Include non-linear elastic and plastic mechanics into the HMSS model. This addition could be valuable to investigate damage-related processes in materials.

The models developed in this study can be valuable tools for the various future research areas stated in the following:

- Evaluation and prediction of the effects of climate change on the HMSS in building assemblies and artefacts housed in historical buildings.
- Establishment of guidelines for future indoor climate demands based on numerically simulated findings to prevent predicted damages to building assemblies and artefacts found in historical buildings.
- Investigation of the cause of damage-related processes in building assemblies and artefacts of heritage sites.

10 References

- Björk, C., Kallstenius, P., Reppen, L. (2002): *Så byggdes husen 1880-2000, Arkitektur, konstruktion och material i våra flerbostadshus under 120 år* (As the houses were built 1880-2000, Architecture, construction and materials in our multi-residential buildings during 120 years. In Swedish), Forskningsrådet Formas, Sweden, 166 pp.
- Chandrupatla, T., Belegundu, A.D. (1997): *Introduction to the Finite Elements in Engineering, Second Edition*. Prentice Hall.
- COMSOL AB (1998-2010): *COMSOL Multiphysics Version 4.1*.
- Eschenauer, H., Olhoff, N., Schnell, W. (1997): *Applied Structural Mechanics*, Springer-Verlag, Berlin, Germany.
- European Provisional Standard prEN 15026 (2005): *Hygrothermal Performance of Building Components and Building Elements – Assessment of Moisture Transfer by Numerical Simulation*.
- Fraunhofer Institut Bauphysik (IBP) Holzkirchen (2010): *WUFI 2D Version 3.3*.
- Hagentoft, C.E. (2001): *Introduction to Building Physics*. Studentlitteratur, Lund, Sweden.
- International Institute of Conservation (ICA) (2010): *The Plus/Minus Dilemma: The Way Forward in Environmental Guidelines - Edited transcription of the roundtable (13 May 2010)*, London, United Kingdom, www.iiconservation.org/dialogues/Plus_Minus_trans.pdf.
- Jakiela, S., Bratasz, L., Kozłowski, R. (2007): Numerical modeling of moisture movement and related stress field in lime wood subjected to changing climate conditions. *Wood Sci Technol*, 2008, 42:21-37.
- Kasteel van Gaasbeek (2011). *Kasteel van Gaasbeek*, www.kasteelvangaasbeek.be.
- Kramer, R.P. (2011): *The impact of climate change on the inside climate of monumental buildings*. Master project. Department of Building Services, Eindhoven University of Technology, Eindhoven, Netherlands.
- Kunsten en Erfgoed (2006): *Erkend Cultureel Archief - Kasteel van Gaasbeek*, Flemish government, Belgium, <http://www.kunstenerfgoed.be/ake/view/nl/3781662-Kasteel+van+Gaasbeek.html>.
- Mecklenburg, M. F. (2007): Micro climates and moisture induced damage to paintings. *Museum Microclimates - Contributions to the Copenhagen conference (19-23 November 2007)*, National Museum of Denmark, Copenhagen, Denmark, http://www.natmus.dk/graphics/konferencer_mm/microclimates/pdf/musmic150.pdf.
- Ottosen, N., Petersson, H. (1992): *Introduction to the Finite Element Method*. Pearson Prentice Hall, University of Lund, Lund, Sweden.
- Rachwal, B., Bratasz, L., Lukomski, M., Kozłowski, R. (2010): Response of wood supports in panel paintings subjected to changing climate conditions. *Strain – An International Journal for Experimental Mechanics*, STRAIN-0631.

- Sasic Kalagasidis, A. (2010): *Getting Started with COMSOL Multiphysics, A step-by-step manual - Part II*. Department of Civil and Environmental Engineering, Chalmers University of Technology, Göteborg, Sweden.
- Schellen, H.L., van Schijndel, A.W.M. (2010): *Numerical modelling of moisture related mechanical stress in wooden cylindrical objects using COMSOL: a comparative benchmark*, Eindhoven University of Technology, Eindhoven Netherlands.
- Schellen, H.L., Ankersmit, B., Neuhaus, E., Martens, M. (2008): Een bouwfysisch verantwoord binnenklimaat in monumenten met een museale functie (A sound indoor climate for a museum in a monumental building. In Dutch.). *Bouwfysica van Monumenten*, Nederlands Vlaamse Bouwfysica Vereniging, 4-2008, pp.2-11.
- Schellen, H.L., van Schijndel, A.W.M. (2007): An Overview of Experimental and Simulation Work on Indoor Climate and Control in Historic Houses and Monumental Buildings. *Contributions to the Experts' Roundtable on Sustainable Climate Management Strategies (April 2007)*, The Getty Conservation Institute, Tenerife, Spain.
- Schellen, H.L. (2002): *Heating Monumental Churches, Indoor Climate and Preservation of Cultural Heritage*. Ph.D. Thesis. Eindhoven University of Technology, Eindhoven Netherlands.
- Smulders H., Martens, M. (2008): *Physics of Monument*. Eindhoven University of Technology, Eindhoven, Netherlands, <http://www.monumenten.bwk.tue.nl/>.
- Sulaiman R., Schellen H.L., Hensen J.L.M. (2010): Pilot study on indoor climate investigation and computer simulation in historical museum building: Amerongen Castle, the Netherlands. *Journal of Design and the Built Environment*, 7:75-94.
- The Getty Conservation Institute (1995): *The Structural Conservation of Panel Paintings – Proceedings of a symposium at the J. Paul Getty Museum (24-28 April 1995)*, Los Angeles, US, http://www.getty.edu/conservation/publications/pdf_publications/panelpaintings3.pdf.
- van Schijndel, A.W.M., Schellen, H.L. (2009): *Heat and Moisture in Building Envelopes – Numerical Exercises using Multiphysics package COMSOL*. Faculty of Architecture, Building and Planning, Eindhoven University of Technology, Eindhoven, Netherlands, http://sts.bwk.tue.nl/7s532/readers/.%5C02a_7S532_Exercises_2009_ENG_V1.pdf.

11 Appendices

11.1 Network analysis

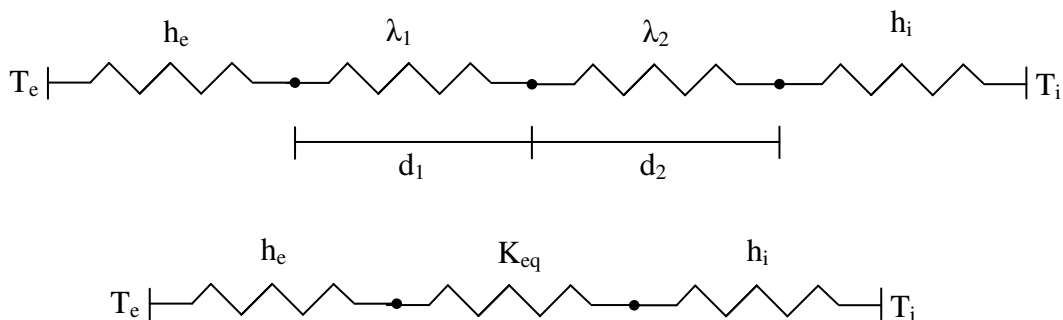
The one-dimensional decoupled HM stationary model was validated by comparison with network analysis. The validation results for both models are presented in the following. It was observed that the simulation results obtained from the HM COMSOL model agrees with the network analysis.

11.1.1 Heat Transfer

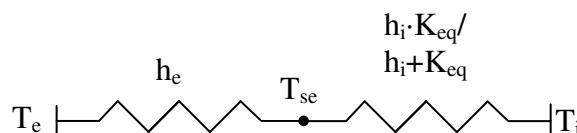
General parameters:

| Name | Expression | Description |
|----------------|-----------------------------|------------------------------------|
| Te | -10 [degC] | Exterior temperature |
| Ti | 20 [degC] | Interior temperature |
| he | 25 [W/(m ² *K)] | Exterior heat transfer coefficient |
| hi | 7.7 [W/(m ² *K)] | Interior heat transfer coefficient |
| λ_1 | 0.6 [W/(m*K)] | Thermal conductivity – Material 1 |
| λ_2 | 1 [W/(m*K)] | Thermal conductivity – Material 2 |
| d ₁ | 0.38 [m] | Thickness – Material 1 |
| d ₂ | 0.02 [m] | Thickness – Material 2 |

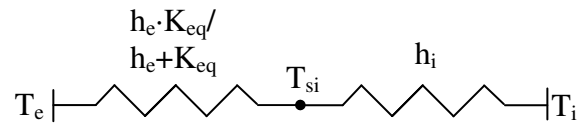
Network analysis – Solving for equivalent surface temperatures:



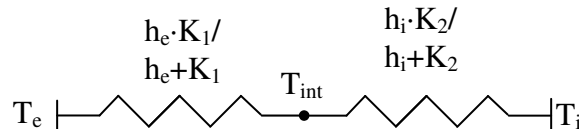
Solving for exterior surface temperature, T_{se} , at $x = 0.00$ m:



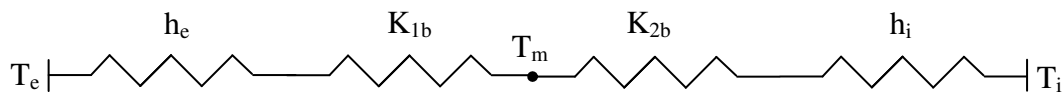
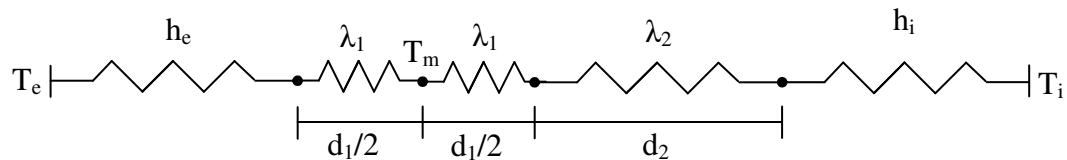
Solving for interior surface temperature, T_{si} , at $x = 0.40$ m:



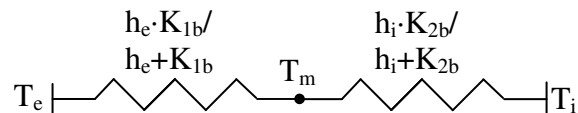
Solving for material interface temperature, T_{int} , at $x = 0.38$ m:



Network analysis – Solving for internal temperatures:



Solving for temperature at middle, T_m , at $x = 0.19$ m:



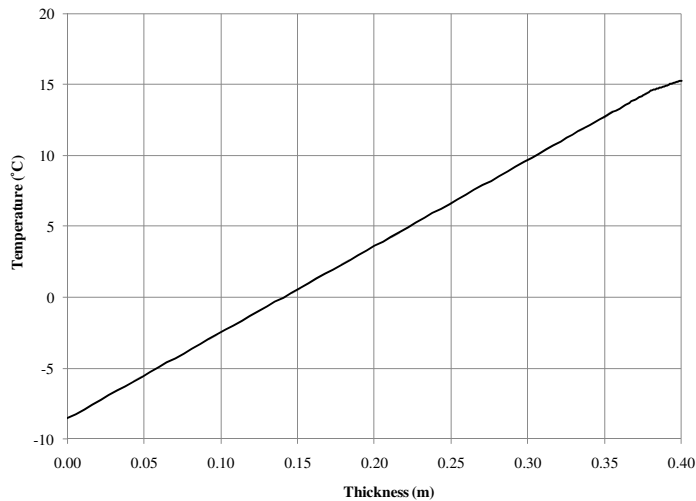
Network analysis results:

| Name | Calculated value | Description |
|----------|------------------------------|--|
| K_1 | 1.58 [W/(m ² *K)] | Thermal conductance – Material 1 |
| K_2 | 50 [W/(m ² *K)] | Thermal conductance – Material 2 |
| K_{eq} | 1.53 [W/(m ² *K)] | Equivalent thermal conductance |
| K_{1b} | 3.16 [W/(m ² *K)] | Thermal conductance – Half of Material 1 |
| K_{2b} | 2.97 [W/(m ² *K)] | Thermal conductance – Half of |

| | | Material 1 an Material 2 |
|-----------|--------------|---|
| T_{se} | -8.54 [degC] | Exterior surface temperature (<i>where $x = 0.00 m$</i>) |
| T_m | 3.00 [degC] | Internal temperature (<i>where $x = 0.19 m$</i>) |
| T_{int} | 14.54 [degC] | Internal temperature (<i>where $x = 0.38 m$</i>) |
| T_{si} | 15.27 [degC] | Interior surface temperature (<i>where $x = 0.40 m$</i>) |

COMSOL model outputs:

| Name | Model output | Description |
|-----------|--------------|---|
| T_{se} | -8.54 [degC] | Exterior surface temperature (<i>where $x = 0.00 m$</i>) |
| T_m | 3.00 [degC] | Internal temperature (<i>where $x = 0.19 m$</i>) |
| T_{int} | 14.54 [degC] | Internal temperature (<i>where $x = 0.38 m$</i>) |
| T_{si} | 15.27 [degC] | Interior surface temperature (<i>where $x = 0.40 m$</i>) |

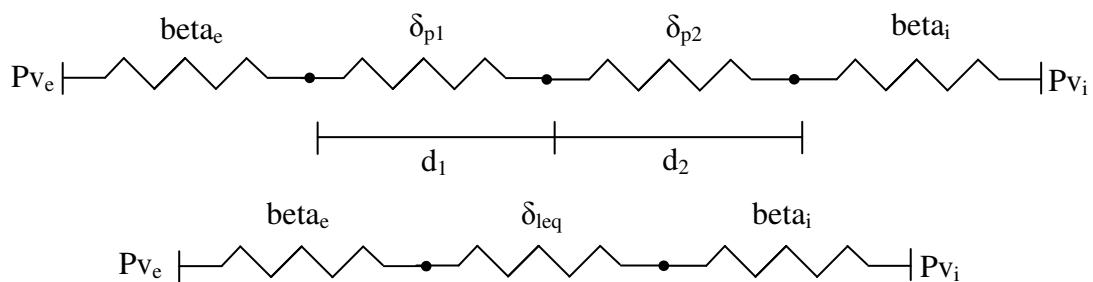


11.1.2 Moisture Transfer

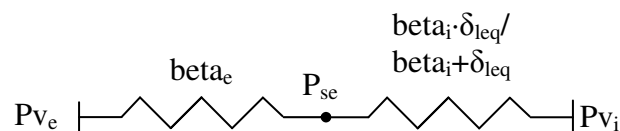
General parameters:

| Name | Expression | Description |
|----------------|--------------------------------------|--|
| Te | -10 [degC] | Exterior temperature |
| Ti | 20 [degC] | Interior temperature |
| To | 10 [degC] | Initial temperature |
| RHe | 0.8 | Exterior relative humidity |
| RHi | 0.5 | Interior relative humidity |
| RHo | 0.5 | Initial relative humidity |
| beta_e | 6.00E-07 [kg/(m ² *s*Pa)] | Exterior moisture transfer coefficient |
| beta_i | 3.00E-08 [kg/(m ² *s*Pa)] | Interior moisture transfer coefficient |
| δ_{p1} | 1.07E-11 [kg/(m*s*Pa)] | Vapour permeability – Material 1 |
| δ_{p2} | 8.24E-12 [kg/(m*s*Pa)] | Vapour permeability – Material 2 |
| d ₁ | 0.38 [m] | Thickness – Material 1 |
| d ₂ | 0.02 [m] | Thickness – Material 2 |

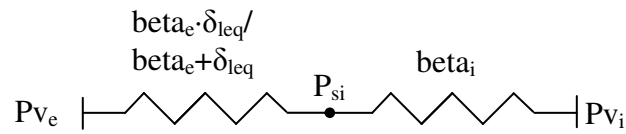
Network analysis – Solving for equivalent surface pressure:



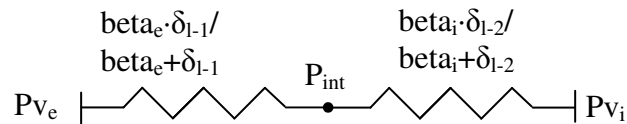
Solving for exterior surface pressure, P_{se} , at $x = 0.00$ m:



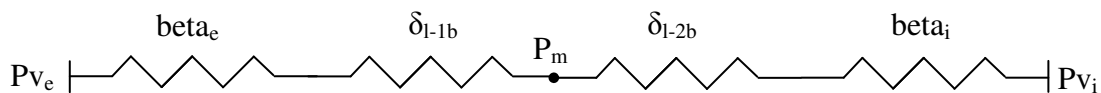
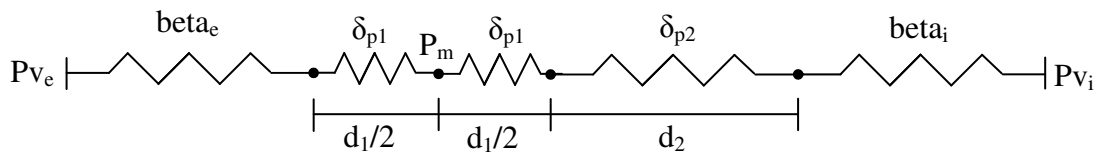
Solving for interior surface temperature, P_{si} , at $x = 0.40$ m:



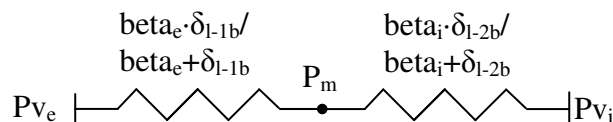
Solving for material interface pressure, P_{int} , at $x = 0.38$ m:



Network analysis – Solving for internal pressures:



Solving for pressure at middle, P_m , at $x = 0.19$ m:



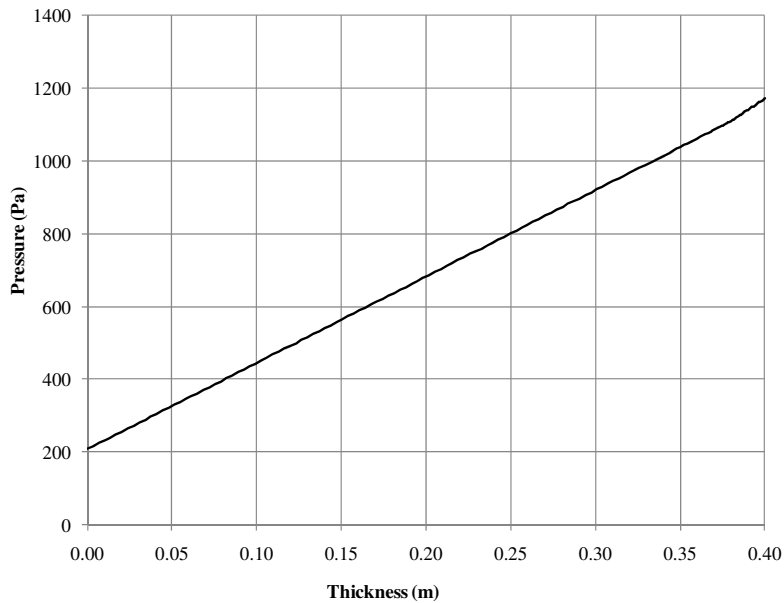
Network analysis results:

| Name | Calculated value | Description |
|-----------------|--------------------------------------|---|
| δ_{1-1} | 2.82E-11 [kg/(m ² *s*Pa)] | Vapour permeance – Material 1 |
| δ_{1-2} | 4.12E-10 [kg/(m ² *s*Pa)] | Vapour permeance – Material 2 |
| δ_{1eq} | 2.64E-11 [kg/(m ² *s*Pa)] | Equivalent vapour permeance |
| δ_{1-1b} | 5.64E-11 [kg/(m ² *s*Pa)] | Equivalent vapour permeance for interior part 1 |
| δ_{1-2b} | 4.96E-11 [kg/(m ² *s*Pa)] | Equivalent vapour permeance for |

| | | |
|-----------|--------------|--|
| | | interior part 2 |
| P_{se} | 207.91 [Pa] | Exterior surface pressure (<i>where $x = 0.00$ m</i>) |
| P_m | 658.37 [Pa] | Internal pressure (<i>where $x = 0.19$ m</i>) |
| P_{int} | 1108.82[Pa] | Internal pressure (<i>where $x = 0.38$ m</i>) |
| P_{si} | 1170.46 [Pa] | Interior surface pressure (<i>where $x = 0.40$ m</i>) |

COMSOL model outputs:

| Name | Model output | Description |
|-----------|--------------|--|
| P_{se} | 207.91 [Pa] | Exterior surface pressure (<i>where $x = 0.00$ m</i>) |
| P_m | 658.40 [Pa] | Internal pressure (<i>where $x = 0.19$ m</i>) |
| P_{int} | 1108.89 [Pa] | Internal pressure (<i>where $x = 0.38$ m</i>) |
| P_{si} | 1170.46 [Pa] | Interior surface pressure (<i>where $x = 0.40$ m</i>) |



11.2 Material properties

The material properties used in the case studies obtained from the Fraunhofer-Institut Bauphysik (IBP) Holzkirchen material database are summarized in the following tables.

Summary of basic values:

| Property | Material | |
|--|-------------------------|-------------------------|
| | Solid brick, historical | Cement plaster (stucco) |
| Bulk density (kg/m ³) | 1800 | 2000 |
| Porosity (m ³ /m ³) | 0.31 | 0.3 |
| Specific heat capacity, dry (J/kg·K) | 850 | 850 |
| Thermal conductivity, dry (W/m·K) | 0.6 | 1.2 |
| Water vapour diffusion resistance factor (-) | 15 | 25 |

Moisture storage functions:

| Material: Solid brick, historical | |
|-----------------------------------|------------------------------------|
| Relative humidity (-) | Water content (kg/m ³) |
| 0 | 0 |
| 0.5 | 3 |
| 0.65 | 3.4 |
| 0.8 | 4.5 |
| 0.93 | 8.7 |
| 0.99 | 22 |
| 0.997 | 32 |
| 0.999 | 110 |
| 0.9997 | 200 |

| 1.0 | 230 |
|-----------------------------------|------------------------------------|
| Material: Cement plaster (stucco) | |
| Relative humidity (-) | Water content (kg/m ³) |
| 0 | 0 |
| 0.1 | 1.11 |
| 0.2 | 2.48 |
| 0.3 | 4.22 |
| 0.4 | 6.51 |
| 0.5 | 9.66 |
| 0.55 | 11.71 |
| 0.6 | 14.24 |
| 0.65 | 17.42 |
| 0.7 | 21.54 |
| 0.75 | 27.1 |
| 0.8 | 35 |
| 0.85 | 47.13 |
| 0.9 | 68.11 |
| 0.91 | 74.29 |
| 0.92 | 81.52 |
| 0.93 | 90.1 |
| 0.94 | 100.46 |
| 0.95 | 113.19 |
| 0.96 | 129.23 |
| 0.97 | 150.06 |
| 0.98 | 178.18 |
| 0.99 | 218.27 |

| | |
|-----|-----|
| 1.0 | 280 |
|-----|-----|

Calculated Moisture capacity:

| Material: Solid brick, historical | |
|-----------------------------------|------------------------------------|
| Relative humidity (-) | Water content (kg/m ³) |
| 0 | 0.00 |
| 0.5 | 6.00 |
| 0.65 | 2.67 |
| 0.8 | 7.33 |
| 0.93 | 32.31 |
| 0.99 | 221.67 |
| 0.997 | 1428.57 |
| 0.999 | 39000.00 |
| 0.9997 | 128571.00 |
| 1.0 | 100000.00 |
| Material: Cement plaster (stucco) | |
| Relative humidity (-) | Water content (kg/m ³) |
| 0 | 0.00 |
| 0.1 | 11.10 |
| 0.2 | 13.70 |
| 0.3 | 17.40 |
| 0.4 | 22.90 |
| 0.5 | 31.50 |
| 0.55 | 41.00 |
| 0.6 | 50.60 |
| 0.65 | 101.00 |
| 0.7 | 106.00 |

| | |
|------|---------|
| 0.75 | 111.00 |
| 0.8 | 158.00 |
| 0.85 | 243.00 |
| 0.9 | 420.00 |
| 0.91 | 618.00 |
| 0.92 | 723.00 |
| 0.93 | 858.00 |
| 0.94 | 1040.00 |
| 0.95 | 1270.00 |
| 0.96 | 1600.00 |
| 0.97 | 2080.00 |
| 0.98 | 2810.00 |
| 0.99 | 4010.00 |
| 1.0 | 6170.00 |

Liquid transport coefficients:

| Material: Solid brick, historical | | |
|---------------------------------------|--------------------------------------|---|
| Water content (kg/m ³) | DWS (Suction) (m ² /s) | DWW (Redistribution) (m ² /s) |
| 0 | 0 | 0 |
| 23 | 7.00E-08 | 7.00E-09 |
| 160 | 7.00E-07 | 7.00E-09 |
| 184 | 3.00E-06 | 5.00E-08 |
| 207 | 5.00E-05 | 1.00E-07 |
| 230 | 3.00E-04 | 9.00E-05 |
| Material: Cement plaster (stucco) | | |
| Water content | DWS (Suction) | DWW (Redistribution) |

| | | |
|----------------------|---------------------|---------------------|
| (kg/m ³) | (m ² /s) | (m ² /s) |
| 0 | 0 | 0 |
| 25 | 9.00E-12 | 9.00E-12 |
| 280 | 2.90E-09 | 3.00E-10 |

Thermal conductivity, moisture dependent:

| | |
|---------------------------------------|----------------------------------|
| Material: Solid brick, historical | |
| Water content (kg/m ³) | Thermal conductivity (W/ m·K) |
| 0 | 0.6 |
| 310 | 2.15 |
| Material: Cement plaster (stucco) | |
| Water content (kg/m ³) | Thermal conductivity (W/ m·K) |
| 0 | 1.2 |
| 300 | 3.0 |

11.3 Matlab files

11.3.1 Saturation vapour pressure

```
% Calculation of the saturation vapour pressure according to
% IEA Annex 24 Final Report, Task 1, Modelling, by Hugo Hens
% Search formulas in Appendix
%
% psat = psatf(t)
% t = temperature in degrees Celcius
% psat = saturation vapour pressure (Pa)
%
% If t is a vector, the function returns a vector of the same size.
%
% Example
% t=[16:18];
% psat=psatf(t)
% psat = 1.0e+003*[1.8215, 1.9412, 2.0678];
% Author: Martin de Wit 22-May-1998;

function psat=psatf(t)

%Define temperature range (i.e. -30 to 80+ deg C w/ 1 deg step) / NWP
t=-30:1:80;

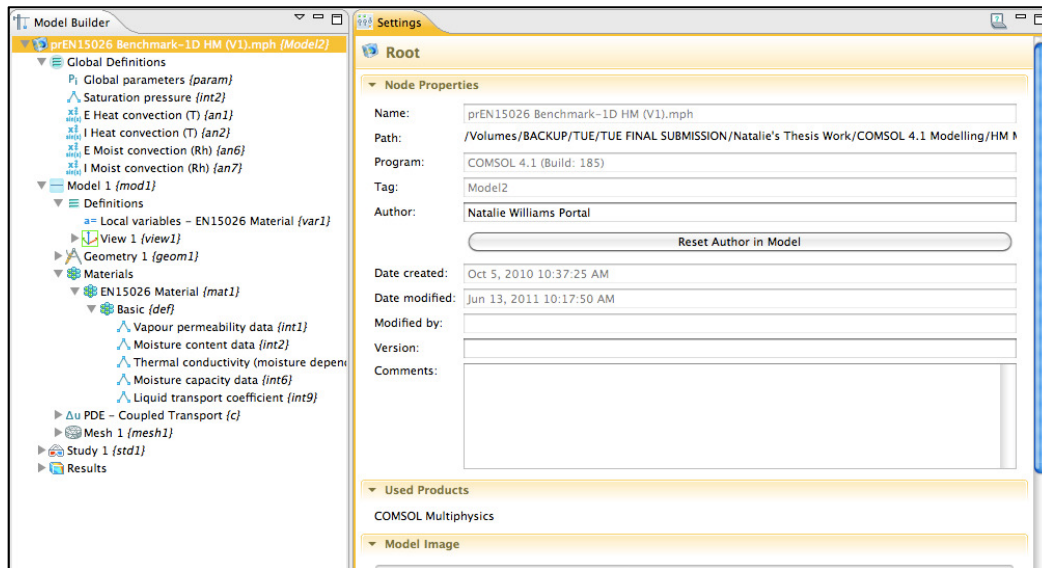
psat=611*exp(17.08*t./(234.18+t));
f=find(t<0);
psat(f)=611*exp(22.44*t(f)./(272.44+t(f)));
end

%Generate data text files to be inputted into COMSOL - Saturation vapour pressure %[Pa] with respect
to temperature [degC] / NWP
fid=fopen('psatf.txt','w');
fprintf(fid,'%s\t','%temperature');
fprintf(fid,'%s\r\n', '');
fprintf(fid,'%s\t', t);
fprintf(fid,'%s\r\n', '');
fprintf(fid,'%s\t','%data');
fprintf(fid,'%s\r\n', '');
fprintf(fid,'%s\t', psat);
fclose(fid);
```

11.3.2 M-file for HM model

```
function out = model
% prEN15026 Benchmark-1D HM (V1).m
% Model exported on Jun 13 2011, 10:17 by COMSOL 4.1.0.185.

import com.comsol.model.*
import com.comsol.model.util.*
model = ModelUtil.create('Model');
model.modelPath('/Verification - prEN15026 Benchmark/COMSOL Models');
model.name('prEN15026 Benchmark-1D HM (V1).mph');
```

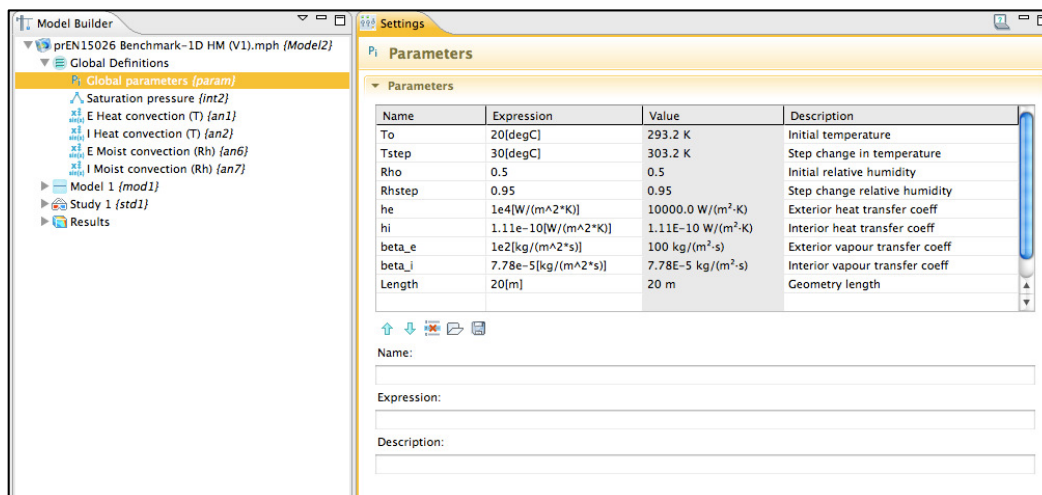


% Global Definitions: Global parameters

```

model.param.set('To', '20[degC]', 'Initial temperature');
model.param.set('Tstep', '30[degC]', 'Step change in temperature');
model.param.set('Rho', '0.5', 'Initial relative humidity');
model.param.set('Rhstep', '0.95', 'Step change relative humidity');
model.param.set('he', '1E4[W/(m^2*K)]', 'Exterior heat transfer coeff');
model.param.set('hi', '1.11E-10[W/(m^2*K)]', 'Interior heat transfer coeff');
model.param.set('beta_e', '1E2[kg/(m^2*s)]', 'Exterior vapour transfer coeff');
model.param.set('beta_i', '2.45E-8[kg/(m^2*s)]', 'Interior vapour transfer coeff');
model.param.set('Length', '20[m]', 'domain length');

```



% Global Definitions: Interpolation functions

```

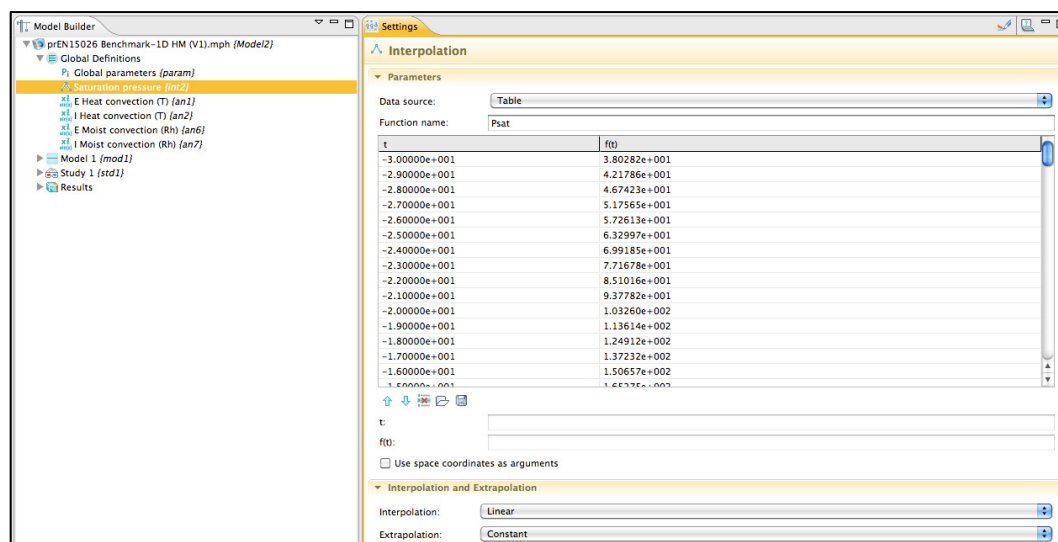
model.func.create('int2', 'Interpolation');
model.func('int2').name('Saturation pressure');
model.func('int2').set('funcname', 'Psat');
model.func('int2').set('table', {'-3.00000e+001' '3.80282e+001'; '-2.90000e+001' '4.21786e+001'; '-2.80000e+001' '4.67423e+001'; '-2.70000e+001' '5.17565e+001'; '-2.60000e+001' '5.72613e+001'; '-2.50000e+001' '6.32997e+001'; '-2.40000e+001' '6.99185e+001'; '-2.30000e+001' '7.71678e+001'; '-2.20000e+001' '8.51016e+001'; '-2.10000e+001' '9.37782e+001'; '-2.00000e+001' '1.03260e+002'; '-1.90000e+001' '1.13614e+002'; '-1.80000e+001' '1.24912e+002'; '-1.70000e+001' '1.37232e+002'; '-1.60000e+001' '1.50657e+002'; '-1.50000e+001' '1.65275e+002'; '-1.40000e+001' '1.81181e+002'; '-1.30000e+001' '1.98477e+002'; '-1.20000e+001' '2.17273e+002'; '-1.10000e+001' '2.37684e+002'; '-1.00000e+001' '2.59834e+002'; '-9.00000e+000' '2.83857e+002'; '-8.00000e+000' '3.09893e+002';

```

```

7.00000e+000' '3.38094e+002'; '-6.00000e+000' '3.68620e+002'; '-5.00000e+000' '4.01643e+002'; '-
4.00000e+000' '4.37344e+002'; '-3.00000e+000' '4.75918e+002'; '-2.00000e+000' '5.17570e+002'; '-
1.00000e+000' '5.62520e+002'; '0.00000e+000' '6.11000e+002'; '1.00000e+000' '6.57025e+002';
'2.00000e+000' '7.06083e+002'; '3.00000e+000' '7.58343e+002'; '4.00000e+000' '8.13982e+002';
'5.00000e+000' '8.73187e+002'; '6.00000e+000' '9.36151e+002'; '7.00000e+000' '1.00308e+003';
'8.00000e+000' '1.07417e+003'; '9.00000e+000' '1.14966e+003'; '1.00000e+001' '1.22977e+003';
'1.10000e+001' '1.31474e+003'; '1.20000e+001' '1.40481e+003'; '1.30000e+001' '1.50025e+003';
'1.40000e+001' '1.60133e+003'; '1.50000e+001' '1.70833e+003'; '1.60000e+001' '1.82153e+003';
'1.70000e+001' '1.94124e+003'; '1.80000e+001' '2.06777e+003'; '1.90000e+001' '2.20145e+003';
'2.00000e+001' '2.34262e+003'; '2.10000e+001' '2.49163e+003'; '2.20000e+001' '2.64884e+003';
'2.30000e+001' '2.81463e+003'; '2.40000e+001' '2.98940e+003'; '2.50000e+001' '3.17353e+003';
'2.60000e+001' '3.36746e+003'; '2.70000e+001' '3.57162e+003'; '2.80000e+001' '3.78646e+003';
'2.90000e+001' '4.01244e+003'; '3.00000e+001' '4.25004e+003'; '3.10000e+001' '4.49976e+003';
'3.20000e+001' '4.76210e+003'; '3.30000e+001' '5.03760e+003'; '3.40000e+001' '5.32681e+003';
'3.50000e+001' '5.63029e+003'; '3.60000e+001' '5.94861e+003'; '3.70000e+001' '6.28238e+003';
'3.80000e+001' '6.63222e+003'; '3.90000e+001' '6.99877e+003'; '4.00000e+001' '7.38267e+003';
'4.10000e+001' '7.78461e+003'; '4.20000e+001' '8.20528e+003'; '4.30000e+001' '8.64540e+003';
'4.40000e+001' '9.10571e+003'; '4.50000e+001' '9.58696e+003'; '4.60000e+001' '1.00899e+004';
'4.70000e+001' '1.06154e+004'; '4.80000e+001' '1.11643e+004'; '4.90000e+001' '1.17374e+004';
'5.00000e+001' '1.23355e+004'; '5.10000e+001' '1.29596e+004'; '5.20000e+001' '1.36105e+004';
'5.30000e+001' '1.42893e+004'; '5.40000e+001' '1.4969e+004'; '5.50000e+001' '1.57342e+004';
'5.60000e+001' '1.65023e+004'; '5.70000e+001' '1.73023e+004'; '5.80000e+001' '1.81352e+004';
'5.90000e+001' '1.90021e+004'; '6.00000e+001' '1.99040e+004'; '6.10000e+001' '2.08423e+004';
'6.20000e+001' '2.18180e+004'; '6.30000e+001' '2.28323e+004'; '6.40000e+001' '2.38865e+004';
'6.50000e+001' '2.49819e+004'; '6.60000e+001' '2.61197e+004'; '6.70000e+001' '2.73012e+004';
'6.80000e+001' '2.85278e+004'; '6.90000e+001' '2.98009e+004'; '7.00000e+001' '3.11218e+004';
'7.10000e+001' '3.24921e+004'; '7.20000e+001' '3.39131e+004'; '7.30000e+001' '3.53865e+004';
'7.40000e+001' '3.69136e+004'; '7.50000e+001' '3.84962e+004'; '7.60000e+001' '4.01357e+004';
'7.70000e+001' '4.18339e+004'; '7.80000e+001' '4.35923e+004'; '7.90000e+001' '4.54126e+004';
'8.00000e+001' '4.72967e+004');

```

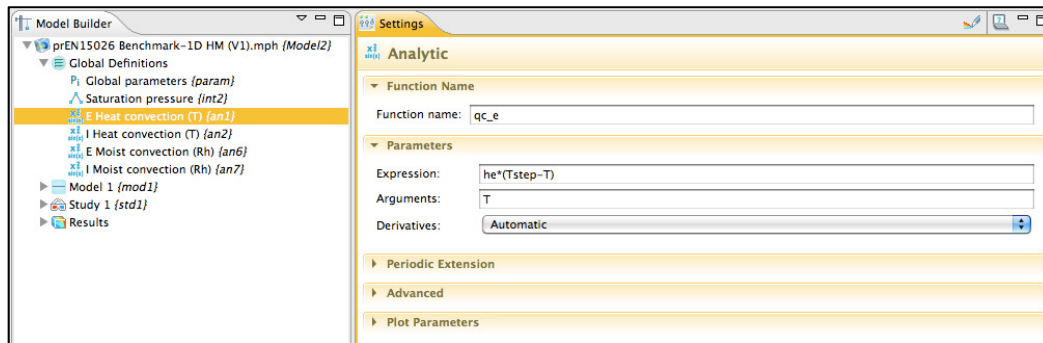


% Global Definitions: Analytical functions

```

model.func.create('an1', 'Analytic');
model.func('an1').name('E Heat convection (T)');
model.func('an1').set('funcname', 'qc_e');
model.func('an1').set('expr', 'he*(Tstep-T)');
model.func('an1').set('args', {'T'});
model.func('an1').set('plotargs', {'T' " "});

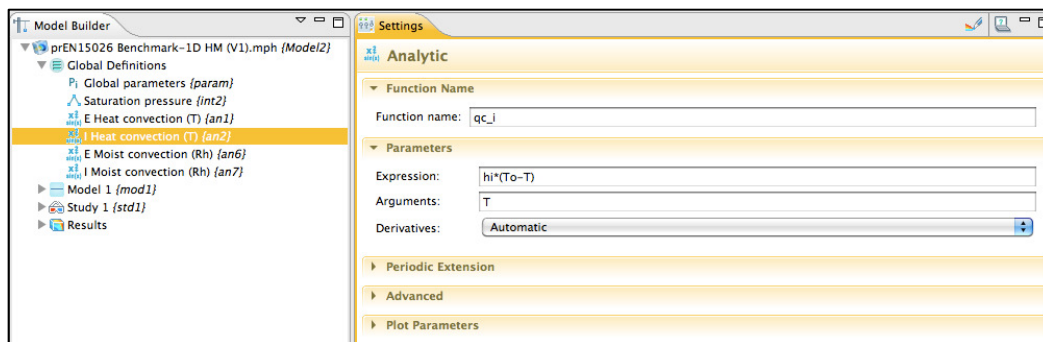
```



```

model.func.create('an2', 'Analytic');
model.func('an2').name('I Heat convection (T)');
model.func('an2').set('funcname', 'qc_i');
model.func('an2').set('expr', 'hi*(To-T)');
model.func('an2').set('args', {'T'});
model.func('an2').set('plotargs', {'T' " "});

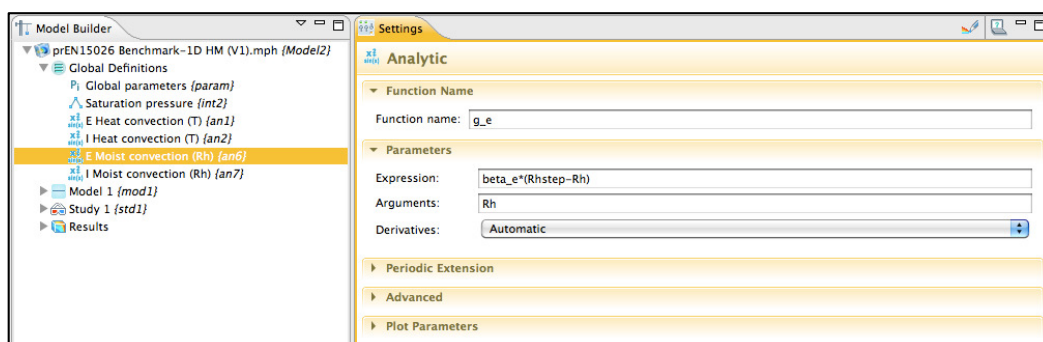
```



```

model.func.create('an6', 'Analytic');
model.func('an6').name('E Moist convection (Rh)');
model.func('an6').set('funcname', 'g_e');
model.func('an6').set('expr', 'beta_e*(Rhstep-Rh)');
model.func('an6').set('args', {'Rh'});
model.func('an6').set('plotargs', {'Rh' " "});

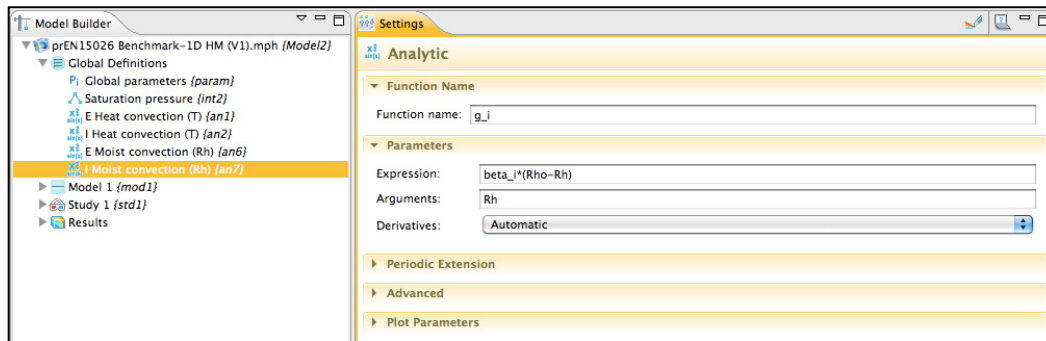
```



```

model.func.create('an7', 'Analytic');
model.func('an7').name('I Moist convection (Rh)');
model.func('an7').set('funcname', 'g_i');
model.func('an7').set('expr', 'beta_i*(Rho-Rh)');
model.func('an7').set('args', {'Rh'});
model.func('an7').set('plotargs', {'Rh' " "});

```

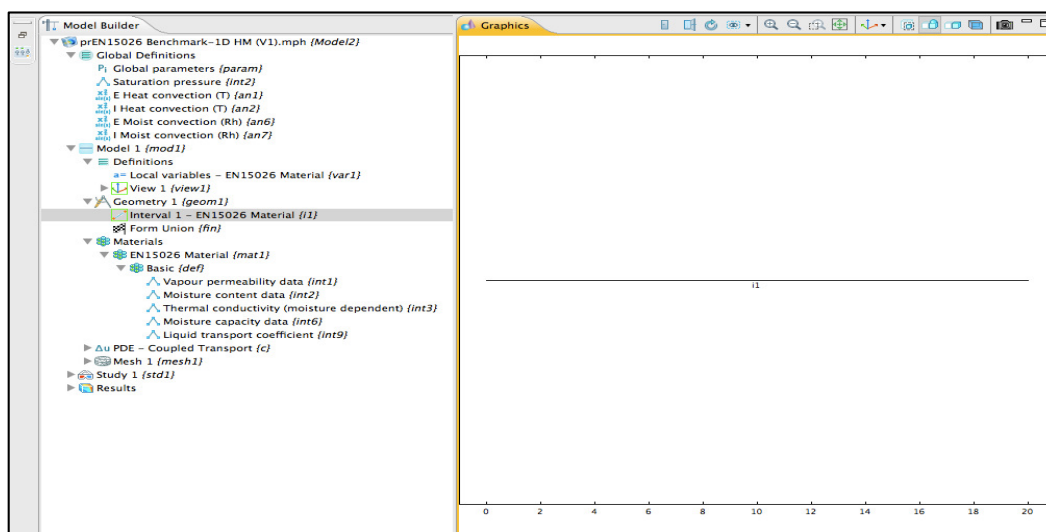
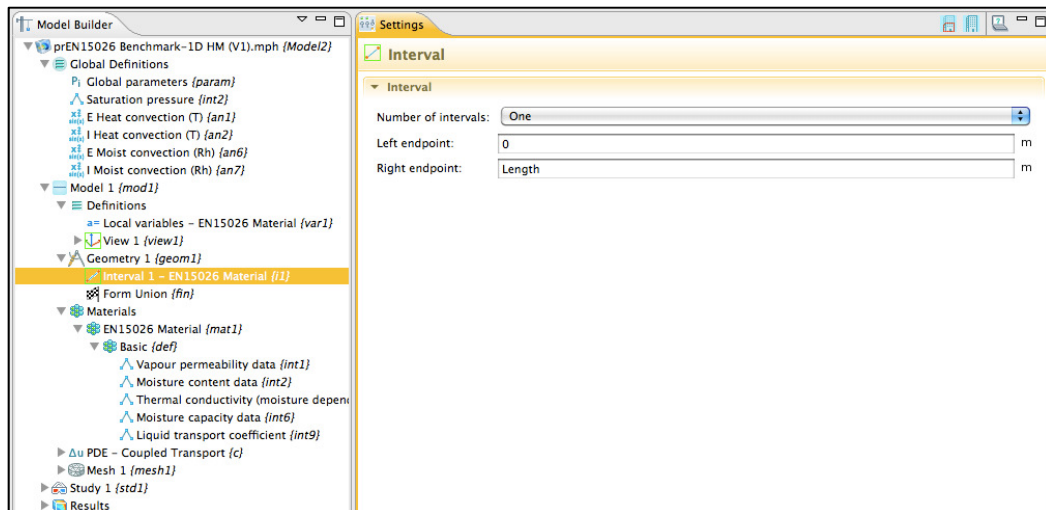


% Model 1

```
model.modelNode.create('mod1');
```

% Model 1: Geometry

```
model.geom.create('geom1', 1);
model.geom('geom1').feature.create('i1', 'Interval');
model.geom('geom1').feature('i1').name('Interval 1 - EN15026 Material');
model.geom('geom1').feature('i1').set('p2', 'Length');
model.geom('geom1').run;
```



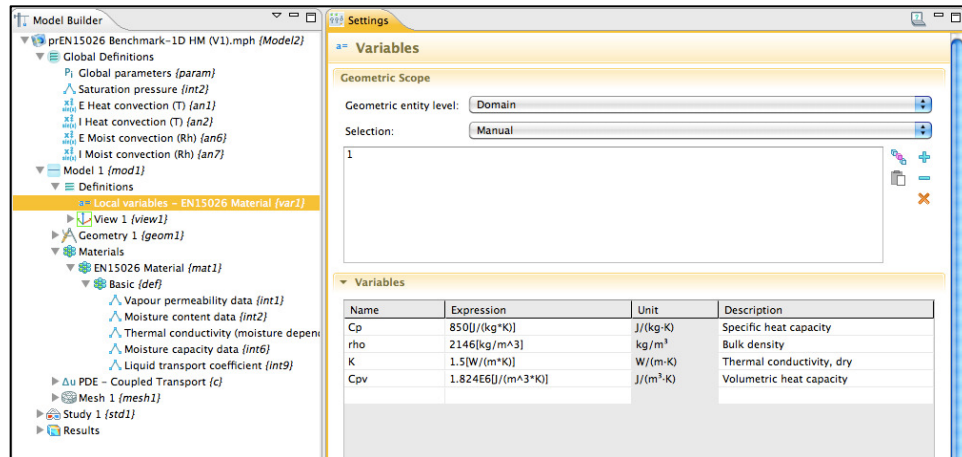
% Model 1: Definitions

```
model.variable.create('var1');
```

```

model.variable('var1').model('mod1');
model.variable('var1').name('Local variables - EN15026 Material');
model.variable('var1').set('Cp', '850[J/(kg*K)]', 'Specific heat capacity');
model.variable('var1').set('rho', '2146[kg/m^3]', 'Bulk density');
model.variable('var1').set('K', '1.5[W/(m*K)]', 'Thermal conductivity, dry');
model.variable('var1').set('Cpv', '1.824E6[J/(m^3*K)]', 'Volumetric heat capacity');
model.variable('var1').selection.geom('geom1', 1);
model.variable('var1').selection.set([1]);

```

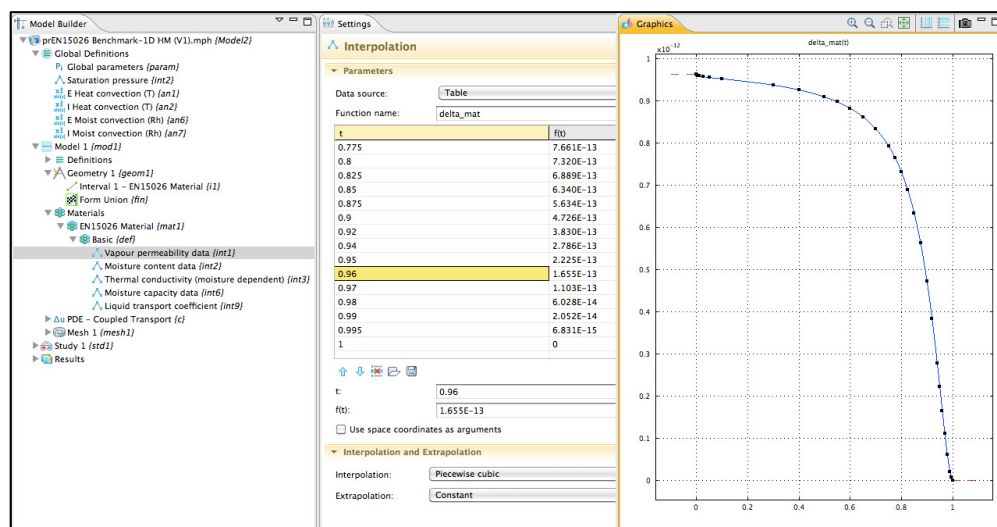


% Model 1: Materials

```

model.material.create('mat1');
model.material('mat1').name('EN15026 Material');
model.material('mat1').materialModel('def').func.create('int1', 'Interpolation');
model.material('mat1').materialModel('def').func('int1').name('Vapour permeability data');
model.material('mat1').materialModel('def').func('int1').set('funcname', 'delta_mat');
model.material('mat1').materialModel('def').func('int1').set('table', { '0' '9.638E-13'; '0.0001' '9.621E-13'; '0.0006' '9.615E-13'; '0.0035' '9.605E-13'; '0.01' '9.595E-13'; '0.025' '9.58E-13'; '0.05' '9.562E-13'; '0.1' '9.53E-13'; '0.3' '9.381E-13'; '0.4' '9.268E-13'; '0.5' '9.100E-13'; '0.55' '8.983E-13'; '0.6' '8.830E-13'; '0.65' '8.625E-13'; '0.7' '8.343E-13'; '0.75' '7.935E-13'; '0.775' '7.661E-13'; '0.8' '7.320E-13'; '0.825' '6.889E-13'; '0.85' '6.340E-13'; '0.875' '5.634E-13'; '0.9' '4.726E-13'; '0.92' '3.830E-13'; '0.94' '2.786E-13'; '0.95' '2.225E-13'; '0.96' '1.655E-13'; '0.97' '1.103E-13'; '0.98' '6.028E-14'; '0.99' '2.052E-14'; '0.995' '6.831E-15'; '1' '0'});
model.material('mat1').materialModel('def').set('delta_mat', 'delta_mat1[kg/(m*s*Pa)]');

```



```

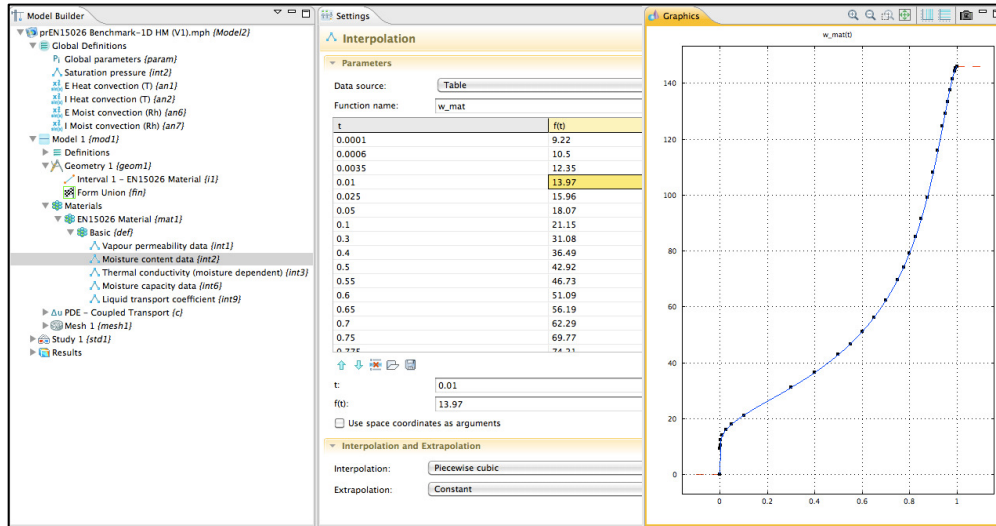
model.material('mat1').materialModel('def').func.create('int2', 'Interpolation');
model.material('mat1').materialModel('def').func('int2').name('Moisture content data');

```

```

model.material('mat1').materialModel('def').func('int2').set('funcname', 'w_mat');
model.material('mat1').materialModel('def').func('int2').set('table', {'0' '0'; '0.0001' '9.22'; '0.0006' '10.5';
'0.0035' '12.35'; '0.01' '13.97'; '0.025' '15.96'; '0.05' '18.07'; '0.1' '21.15'; '0.3' '31.08'; '0.4' '36.49'; '0.5'
'42.92'; '0.55' '46.73'; '0.6' '51.09'; '0.65' '56.19'; '0.7' '62.29'; '0.75' '69.77'; '0.775' '74.21'; '0.8' '79.23';
'0.825' '84.96'; '0.85' '91.55'; '0.875' '99.17'; '0.9' '107.98'; '0.92' '115.93'; '0.94' '124.56'; '0.95' '129.02';
'0.96' '133.44'; '0.97' '137.67'; '0.98' '141.46'; '0.99' '144.45'; '0.995' '145.49'; '1' '146.00'});
model.material('mat1').materialModel('def').set('w_mat', 'w_mat1[kg/m^3]');

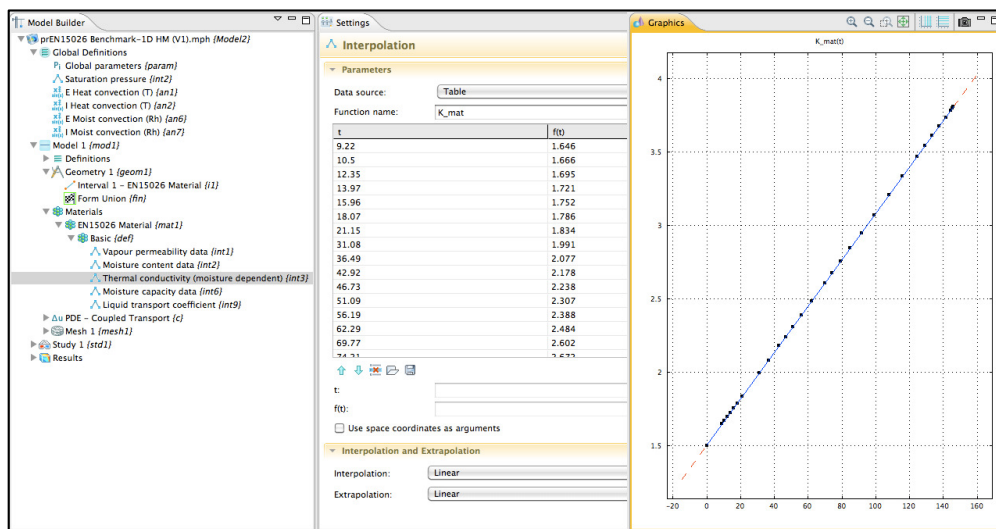
```



```

model.material('mat1').materialModel('def').func.create('int3', 'Interpolation');
model.material('mat1').materialModel('def').func('int3').name('Thermal conductivity (moisture dependent)');
model.material('mat1').materialModel('def').func('int3').set('funcname', 'K_mat');
model.material('mat1').materialModel('def').func('int3').set('table', {'0' '1.5'; '9.22' '1.646'; '10.5' '1.666';
'12.35' '1.695'; '13.97' '1.721'; '15.96' '1.752'; '18.07' '1.786'; '21.15' '1.834'; '31.08' '1.991'; '36.49'
'2.077'; '42.92' '2.178'; '46.73' '2.238'; '51.09' '2.307'; '56.19' '2.388'; '62.29' '2.484'; '69.77' '2.602';
'74.21' '2.672'; '79.23' '2.752'; '84.96' '2.842'; '91.55' '2.946'; '99.17' '3.067'; '107.98' '3.206'; '115.93'
'3.332'; '124.56' '3.468'; '129.02' '3.539'; '133.44' '3.608'; '137.67' '3.675'; '141.46' '3.735'; '144.45'
'3.782'; '145.49' '3.799'; '146.00' '3.807'});
model.material('mat1').materialModel('def').set('K_mat', 'K_mat1[W/(m*K)]');

```



```

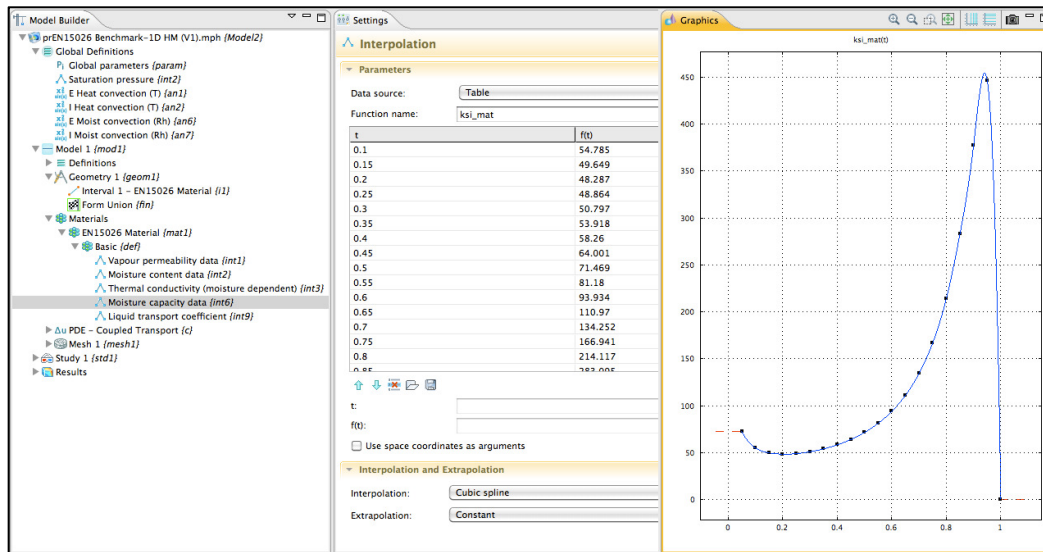
model.material('mat1').materialModel('def').func.create('int6', 'Interpolation');
model.material('mat1').materialModel('def').func('int6').name('Moisture capacity data');
model.material('mat1').materialModel('def').func('int6').set('funcname', 'ksi_mat');

```

```

model.material('mat1').materialModel('def').func('int6').set('table', {'0.05' '72.114'; '0.1' '54.785'; '0.15'
'49.649'; '0.2' '48.287'; '0.25' '48.864'; '0.3' '50.797'; '0.35' '53.918'; '0.4' '58.26'; '0.45' '64.001'; '0.5'
'71.469'; '0.55' '81.18'; '0.6' '93.934'; '0.65' '110.97'; '0.7' '134.252'; '0.75' '166.941'; '0.8' '214.117'; '0.85'
'283.095'; '0.9' '377.602'; '0.95' '446.165'; '1' '0'});
model.material('mat1').materialModel('def').set('ksi_mat', 'ksi_mat1[kg/m^3]');

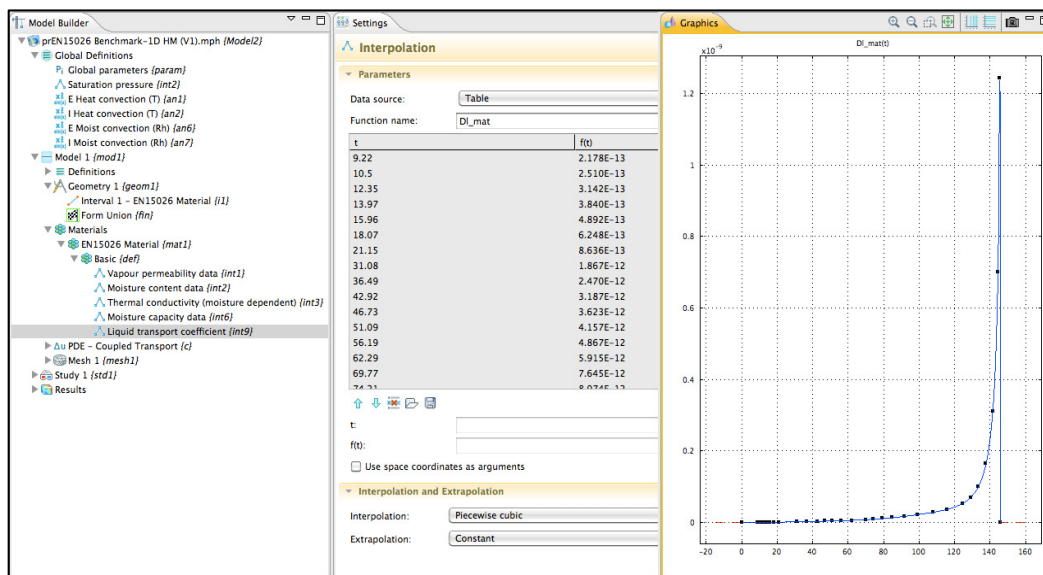
```



```

model.material('mat1').materialModel('def').func.create('int9', 'Interpolation');
model.material('mat1').materialModel('def').func('int9').name('Liquid transport coefficient');
model.material('mat1').materialModel('def').func('int9').set('funcname', 'Dl_mat');
model.material('mat1').materialModel('def').func('int9').set('table', {'0' '0'; '9.22' '2.178E-13'; '10.5'
'2.510E-13'; '12.35' '3.142E-13'; '13.97' '3.840E-13'; '15.96' '4.892E-13'; '18.07' '6.248E-13'; '21.15'
'8.636E-13'; '31.08' '1.867E-12'; '36.49' '2.470E-12'; '42.92' '3.187E-12'; '46.73' '3.623E-12'; '51.09'
'4.157E-12'; '56.19' '4.867E-12'; '62.29' '5.915E-12'; '69.77' '7.645E-12'; '74.21' '8.974E-12'; '79.23'
'1.081E-11'; '84.96' '1.337E-11'; '91.55' '1.694E-11'; '99.17' '2.186E-11'; '107.98' '2.870E-11'; '115.93'
'3.697E-11'; '124.56' '5.312E-11'; '129.02' '6.961E-11'; '133.44' '1.005E-10'; '137.67' '1.642E-10';
'141.46' '3.097E-10'; '144.45' '6.997E-10'; '145.49' '1.243E-09'; '146.00' '0'});

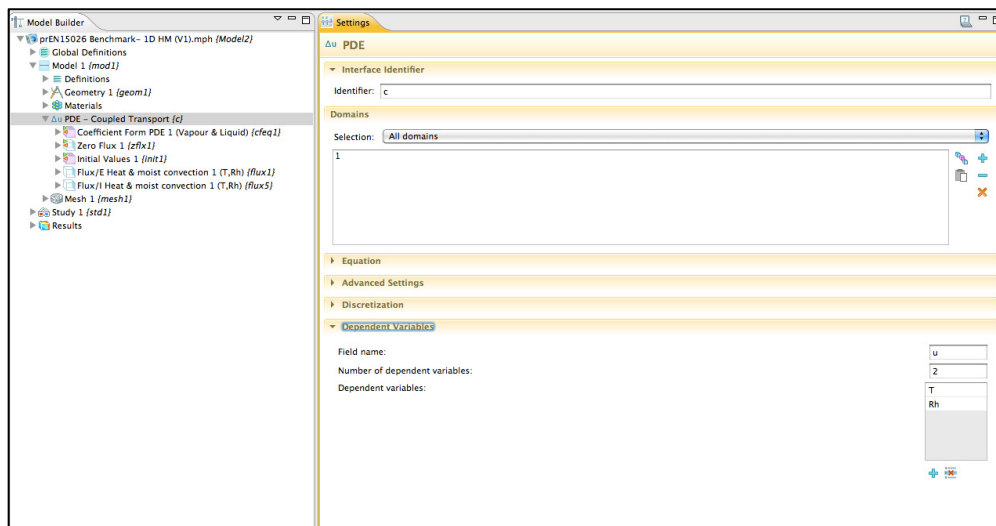
```



```

% Model 1: PDE – Coupled Transport (c)
model.physics.create('c', 'CoefficientFormPDE', 'geom1');
model.physics('c').field('dimensionless').component({'T' 'Rh'});

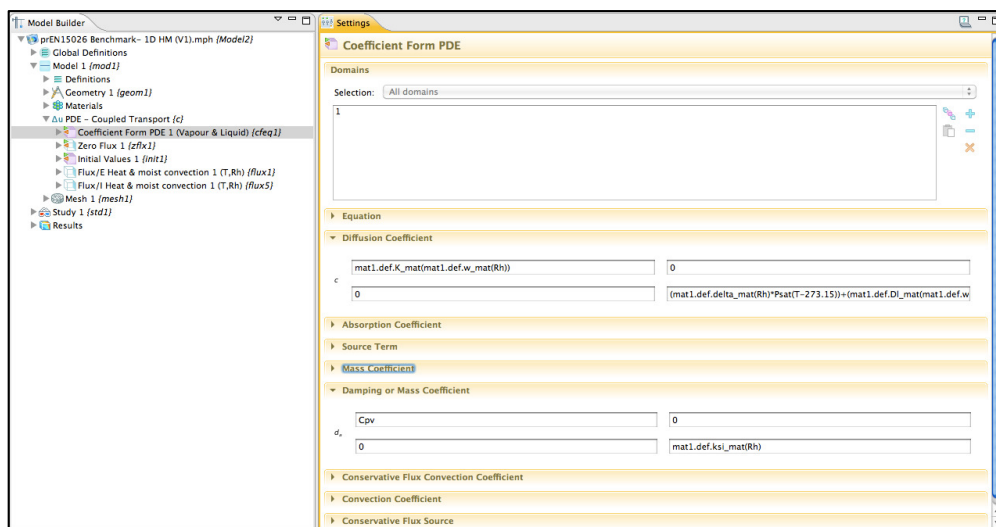
```



```

model.physics('c').feature.create('cfeq1', 'CoefficientFormPDE', 1);
model.physics('c').feature('cfeq1').selection.all;
model.physics('c').feature('cfeq1').name('Coefficient Form PDE 1 (Vapour & Liquid)');
model.physics('c').feature('cfeq1').set('c', {mat1.def.K_mat(mat1.def.w_mat(Rh)); '0'; '0';
'(mat1.def.delta_mat(Rh)*Psat(T-
273.15))+(mat1.def.DI_mat(mat1.def.w_mat(Rh))*mat1.def.ksi_mat(Rh))});
model.physics('c').feature('cfeq1').set('f', {'0'; '0'});
model.physics('c').feature('cfeq1').set('da', {'Cpv'; '0'; '0'; 'mat1.def.ksi_mat(Rh)'});

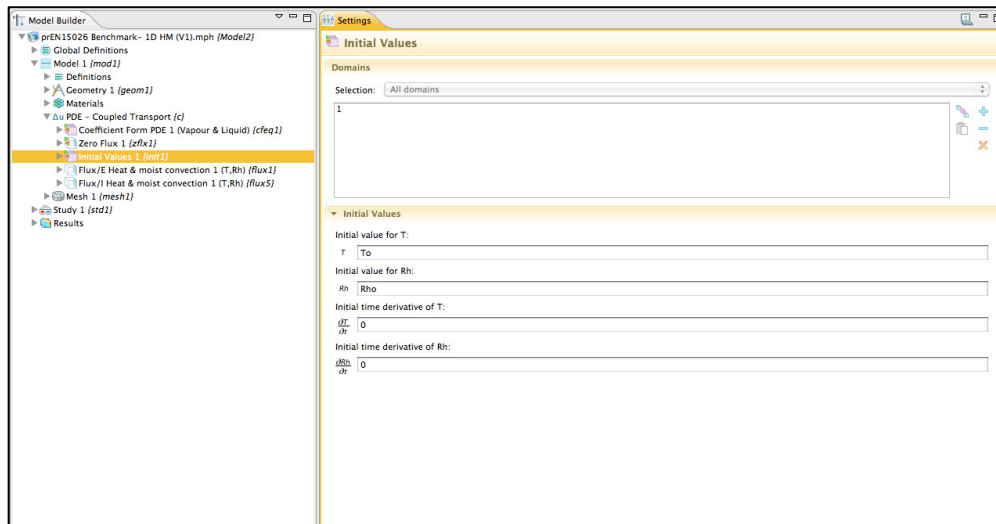
```



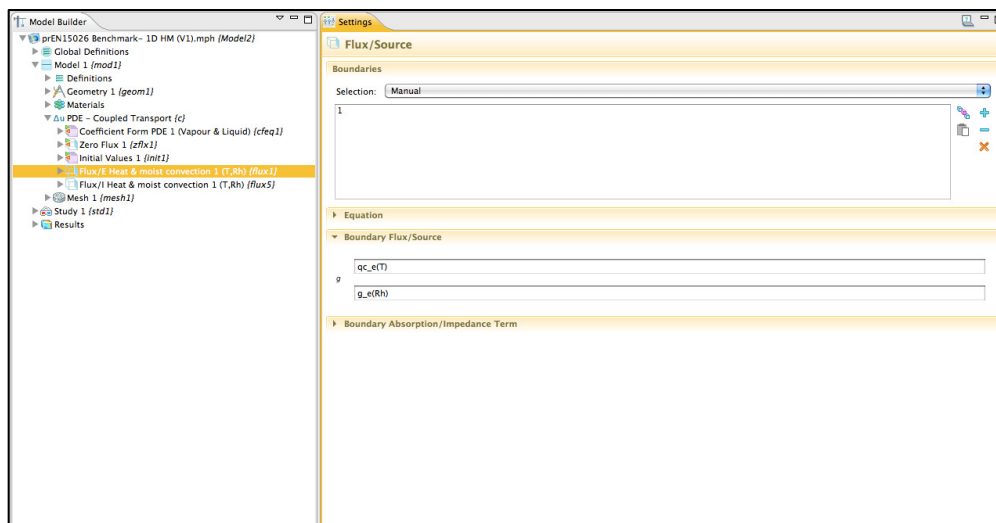
```

model.physics('c').feature('init1').set('T', 'To');
model.physics('c').feature('init1').set('Rh', 'Rho');

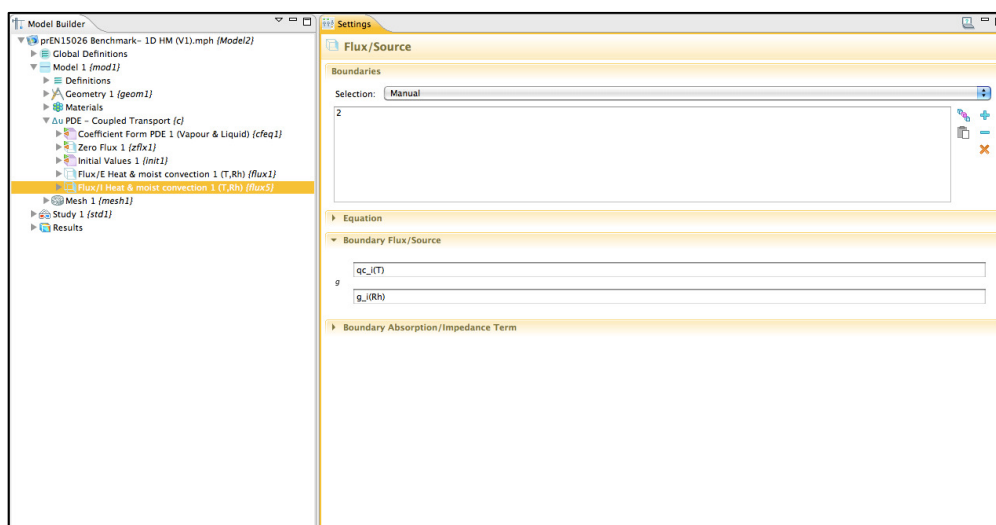
```



```
model.physics('c').feature('flux1').set('g', {'qc_e(T)'; 'g_e(Rh)'});
model.physics('c').feature('flux1').name('Flux/E Heat & moist convection 1 (T,Rh)');
```



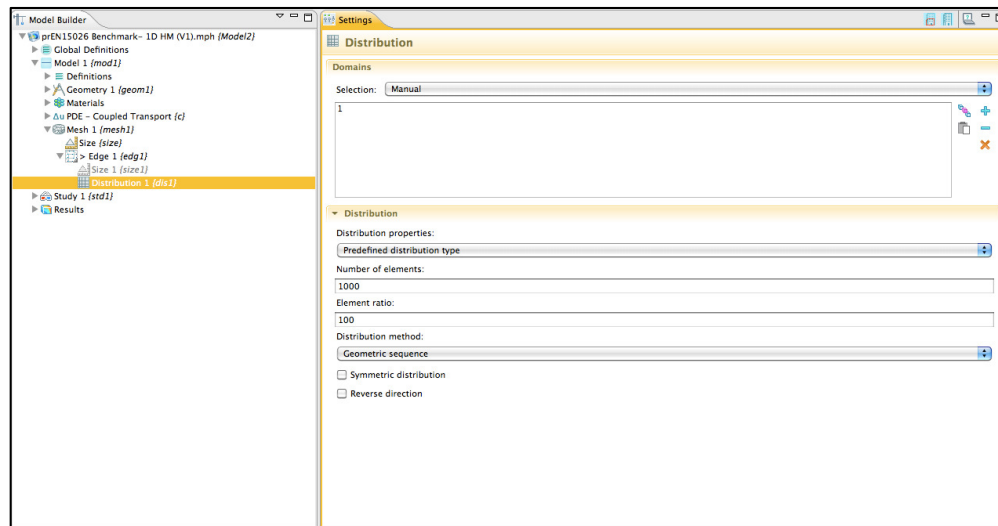
```
model.physics('c').feature('flux5').set('g', {'qc_i(T)'; 'g_i(Rh)'});
model.physics('c').feature('flux5').name('Flux/I Heat & moist convection 1 (T,Rh)');
```



```

model.mesh.create('mesh1', 'geom1');
model.mesh('mesh1').feature.create('edg1', 'Edge');
model.mesh('mesh1').feature('edg1').selection.geom('geom1', 1);
model.mesh('mesh1').feature('edg1').selection.set([1]);
model.mesh('mesh1').feature('edg1').feature.create('size1', 'Size');
model.mesh('mesh1').feature('edg1').feature('size1').active(false);
model.mesh('mesh1').feature('edg1').feature.create('dis1', 'Distribution');
model.mesh('mesh1').feature('edg1').feature('dis1').set('type', 'predefined');
model.mesh('mesh1').feature('edg1').feature('dis1').set('elemcount', '1000');
model.mesh('mesh1').feature('edg1').feature('dis1').set('elemratio', '100');
model.mesh('mesh1').feature('edg1').feature('dis1').set('method', 'geometric');
model.mesh('mesh1').run('edg1');

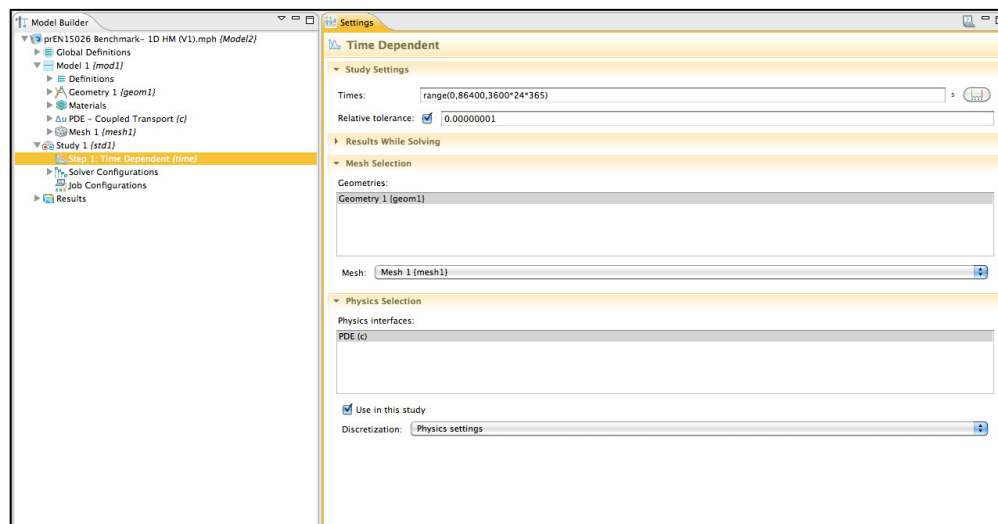
```



```

model.study.create('std1');
model.study('std1').feature.create('time', 'Transient');
model.study('std1').feature('time').set('tlist', 'range(0,3600,3600*24*365)');
model.study('std1').feature('time').set('rtol', '0.00000001');
model.study('std1').feature('time').set('rtolactive', true);

```



```

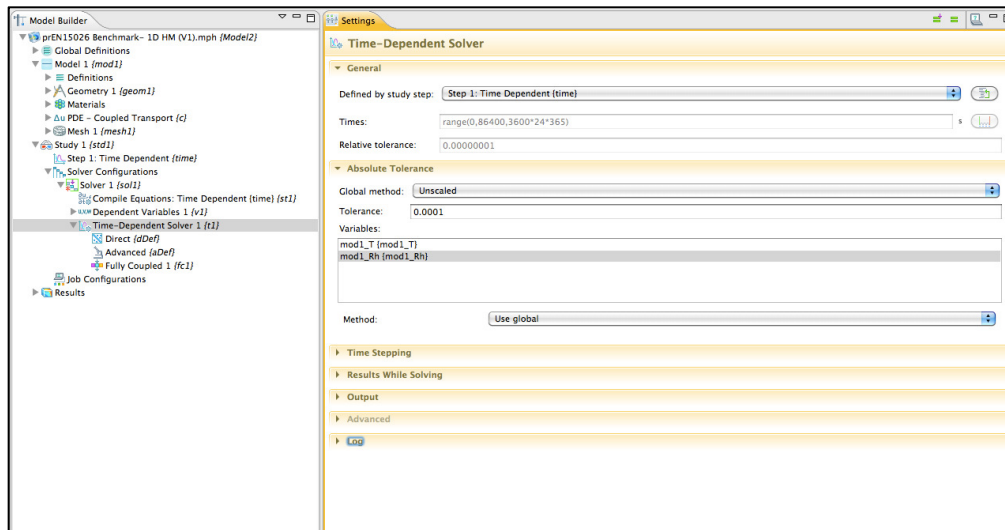
model.sol.create('sol1');
model.sol('sol1').study('std1');
model.sol('sol1').attach('std1');
model.sol('sol1').feature.create('st1', 'StudyStep');
model.sol('sol1').feature.create('v1', 'Variables');

```

```

model.sol('sol1').feature.create('t1', 'Time');
model.sol('sol1').feature('st1').name('Compile Equations: Time Dependent {time}');
model.sol('sol1').feature('st1').set('studystep', 'time');
model.sol('sol1').feature('t1').feature.create('fc1', 'FullyCoupled');
model.sol('sol1').feature('t1').feature.remove('fcDef');
model.sol('sol1').feature('t1').set('tlist', 'range(0,3600,3600*24*365)');
model.sol('sol1').feature('t1').set('rtol', '1.0E-7');
model.sol('sol1').feature('t1').set('atolglobal', '0.00010');

```



```

model.sol('sol1').runAll;
model.result('pg1').run;

```

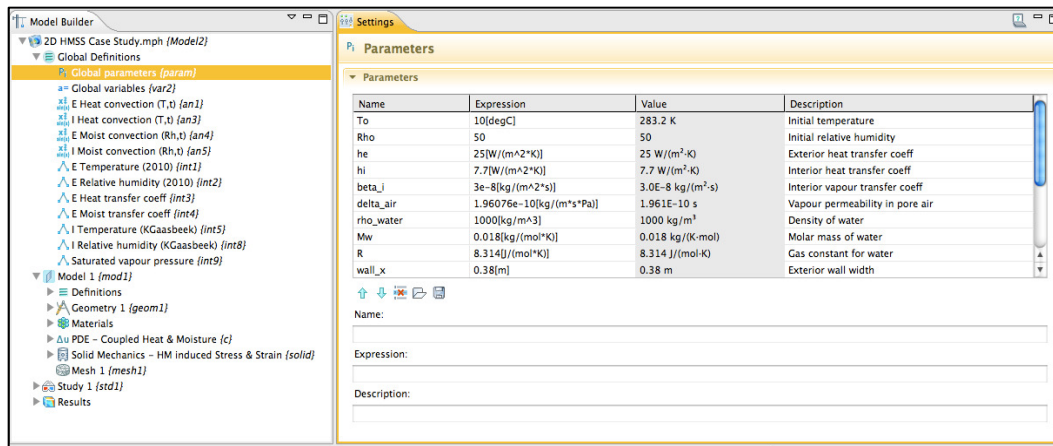
11.3.3 M-file for HMSS model

```
function out = model
% 2D HMSS Case study.m
% Model exported on Jun 13 2011, 09:08 by COMSOL 4.1.0.88.
```

```
import com.comsol.model.*
import com.comsol.model.util.*
model = ModelUtil.create('Model');
model.modelPath('Case study - Wall and panel\COMSOL Model');
model.modelNode.create('mod1');
```

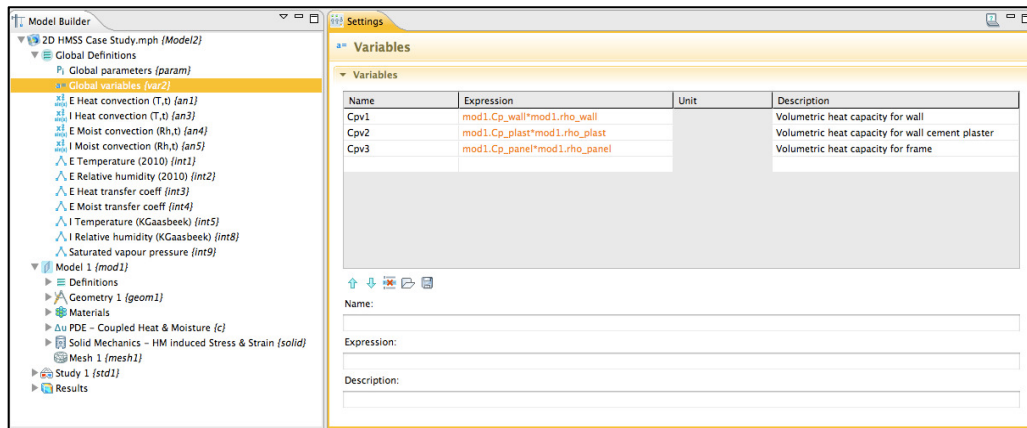
% Global Definitions: Global parameters

```
model.param.set('To', '20[degC]', 'Initial temperature');
model.param.set('Rho', '50', 'Initial relative humidity');
model.param.set('he', '25[W/(m^2*K)]', 'Exterior heat transfer coeff');
model.param.set('hi', '7.7[W/(m^2*K)]', 'Interior heat transfer coeff');
model.param.set('beta_i', '3E-8[kg/(m^2*s)]', 'Interior vapour transfer coeff');
model.param.set('delta_air', '1.96076E-10[kg/(m*s*Pa)]', 'Vapour permeability in pore air');
model.param.descr('rho_water', '1000[kg/m^3]', 'Density of water');
model.param.descr('Mw', '0.018[kg/(mol*K)]', 'Molar mass of water');
model.param.descr('R', '8.314[J/(mol*K)]', 'Universal gas constant for water');
model.param.set('wall_x', '0.38[m]', 'Exterior wall width');
model.param.set('wall_y', '1.5[m]', 'Exterior wall height');
model.param.set('panel_x', '0.01[m]', 'Picture frame width');
model.param.set('panel_y', '0.36[m]', 'Picture frame height');
model.param.set('plaster_x', '0.02[m]', 'Cement mortar width');
```



% Global Definitions: Global variables

```
model.variable('var2').set('Cpv1', 'mod1.Cp_wall*mod1.rho_wall', 'Volumetric heat capacity for wall');
model.variable('var2').set('Cpv2', 'mod1.Cp_plast*mod1.rho_plast', 'Volumetric heat capacity for cement plaster');
model.variable('var2').set('Cpv3', 'mod1.Cp_panel*mod1.rho_panel', 'Volumetric heat capacity for frame');
```

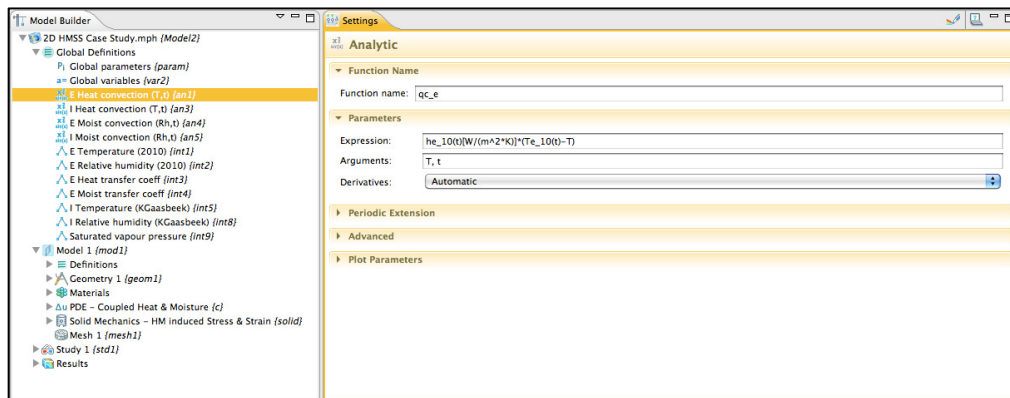


% Global Definitions: Analytic functions

```

model.func.create('an1', 'Analytic');
model.func('an1').name('E Heat convection (T,t)');
model.func('an1').set('funcname', 'qc_e');
model.func('an1').set('expr', 'he_10(t)[W/(m^2*K)]*(Te_10(t)-T)');
model.func('an1').set('args', {'T,t'});
model.func('an1').set('plotargs', {'T,t' " "});

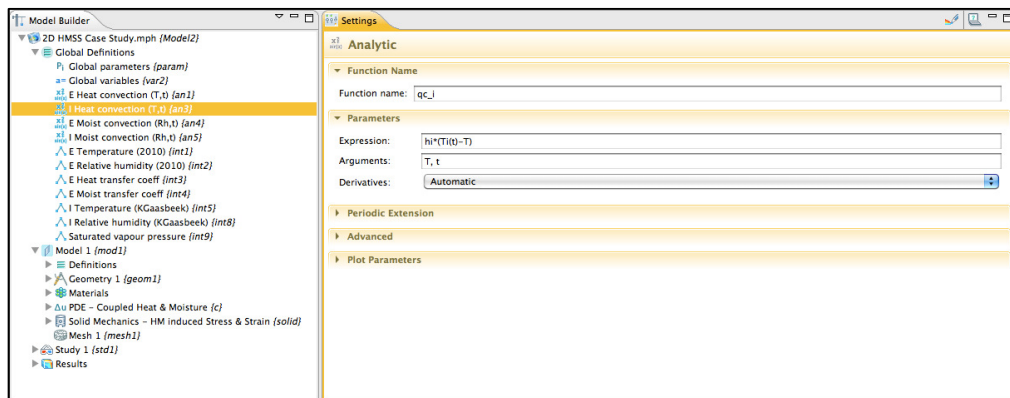
```



```

model.func.create('an3', 'Analytic');
model.func('an1').name('I Heat convection (T,t)');
model.func('an1').set('funcname', 'qc_i');
model.func('an1').set('expr', 'hi*(Ti(t)-T)');
model.func('an1').set('args', {'T,t'});
model.func('an1').set('plotargs', {'T,t' " "});

```



```

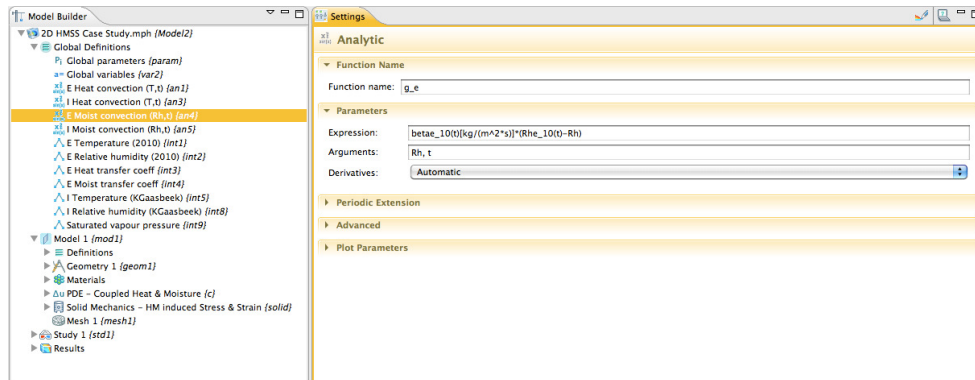
model.func.create('an4', 'Analytic');

```

```

model.func('an1').name('E Moist convection (Rh,t)');
model.func('an1').set('funcname', 'g_e');
model.func('an1').set('expr', 'betae_10(t)[kg/(m^2*s)]*(Rhe_10(t)-Rh)');
model.func('an1').set('args', {'Rh,t'});
model.func('an1').set('plotargs', {'Rh,t' " "});

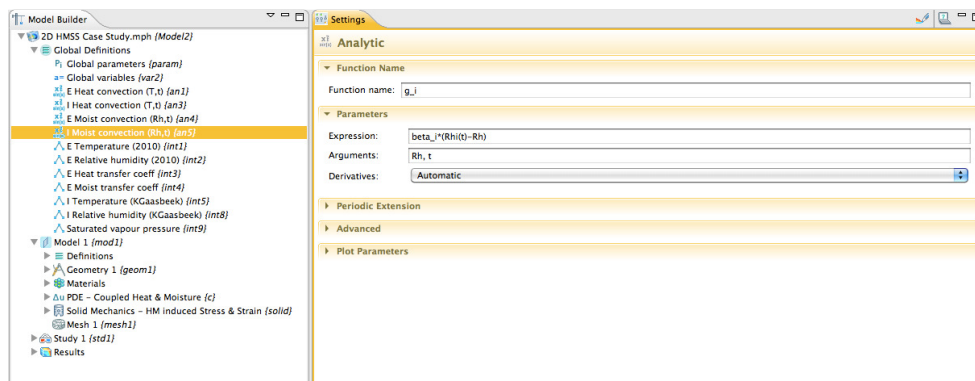
```



```

model.func.create('an5', 'Analytic');
model.func('an1').name('I Moist convection (Rh,t)');
model.func('an1').set('funcname', 'g_i');
model.func('an1').set('expr', 'beta_i*(Rhi(t)-Rh)');
model.func('an1').set('args', {'Rh,t'});
model.func('an1').set('plotargs', {'Rh,t' " "});

```

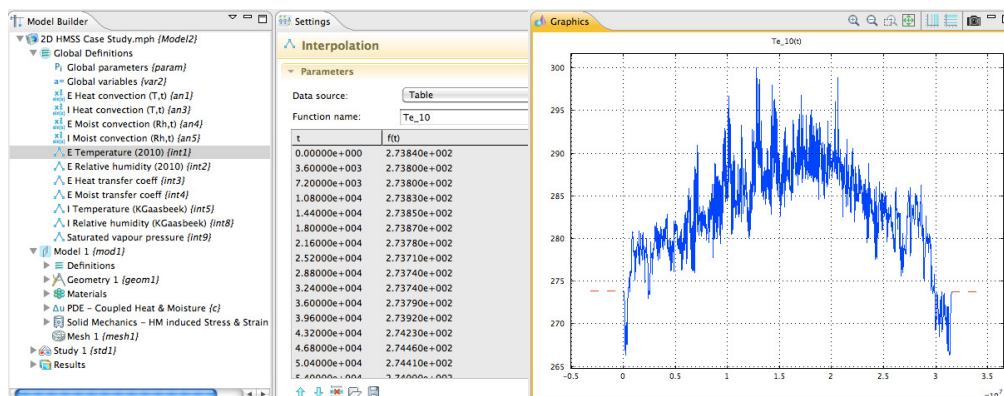


% Global Definitions: Interpolation functions

```

model.func.create('int1', 'Interpolation');
model.func('int1').name('E Temperature (2010)');
model.func('int1').set('funcname', 'Te_10');

```



```

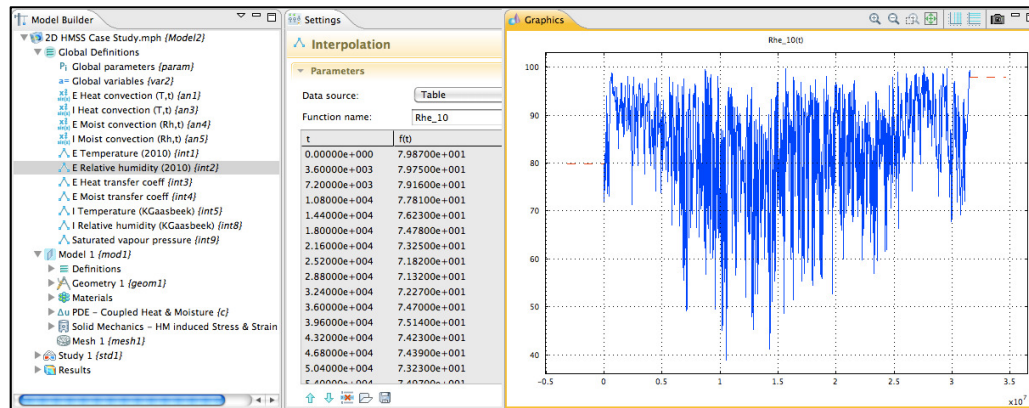
model.func.create('int2', 'Interpolation');

```

```

model.func('int2').name('E Relative humidity (2010)');
model.func('int2').set('funcname', 'Rhe_10');

```



```

model.func.create('int3', 'Interpolation');
model.func('int3').name('E Heat transfer coeff');
model.func('int3').set('funcname', 'he_10');

```

```

model.func.create('int4', 'Interpolation');
model.func('int4').name('E Moist transfer coeff');
model.func('int4').set('funcname', 'betae_10');

```

```

model.func.create('int5', 'Interpolation');
model.func('int5').name('I Temperature (KGaasbeek)');
model.func('int5').set('funcname', 'Ti');

```

```

model.func.create('int8', 'Interpolation');
model.func('int8').name('I Temperature (KGaasbeek)');
model.func('int8').set('funcname', 'Rhi');

```

```

model.func.create('int9', 'Interpolation');
model.func('int9').name('Saturated vapour pressure');
model.func('int9').set('funcname', 'Psat');

```

```

% Model 1

```

```

model.modelNode.create('mod1');

```

```

% Model 1: Geometry

```

```

model.geom.create('geom1', 2);
model.geom('geom1').feature.create('r1', 'Rectangle');
model.geom('geom1').feature('r1').setIndex('size', 'panel_x', 0);
model.geom('geom1').feature('r1').setIndex('size', 'panel_y', 1);
model.geom('geom1').feature('r1').setIndex('pos', 'wall_x+panel_x/2', 0);
model.geom('geom1').feature('r1').setIndex('pos', 'wall_y/2', 1);
model.geom('geom1').feature('r1').set('base', 'center');
model.geom('geom1').feature('r1').name('Rectangle 1 - Panel painting (Limewood)');
model.geom('geom1').run('r1');

```

```

model.geom('geom1').feature.create('r2', 'Rectangle');
model.geom('geom1').feature('r2').setIndex('size', '0.1*panel_x', 0);
model.geom('geom1').feature('r2').setIndex('size', 'panel_y', 1);
model.geom('geom1').feature('r2').setIndex('pos', 'wall_x+panel_x+0.05*panel_x', 0);
model.geom('geom1').feature('r2').setIndex('pos', 'wall_y/2', 1);
model.geom('geom1').feature('r2').set('base', 'center');
model.geom('geom1').feature('r2').name('Rectangle 2 - Panel painting (Gesso)');
model.geom('geom1').run('r2');

```

```

model.geom('geom1').feature.create('r3', 'Rectangle');
model.geom('geom1').feature('r3').setIndex('size', 'wall_x', 0);
model.geom('geom1').feature('r3').setIndex('size', 'wall_y', 1);
model.geom('geom1').feature('r3').setIndex('pos', '0', 0);
model.geom('geom1').feature('r3').setIndex('pos', '0', 1);
model.geom('geom1').feature('r3').set('base', 'corner');
model.geom('geom1').feature('r3').name('Rectangle 3 – Exterior wall (Brick)');
model.geom('geom1').run('r3');

```

```

model.geom('geom1').feature.create('r4', 'Rectangle');
model.geom('geom1').feature('r4').setIndex('size', 'plaster_x', 0);
model.geom('geom1').feature('r4').setIndex('size', 'wall_y', 1);
model.geom('geom1').feature('r4').setIndex('pos', 'wall_x', 0);
model.geom('geom1').feature('r4').setIndex('pos', '0', 1);
model.geom('geom1').feature('r4').set('base', 'corner');
model.geom('geom1').feature('r4').name('Rectangle 4 – Exterior wall (Cement)');
model.geom('geom1').run('r4');

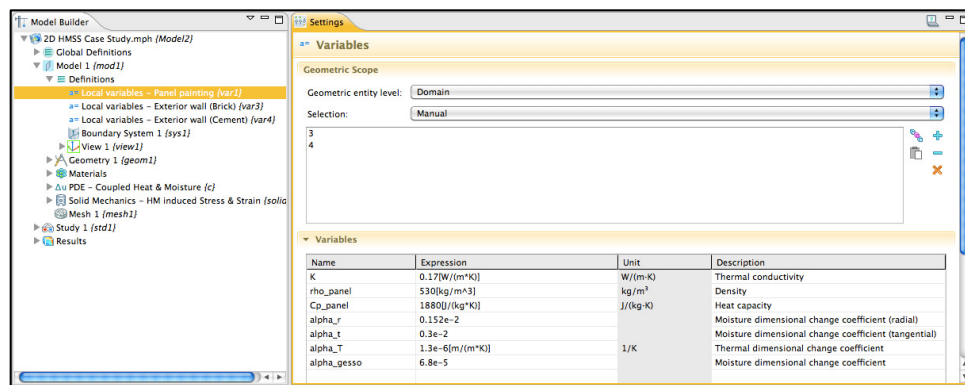
```

% Model 1: Definitions

```

model.variable.create('var1');
model.variable('var1').model('mod1');
model.variable('var1').selection.geom('geom1', 3,4);
model.variable('var1').name('Local variables - Picture painting');

```



```

model.variable.create('var3');
model.variable('var3').model('mod1');
model.variable('var3').selection.geom('geom1', 1);
model.variable('var3').name('Local variables - Exterior wall (Brick)');

```

```

model.variable.create('var4');
model.variable('var4').model('mod1');
model.variable('var4').selection.geom('geom1', 2);
model.variable('var4').name('Local variables - Exterior wall (Cement)');

```

% Model 1: Materials

```

model.material.create('mat1');
model.material('mat1').name('EN15026 Material');
model.material.create('mat2');
% AS SHOWN IN SECTION 11.3.2
model.material('mat2').name('Limewood');
model.material('mat2').materialModel('def').func.create('an1', 'Analytic');
model.material('mat2').materialModel('def').func('an1').name('Moisture content');
model.material('mat2').materialModel('def').func('an1').set('funcname', 'w_mat');
model.material('mat2').materialModel('def').func('an1').set('expr',
'0.61201+0.17236*Rh+0.00018587*Rh^2-0.000467145*Rh^3+0.000000503887*Rh^4');
model.material('mat2').materialModel('def').func('an1').set('args', {'Rh'});
model.material('mat2').materialModel('def').func('an1').set('dermethod', 'manual');

```

```

model.material('mat2').materialModel('def').func('an1').set('argders',{ 'Rh'
'd(0.61201+0.17236*Rh+0.00018587*Rh^2-0.0000467145*Rh^3+0.000000503887*Rh^4, Rh)});
% OTHER MATERIAL PROPERTIES INPUTTED IN SIMILAR OR SAME MANNER
model.material.create('mat3');
model.material('mat3').name('Gesso');
model.material.create('mat4');
model.material('mat4').name('Solid Brick, historical (Fraunhofer-IBP)');
model.material.create('mat5');
model.material('mat5').name('Cement plaster (Fraunhofer-IBP)');

```

.....

% Model 1: PDE – Coupled Transport (c)

```

model.physics.create('c', 'CoefficientFormPDE', 'geom1');
model.physics('c').field('dimensionless').component({'T' 'Rh'});
% SIMILAR TO THAT SHOWN IN SECTION 11.3.2

```

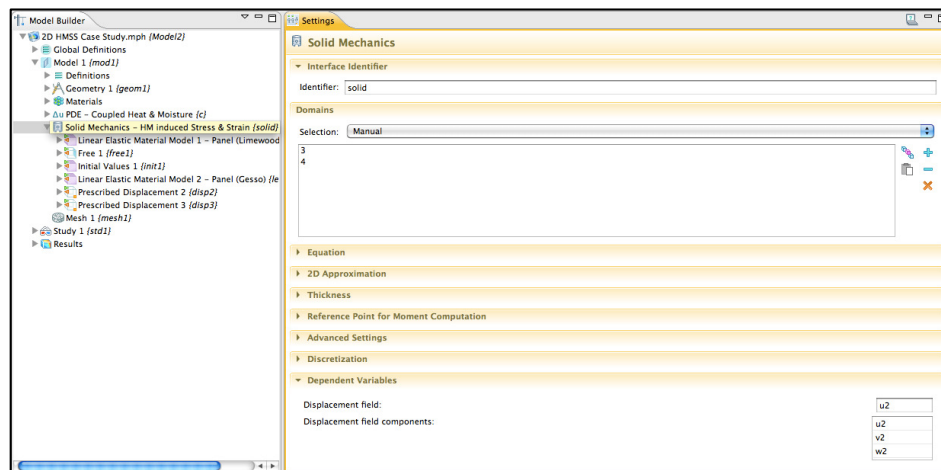
.....

% Model 1: Solid Mechanics – HM induced Stress & Strain

```

model.physics.create('solid', 'SolidMechanics', 'geom1');
model.physics('solid').name('Solid Mechanics -HM induced Stress & Strain');

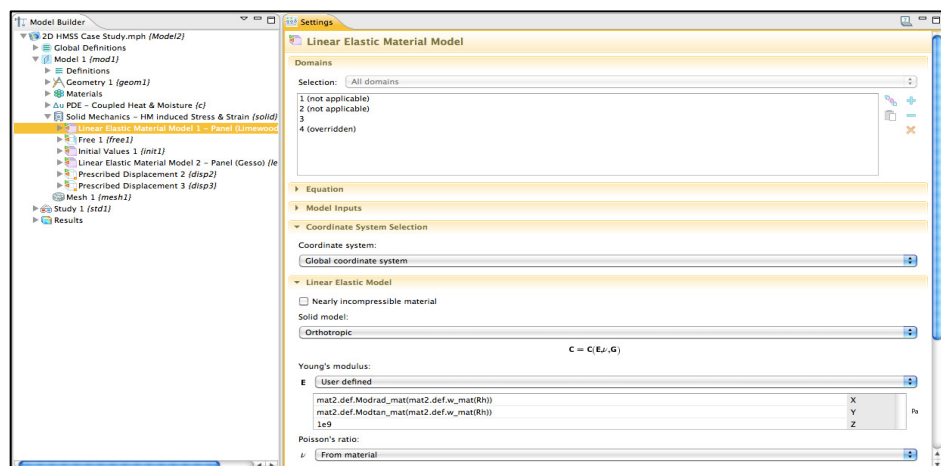
```



```

model.physics('solid').feature.create('lemm1', 'LinearElasticModel', 1);
model.physics('solid').feature('lemm1').name('Linear Elastic Material Model 1 – Panel (Limewood)');
model.physics('solid').feature('lemm1').selection.set([1]);
model.physics('solid').feature('lemm1').set('SolidModel', 1, 'Orthotropic');
model.physics('solid').feature('lemm1').set('Evector_mat', 1, 'userdef');
model.physics('solid').feature('lemm1').set('nuvector_mat', 1, 'from_mat');
model.physics('solid').feature('lemm1').set('Gvector_mat', 1, 'userdef');
model.physics('solid').feature('lemm1').set('rho_mat', 1, 'from_mat');

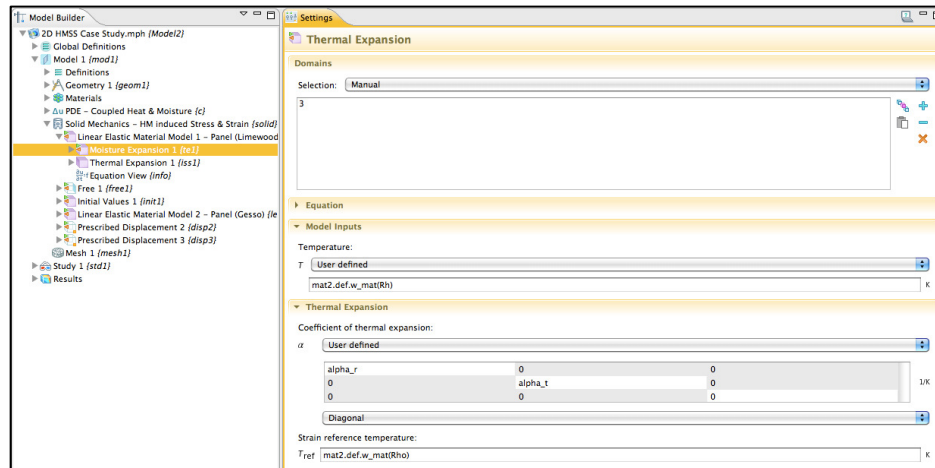
```



```

model.physics('solid').feature('lemm1').feature.create('te1', 'ThermalExpansion', 2);
model.physics('solid').feature('lemm1').feature('te1').name('Moisture Expansion 1');
model.physics('solid').feature('lemm1').feature('te1').set('Tref', 1, 'mat2.def.w_mat(Rho)');
model.physics('solid').feature('lemm1').feature('te1').set('minput_temperature', 1, 'mat2.def.w_mat(Rh)');
model.physics('solid').feature('lemm1').feature('te1').set('alpha', {'alpha_r' '0' '0' '0' 'alpha_t' '0' '0' '0'
'0'});

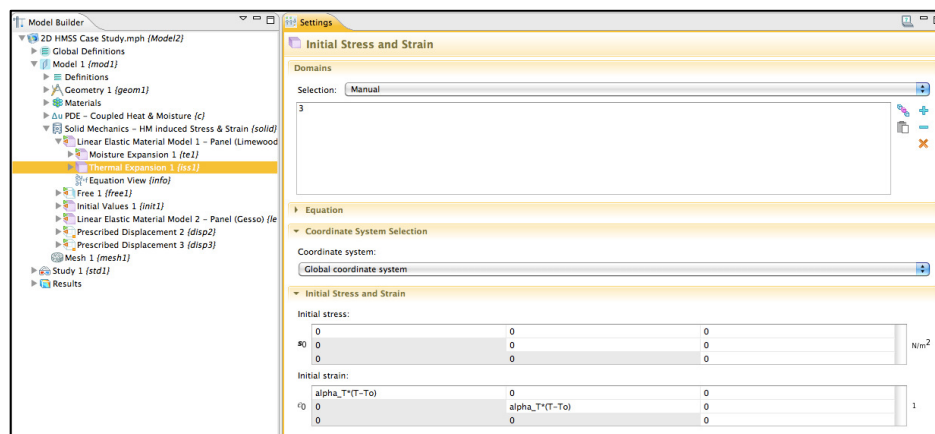
```



```

model.physics('solid').feature('lemm1').feature.create('iss1', 'InitialStressandStrain', 2);
model.physics('solid').feature('lemm1').feature('iss1').name('Thermal Expansion 1');
model.physics('solid').feature('lemm1').feature('iss1').set('ei', {'alpha_T*(T-To)' '0' '0' '0' 'alpha_T*(T-
To)' '0' '0' '0' '0'});

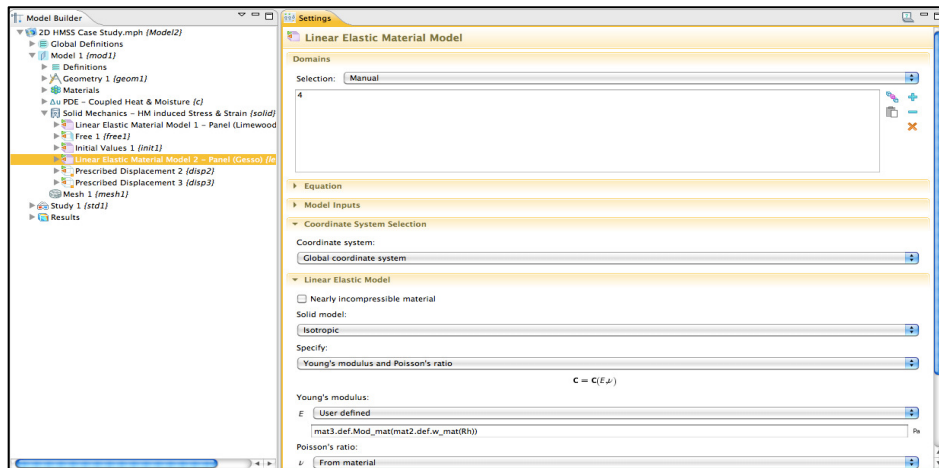
```



```

model.physics('solid').feature.create('lemm2', 'LinearElasticModel', 2);
model.physics('solid').feature('lemm2').name('Linear Elastic Material Model 2 – Panel (Gesso)');
model.physics('solid').feature('lemm2').selection.set([2]);
model.physics('solid').feature('lemm2').set('SolidModel', 1, 'Isotropic');
% FOLLOWING LINES THAT ARE EXCLUDED DESCRIBE MATERIAL DATA INPUT-ETC.

```



```

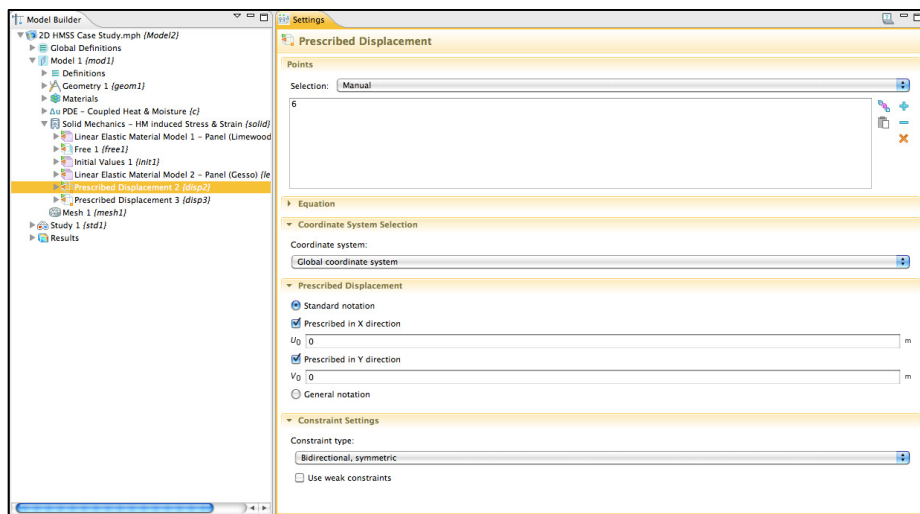
model.physics('solid').feature('lemm2').feature.create('te1', 'ThermalExpansion', 2);
model.physics('solid').feature('lemm2').feature('te1').name('Moisture Expansion 1');
model.physics('solid').feature('lemm2').feature.create('iss1', 'InitialStressandStrain', 2);
model.physics('solid').feature('lemm2').feature('iss1').name('Thermal Expansion 1');
% SAME PROCEDURE AS ABOVE FOR 'LEMM1'

```

```

model.physics('solid').feature('disp2').set('Direction', 1, '0');
model.physics('solid').feature('disp3').set('Direction', 1, '1');

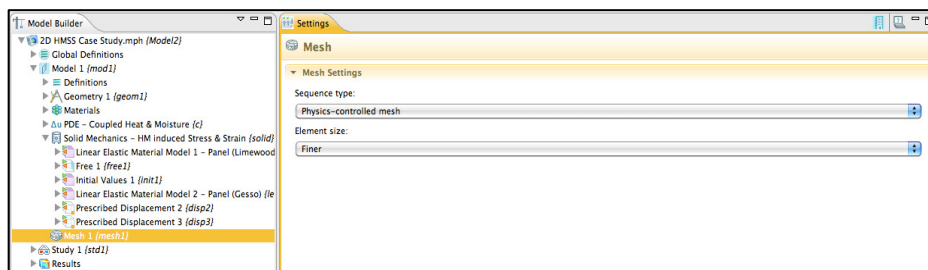
```



```

model.mesh.create('mesh1', 'geom1');

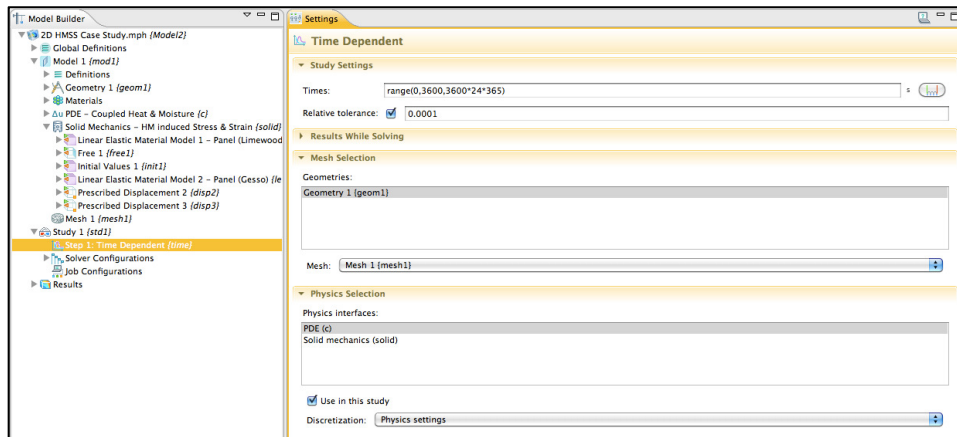
```



```

model.study.create('std1');
model.study('std1').feature.create('time', 'Transient');
model.study('std1').feature('time').set('tlist', 'range(0,3600,3600*24*365)');
model.study('std1').feature('time').set('rtol', '0.0001');
model.study('std1').feature('time').set('rtolactive', true);

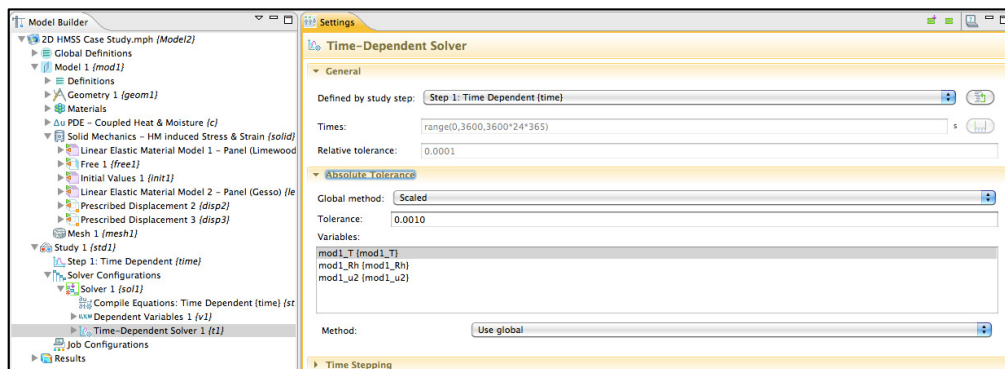
```



```

model.sol.create('sol1');
model.sol('sol1').study('std1');
model.sol('sol1').attach('std1');
model.sol('sol1').feature.create('st1', 'StudyStep');
model.sol('sol1').feature.create('v1', 'Variables');
model.sol('sol1').feature.create('t1', 'Time');
model.sol('sol1').feature('st1').name('Compile Equations: Time Dependent {time}');
model.sol('sol1').feature('st1').set('studystep', 'time');
model.sol('sol1').feature('t1').feature.create('fc1', 'FullyCoupled');
model.sol('sol1').feature('t1').feature.remove('fcDef');
model.sol('sol1').feature('t1').set('tlist', 'range(0,3600,3600*24*365)');
model.sol('sol1').feature('t1').set('rtol', '1.0E-4');
model.sol('sol1').feature('t1').set('atolglobal', '0.0010');

```



```

model.sol('sol1').runAll;
model.result('pg1').run;

```